UNIVERSIDAD DE MEDELLÍN
FACULTAD DE CIENCIAS BÁSICAS

TESIS
Programa de maestría en modelación y ciencia computacional

Selección de nanoanticuerpos contra antígenos tumorales mediante la utilización de una biblioteca sintética expresada en la superficie de fagos filamentosos

Julieta Salazar Uribe

Directores
Alain González Pose, PhD
Ernesto Moreno Frías, PhD
Frank Camacho Casanova, PhD

Medellín, 2023

Agradecimientos

Quiero comenzar agradeciendo a Dios por haberme guiado a este proyecto y brindarme la oportunidad de aprender, adquirir experiencia y disfrutar el camino.

Quiero agradecer a mis tutores, el Dr. Alain y el Dr. Ernesto por su valiosa orientación y enseñanzas a lo largo de esta etapa. Gracias por compartir sus conocimientos y corregirme en el camino. Valoro su dedicación, paciencia y apoyo.

También a mis compañeros de laboratorio Marcela y Yunier por hacer el ambiente de trabajo amigable y por acompañar los momentos de café con análisis de los ensayos y discusiones enriquecedoras. Gracias por su compañía y colaboración en todo momento.

Agradezco a mis padres, les agradezco su amor y apoyo. Gracias mamá por ser una fuente de motivación y recarga. A mi herma por sus aportes creativos y compañía.

Dedico un agradecimiento especial a mi compañero de cuatro patas, Cirilo, por el amor incondicional y compañía durante los días y largas noches de trabajo en esta tesis. Su presencia me ha recordado la importancia de disfrutar de los momentos simples.

Con cariño a mis amigos por siempre motivarme con sus palabras de aliento y comprender mis tiempos ausentes.

Al profesor Frank y Angélica por su disposición para resolver dudas y brindarnos su asesoría.

La realización de este trabajo de tesis fue financiado por el programa NanoBioCáncer de MINCIENCIAS (Código FP44842-211-2018, número de

proyecto 58676) y con el apoyo de la Universidad de Medellín para la matricula a través de un crédito condonable.

Mi gratitud a todas las personas que han contribuido en la realización de esta tesis.

RESUMEN

El factor de crecimiento epidérmico (EGF) se produce principalmente de forma paracrina y su concentración en suero humano es muy variable, pero tiende a ser mayor en paciente con cáncer. Es uno de los ligandos más importantes del receptor del factor de crecimiento epidérmico (EGFR). Otro antígeno importante en el desarrollo de cáncer es el factor de necrosis tumoral alfa TNFα como una citocina proinflamatoria. El TNFα es una citocina de 17 kDa con 157 aminoácidos, producido principalmente por macrófagos activados, linfocitos T y células asesinas naturales (NK), también en menor cantidad por células tumorales. Con el objetivo de generar nanoanticuerpos específicos contra diversos antígenos a partir de una biblioteca sintética mediante la tecnología de la presentación de proteínas en la superficie de fagos filamentosos, se realizaron dos estrategias de selección. Las variaciones entre las estrategias utilizadas consistieron en modificaciones en los lavados, las eluciones y la cantidad de rondas de enriquecimiento Utilizando cuatro eluciones diferentes consecutivas y tres rondas de enriquecimiento obtuvimos 4 nanoanticuerpos específicos de EGF, mientras que utilizando una única ronda de selección y condiciones astringentes de lavado y elución logramos obtener 21 nanoanticuerpos específicos de TNFα. La metodología de elución que se emplea durante la realización de la técnica de Phage Display podría influir en la diversidad de secuencias de los fagos que reconocen el antígeno de interés.

Palabras claves

Nanoanticuerpos, biblioteca sintética, enriquecimiento por afinidad, phage display, bacteriófago, antígenos tumorales, factor de crecimiento epidérmico EGF.

Contenido

I. INTRODUCCIÓN

Hace 20 años, Hamers-Casterman *et* al. demostraron la presencia de anticuerpos con un peso molecular aproximado de 100 kDa en el suero de camellos (*Camelus dromedarius*), compuestos únicamente por dímeros de la cadena pesada y se les denominó anticuerpos de cadena pesada (HCAbs, del inglés: *heavy-chain antibodies*) (Hamers-Casterman et al., 1993)(Khong Nguyen et al., 2001).

La porción del dominio de unión al antígeno de los anticuerpos de cadena pesada o dominio variable de la cadena pesada del HCAbs (VHH) producidos en sistemas biológicos de manera recombinante, se denomina nanocuerpo o nanoanticuerpo. Su peso molecular entre 12-15 kDa lo convierten en el fragmento de anticuerpo funcional de menor tamaño que se ha encontrado (Pedreáñez et al., 2021a). Su pequeño tamaño le confiere mayor penetrabilidad y extravasación en tejidos débilmente vascularizados y poco accesibles. Característica especialmente útil en el diagnóstico y tratamiento de tumores (Pedreáñez et al., 2021b).

Para seleccionar nanobodies con una alta especificidad frente a un antígeno determinado aplicamos una novedosa técnica para Colombia denominada *phage display* a partir de bibliotecas sintéticas con una gran diversidad genética de 1.5 x 10^8. Esta biblioteca se usó para generar nanoanticuerpos contra los antígenos tumorales EGF, TNFα y VEGF mediante la técnica de presentación de nanoanticuerpos en la superficie de fagos filamentosos.

Con el objetivo de generar nanoanticuerpos específicos contra diversos antígenos a partir de una biblioteca sintética mediante la tecnología de la presentación de

proteínas en la superficie de fagos filamentosos, se realizaron dos estrategias de selección. Las variaciones entre las estrategias utilizadas consistieron en modificaciones en los lavados, las eluciones y la cantidad de rondas de amplificación. La biblioteca usada en esta investigación corresponde a la desarrollada por Moreno E. *et* al. (2022) en el marco del proyecto NanoBioCáncer (Moreno et al., 2022). A la fecha en Colombia no hay evidencia de trabajos investigativos con estas moléculas, convirtiendo a nuestro equipo en el primer grupo de investigación en el país en utilizar la metodología de bibliotecas sintéticas de nanoanticuerpos basadas en la expresión de proteínas sobre la superficie de fagos filamentosos.

II. REVISIÓN BIBLIOGRÁFICA

1. Anticuerpos de cadena pesada

En 1993, Hamers-Casterman *et* al. demostraron la presencia de anticuerpos con un peso molecular aproximado de 100 kDa en el suero de camellos (*Camelus dromedarius*), que a diferencia de las inmunoglobulinas IgG convencionales, están compuestos únicamente por dímeros de la cadena pesada, carecen de cadenas ligeras y del primer dominio constante (CH1), por lo cual se les denominó anticuerpos de cadena pesada (HCAbs, del inglés: *heavy-chain antibodies*). Las cadenas pesadas de HCAbs esta conformada por dos dominios constantes (CH2 y CH3 del inglés: *constant domain in the heavy chain*), una región bisagra y un dominio variable o sitio de unión al antígeno denominado dominio variable de la cadena pesada del HCAbs (VHH del inglés: *Variable domain of the heavy chain of HCAbs*) (Hamers-Casterman et al., 1993). Estos anticuerpos también se encuentran presentes en otros géneros de la familia *Camelidae*, como la llama (*Lama glama*), dromedario (*Camelus dromedarius*) y la alpaca (*Lama pacos*) (Khong Nguyen et al., 2001). Se conocen tres subclases funcionales de IgG presentes en el suero de la familia *Camelidae*, la subclase IgG1 es un heterodímero que consta de cadena pesada y ligera, mientras que las subclases IgG2 e IgG3 sólo tienen cadena pesada y constituyen el 75% de las inmunoglobulinas séricas totales en especie de camellos y entre un 25-20% en llamas y alpacas (Arbabi-Ghahroudi, 2022).

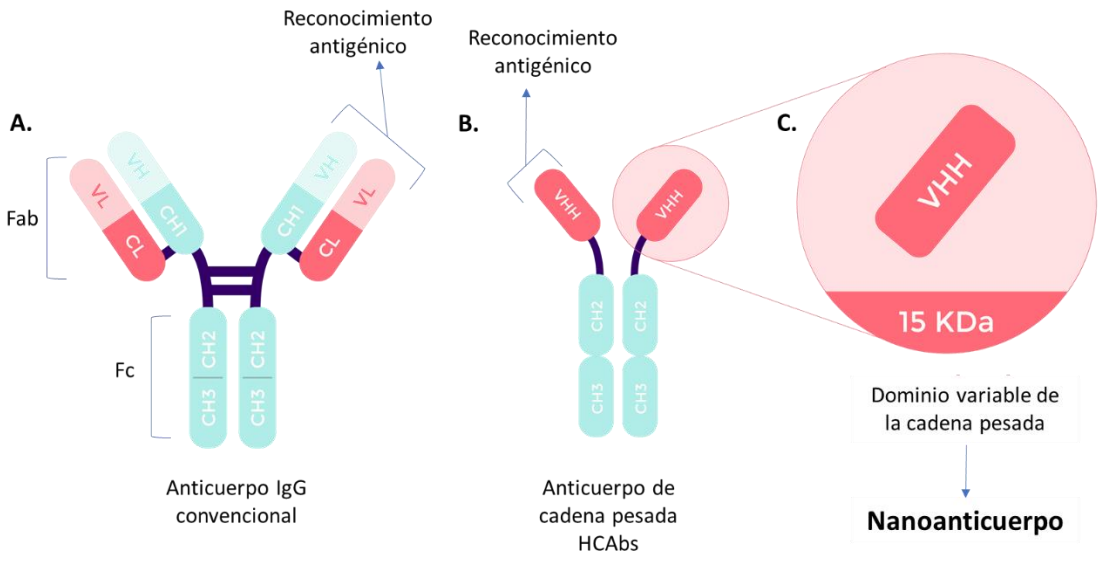

Figura 1. Representación de anticuerpos convencionales y anticuerpos de cadena pesada. (A.) Anticuerpo de tipo IgG compuesto por dos cadenas pesadas (CH3, CH2, CH1 Y VH) y dos cadenas ligeras (CL Y VL); (B.) Anticuerpos de cadena pesada homodímero (CH2 yCH3) y la región de reconocimiento al antígeno (VHH).

Posteriormente, en 1995, Greenberg et al. informaron que en peces cartilaginosos (tiburón nodriza) también se producían una clase similar de inmunoglobulinas, denominado receptor de antígeno nuevo de inmunoglobulina (IgNAR). La estructura del IgNAR es un homodímero con cinco dominios constantes y un dominio variable N-terminal que facilita el reconocimiento del antígeno (vNAR) (Könning et al., 2017)(Greenberg et al., 1995).

Los dominios de unión al antígeno de anticuerpos de cadena pesada (VHH) están compuestos por cuatro regiones con secuencias altamente conservadas denominadas regiones marco (FR, del inglés *framework regions*) y por tres regiones hipervariables determinantes de complementariedad (CDR, del inglés:

complementarity- determining region). Las regiones marco son importantes en la preservación de la estructura, plegamiento y estabilidad de los anticuerpos, mientras que los CDR le confieren variación en la capacidad de reconocimiento de antígenos. A diferencia de los anticuerpos convencionales, la unión de las regiones VHH y CH2 en ausencia del dominio CH1 suele ser alargada y rígida por la presencia de residuos repetidos de prolina, lisina, glutamina o ácido glutámico (Smolarek et al., 2012). Otra característica diferencial de los HCAbs son los CDRs. En los camélidos el CDR3 suele ser mas largo, con una longitud promedio de 16 a 18 aminoácidos en comparación con los 9 a 12 aminoácidos del anticuerpo convencional, un puente disulfuro entre el CDR1 y el CDR3 le proporciona estabilidad al dominio de unión. Esta cualidad le confiere versatilidad para interactuar con las moléculas diana (Hoey et al., 2019). Además, se encontró que el CDR3 es el principal contribuyente a la unión de antígenos, involucrado en aproximadamente el 50% de las interacciones, mientras que al CDR2 se le atribuye el 20% y al CDR1 el 13%. El porcentaje restante corresponde a interacciones en la porción de residuos no CDR, como la región N-terminal de la primera cadena β o la región marco 2 (FR2) (Smolarek et al., 2012).

2. Nanoanticuerpos

La producción recombinante del dominio de unión al antígeno de los anticuerpos de cadena pesada o dominio variable de la cadena pesada del HCAbs (VHH), se denomina nanocuerpo o nanoanticuerpo. La farmacéutica Ablynx registró el nombre comercial de Nanobody ® (Nb). Los nanoanticuerpos se componen aproximadamente de 120 aminoácidos, poseen un peso molecular entre 12-15 kDa y un tamaño de 4 nm de altura con 2,5 nm de diámetro.

Características que lo convierten en el fragmento de anticuerpo funcional de menor tamaño que se ha encontrado. Su tamaño, la conformación convexa y una mayor longitud del CDR3 le confiere la capacidad de unirse a estructuras no reconocidas por los anticuerpos convencionales (Pedreáñez et al., 2021a). Estas características, le permiten mayor flexibilidad que sumado a los puentes disulfuro entre CDR1 y CDR3 le brinda estabilidad al dominio de unión. Las regiones CDR1 y CDR2 también participan en la unión al antígeno, permitiendo una mayor diversidad de paratopos (E. Y. Yang & Shah, 2020).

El encuentro de un fármaco con su diana se da por difusión, este proceso depende del tamaño molecular, su capacidad de extravasación y penetración en los tejidos. Las características de los nanoanticuerpos les permiten difundirse rápidamente a los tejidos y acceder a epítopos que los anticuerpos convencionales o sus derivados como fragmentos Fv de cadena simple (scFv) no podrían acceder, esto los convierte en ideales para el tratamiento del cáncer (Pedreáñez et al., 2021b). Adicionalmente, su pequeño tamaño le confiere mayor penetrabilidad y extravasación en tejidos débilmente vascularizados y poco accesibles. Característica especialmente útil en el diagnóstico y tratamiento de tumores (Pedreáñez et al., 2021b). Para la terapia del cáncer, los nanoanticuerpos se usan como antagonistas para evitar la unión de ligandos y evadir los cambios que conducen a la activación de cascadas de señalización (Jovčevska & Muyldermans, 2020). En 2007, Roovers et al. demostraron la actividad de un nanoanticuerpo contra el receptor del factor de crecimiento epidérmico (EGFR) que bloqueó la señalización mediada por el factor de crecimiento epidérmico (EGF) y la

proliferación celular. Estos nanoanticuerpos retrasaron efectivamente el crecimiento de tumores sólidos *in vivo* (Roovers et al., 2007a). Los nanoanticuerpos también se pueden usar como inhibidores alostéricos para modular la actividad enzimática mediante la alteración del sitio activo de la enzima para evitar la unión a su sustrato (Jovčevska & Muyldermans, 2020).

Otras características adicionales de los VHH incluyen su alta termoestabilidad, pueden tolerar altas temperaturas (60-80°C) y permanecer funcionales luego de someterse a ciclos de calentamiento/enfriamiento. Además, resisten presiones elevadas (500-750 MPa), agentes químicos desnaturalizantes como 2-3 M de cloruro de guanidio y 6-8 M de urea; así como otros entornos hostiles como el pH del tracto gastrointestinal y el pH no fisiológicos (3,0-9,0), lo que incrementa su potencial para la terapia oral. (Arbabi-Ghahroudi, 2022)(E. Y. Yang & Shah, 2020).

Una diferencia adicional entre los HCAbs y sus contrapartes convencionales es la alta solubilidad y alto nivel de expresión en *Escherichia coli* (*E. coli*). Los VHH se han expresado en diferentes sistemas de producción, desde bacterias, levadura y líneas de células de mamíferos, siendo *E. coli* el sistema de expresión que provee mayores ventajas por su estructura, genética y fácil manipulación. En los anticuerpos tradicionales, hay una gran cantidad de residuos hidrofóbicos en la región FR2 donde VH interactúa con VL. Estos residuos hidrofóbicos han sido reemplazados por residuos hidrofílicos en VHH, lo que mejora la solubilidad de VHH (Kinoshita et al., 2022). Esto permite su producción en microorganismos para disminuir significativamente los costos y el tiempo de producción. En la actualidad, muchos VHH se producen con éxito en el periplasma de la bacteria, alcanzando rendimientos de hasta decenas de miligramos por litro (Y. Liu & Huang, 2018).

Debido a las características anteriormente mencionadas, se pueden generan bibliotecas de VHH contra diferentes antígenos de interés y seleccionar de acuerdo a su especificidad y afinidad aplicando la técnica de presentación de nanoanticuerpos en la superficie de fago filamentoso (Phage display).

3. Selección de nanoanticuerpos mediante Phage display.

El concepto de Phage display se introdujo por primera vez en 1985, cuando George P. Smith demostró la expresión de péptidos en la superficie de un virión, haciendo posible insertar fragmentos de ADN foráneos en el gen III de un fago filamentoso y de esta manera crear una proteína de fusión presentada en la superficie del virión sin perder su capacidad de infección (Smith, 1985). Más adelante en 1990, el grupo de Gregory Winter tuvo éxito en la presentación de fragmentos variables de anticuerpos convencionales en los fagos utilizados por Smith (McCafferty et al., 1990). En 2018 estos resultados le otorgaron el Premio Nobel de Química a Smith y Winter por el desarrollo de la técnica de presentación de péptidos y anticuerpos en fagos (Smith, 2019).

La tecnología de presentación en fagos permite la construcción de bibliotecas en las que se muestran varios péptidos y proteínas. Luego, mediante incubación de la biblioteca de fagos con la molécula diana, seguido de la eliminación de los fagos no unidos, se seleccionan los clones afines al antígeno de interés. Por lo tanto, los clones con afinidad por el objetivo de interés se seleccionan a partir de la biblioteca (Nagano & Tsutsumi, 2021).

Para la presentación de moléculas sobre fagos, el bacteriófago filamentoso más usado es el M13, también se usan en menos frecuencia para esta tecnología otros fagos como lambda y T7 (Ul Haq et al., 2012).

a. Bacteriófagos Filamentosos

Los bacteriófagos son los entes más abundantes en la tierra. Estos virus bacterianos tienen material genético en forma de ADN o ARN, encapsulado por una cubierta de proteínas. La cápside está adherida a una cola con proteínas que se utilizan para adherirse a los receptores en la superficie de la célula bacteriana. La mayoría de los fagos tienen cápside poliédrica, excepto los fagos filamentosos que tienen forma cilíndrica (Ul Haq et al., 2012).

Los fagos filamentosos del género *Inovirus* infectan y se propagan en bacterias gram negativas a través del pili sexual sin destruir el huésped durante su ciclo de vida llamado ciclo de vida lisogénico. Dentro del grupo de fagos filamentosos (Ff) están los fagos M13, fd y f1 con un 98% de similitud en sus secuencias de ADN. Este grupo de fagos de ADN monocatenario circular (ssDNA), posee 6400 pb aproximadamente. Tienen un diámetro alrededor de 6,5 nm y un largo aproximado de 930 nm. Su genoma contiene 11 genes, los genes gII, gV y gX codifican las proteínas necesarias en la replicación, los genes gVII, gIX, gVIII, gIII y gVI codifican las proteínas de la cápside y los genes gI, gXI y gIV codifican las proteínas involucradas en el ensamblaje del bacteriófago. La cápside contiene 5 proteínas diferentes, la mayor parte se compone de aproximadamente 2700 copias de la proteína pVIII que cubre la longitud de la partícula viral, las otras cuatro proteínas menores están representadas aproximadamente en 5 copias. En uno de sus extremos están las proteínas pVII y pIX mientras que las proteínas pIII y pVI están en el otro extremo del fago (Shamir & Goldbourt, 2022). Las 5

proteínas proporcionan estabilidad a la estructura, pero la proteína III también esta involucrada en el reconocimiento del huésped y la infección, por lo que es la proteína de mayor tamaño en la cápside (Sidhu, 2001).

b. Ciclo de Vida del Fago Filamentoso

El ciclo de vida de los fagos Ff se compone de tres etapas: infección, replicación del genoma y síntesis de proteínas, y ensamblaje del virión. Además, están involucrados los 11 genes, de los cuales los genes gII, gV y gX codifican las proteínas requeridas en la replicación, las proteínas gVII, gIX, gVIII, gIII y gVI conforman la cápside y algunas están involucradas en el proceso de infección.

El fago filamentoso infecta *E. coli* a través del pili de la bacteria. En esta etapa inicial del ciclo de vida, el dominio N2 de la proteína pIII se une al extremo del pili, un filamento que se extiende desde la superficie bacteriana y contiene proteínas y fosfolípidos. El pili se retrae hacia la envoltura celular, llevando las proteínas pIII y pVI del fago al periplasma, lo que conduce a la apertura de la estructura del virión y la inyección en el citoplasma celular del ADN circular monocatenario denominado forma infectiva.

El material genético que se encuentra dentro de la célula da origen a la replicación del fago mediante el reclutamiento de la ARN polimerasa del huésped, dando como resultado la síntesis de un cebador de ARN que sirve para que la ADN polimerasa III genere la cadena negativa del genoma y la forma replicativa de doble cadena del fago. Una vez que el ADN de fago este cubierto por la proteína principal de la cápside pVIII se unen las proteínas menores pIII y pVI. La proteína

pIII además de cumplir con un papel clave en la infección, también desempeña una función en la liberación de los fagos maduros, donde el dominio C-terminal de pIII está implicado en la unión y en la liberación de los fagos ensamblados (Hay & Lithgow, 2019).

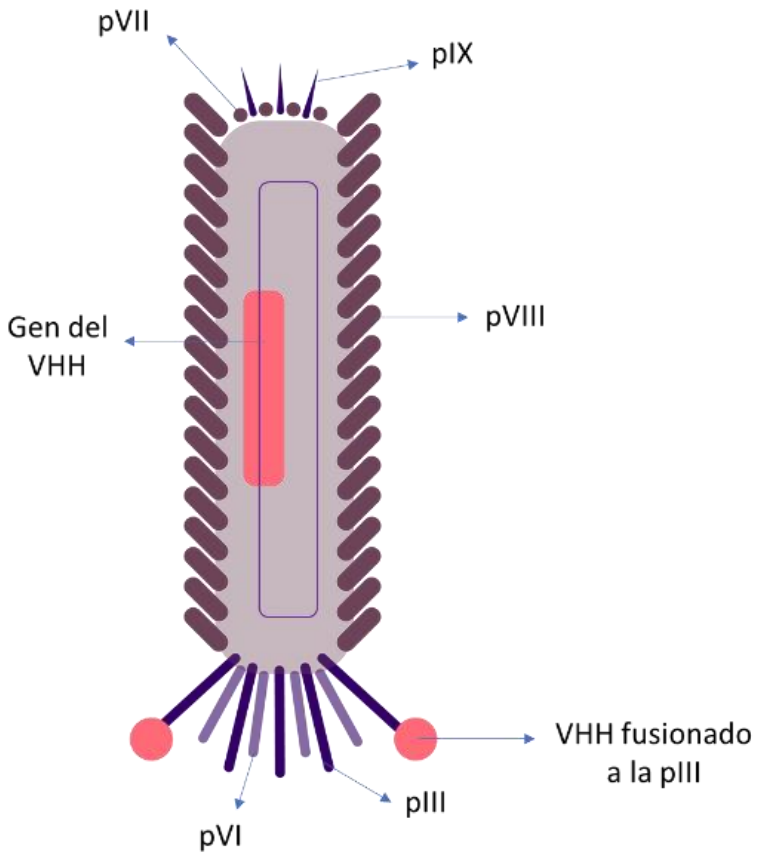

Figura 2. Representación de la estructura del bacteriófago filamentoso M13. Se observa el ADN monocatenario recombinante con el gen que codifica el VHH rodeado por una cápside compuesta principalmente por pVIII y en los extremos las proteínas menores pIII, pVI, pVII y pIX.

c. Phage Display

El método de presentación en fagos se basa en insertar fragmentos de ADN en el gen III del fago filamentoso M13, con el fin de crear una proteína de fusión que no afecta la infectividad y presenta los aminoácidos foráneos en una forma accesible. Los primeros sistemas de presentación en fagos se basaron en fusiones a la proteína pIII o pVIII. Actualmente, el sistema comúnmente utilizado es la presentación de las moléculas deseadas a través del acoplamiento a la proteína pIII del fago filamentoso M13 (Sidhu, 2001). La proteína pIII consta de tres dominios funcionales D1, D2 y D3. El dominio D1 es responsable de la entrada del ADN viral al citoplasma de la célula huésped durante el proceso de infección. El dominio D2 se une al Pili de la bacteria en la etapa inicial del ciclo de vida del virus. El dominio D3 es fundamental para el ensamblaje de la cápside viral (Georgieva & Konthur, 2011). El extremo C-terminal de la proteína pIII debe permanecer sin modificaciones para permitir el ensamble apropiado del fago, de esta manera, sólo es posible la unión de las proteínas foráneas en el extremo N-terminal (Georgieva & Konthur, 2011).

La proteína de fusión puede ser codificada por el genoma propio del fago o por un genoma adicional llamado vector fagémido. Los fagémidos posee un origen de replicación bacteriano y un origen de replicación de fago, una señal de empaquetamiento de fago y el gen de la proteína de cubierta para la fusión. Además, poseen un gen de resistencia antibiótica que permite su selección. Por ejemplo, el fago auxiliador M13KO7 es comúnmente usado y posee un gen de resistencia a la kanamicina. Los vectores fagémidos son encapsulados dentro de

las partículas virales mientras son propagados en las células huésped infectadas con un fago auxiliador. El fago auxiliador provee las proteínas y enzimas necesarias para la replicación y ensamble del virus dentro de la célula y posee un origen de replicación de funcionalidad reducida, lo que favorece que se encapsule preferencialmente las partículas que contienen el genoma del fagémido y de esta manera pueda enriquecerse alrededor de 1000 veces sobre el genoma salvaje del fago (Georgieva & Konthur, 2011) (Bazan et al., 2012).

d. Enriquecimiento por Afinidad Para la Selección de Nanoanticuerpos (Biopanning)

La gran diversidad de anticuerpos que muestran las bibliotecas generadas, hace necesario desarrollar técnicas que permitan la selección de anticuerpos con unas características determinadas que le confieran especificidad por un antígeno determinado. Estos sistemas se basan en la presentación del nanoanticuerpo en la superficie del fago que contienen los genes del nanoanticuerpo correspondiente, de esta forma se establece una relación entre la información genética (genotipo) y la función biológica (fenotipo). En los últimos años, se han desarrollado otros sistemas de expresión en superficie empleando diferentes plataformas de tales como levaduras (McMahon et al., 2018), bacterias (Salema & Fernández, 2017) y células de mamíferos (Lyu et al., 2022).

El procedimiento incluye tres pasos principales para la selección: primero se debe exponer la biblioteca con el antígeno de interés y capturar los fagos específicos; el segundo paso consiste en realizar lavados que permitan eliminar los fagos no

unidos o de baja afinidad y por último, para recuperar los fagos unidos al antígeno, se realizan eluciones de tipo químico, físico o de competencia y se amplifican estos fagos recuperado (Figura 3.). Este proceso generalmente se repite de tres a seis veces como un proceso en el que la diversidad de fagos se reduce mientras se enriquece en clones específicos al antígeno (Alfaleh et al., 2017).

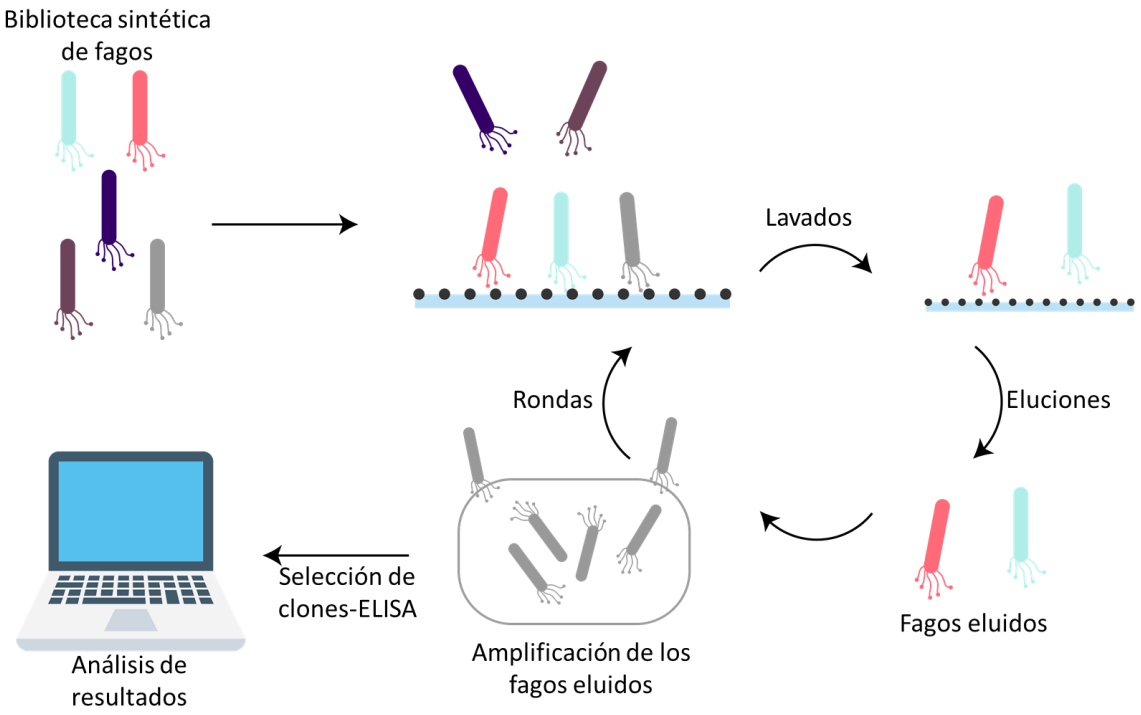

Figura 3. Esquema del proceso de biopanning. Enriquecimiento por afinidad para el aislamiento de nanoanticuerpos de una biblioteca sintética de fagos en función de su afinidad de unión a los antígenos.

4. Bibliotecas de Nanoanticuerpos

La identificación de nanoanticuerpos con especificidad hacia el antígeno depende en gran medida de la biblioteca. Existen tres tipos de bibliotecas que se utilizan para la selección de nanoanticuerpos: bibliotecas inmunes, no inmunes o naïve y sintéticas.

Las bibliotecas inmunes de nanoanticuerpos se obtienen a partir de animales pertenecientes a la familia *Camelidae* como llamas, alpacas y camellos, previamente inmunizados con una o varias moléculas para activar el sistema inmune. Una vez se completa la inmunización, el ARN mensajero (ARNm) se extrae de los linfocitos, se transforma en ADN complementario (ADNc) para amplificar la región variable de los anticuerpos de cadena pesada mediante PCR. Los extremos de los amplicones se digieren con enzimas de restricción, se ligan al vector fagémido y se transforman en *E. coli*. A pesar de sus ventajas en cuanto a la alta afinidad de unión, las bibliotecas inmunes también presentan inconvenientes como el manejo de animales, efecto adverso del antígeno, el tiempo y costo requerido para la inmunización. Otra desventaja incluye la necesidad de usar múltiples bibliotecas para cada antígeno (Ortega-Portilla et al., 2021) (Valdés-Tresanco et al., 2022).

Las bibliotecas naïve, son bibliotecas no inmunes, donde se toman linfocitos de sangre periférica de un animal no inmunizado, destacando la diversidad inmunológica natural del animal sin necesidad de hacer inmunización. Sin embargo, debido a que se omite el paso de inmunización, no se da la maduración de afinidad *in vivo* y puede requerir pasos adicionales para mejorar la afinidad de

unión al antígeno. Además, se requiere un mayor volumen de sangre para producir una biblioteca de gran tamaño, teniendo en cuenta que los linfocitos B están representados en un menor porcentaje, de los cuales aproximadamente el 50% podrían estar expresando HCAb.

Por otro lado, las bibliotecas sintéticas se generan a partir de la aleatorización *in vitro* de codones que forman las regiones hipervariables involucrados en la unión al antígeno. Para la construcción de una biblioteca sintética es necesario definir una única secuencia para las regiones marco de todos los nanoanticuerpos, además del diseño de la aleatorización de los CDRs. La diversidad dependerá de aleatorizar las regiones hipervariables tanto como sea posible incluso la longitud de cada CDR (Muyldermans, 2021a).

Actualmente, las bibliotecas comúnmente usadas se basan en inmunizar especies de camélidos. Sin embargo, las bibliotecas sintéticas traen beneficios frente a las bibliotecas inmunes: No requiere la inmunización ni manipulación de animales, una sola biblioteca sirve para múltiples antígenos y se puede usar para la selección de nanoanticuerpos contra antígenos tóxicos o moléculas no inmunogénicas (Muyldermans, 2021b).

Existen diferentes estrategias para seleccionar la región marco adecuada para una biblioteca. Una de las propiedades para tener en cuenta es la solubilidad, que puede afectar la producción de los nanoanticuerpos, dando como resultado la precipitación de las proteínas y la afectación de su funcionabilidad. La temperatura de desnaturalización (Tm), es otro factor fundamental que influye en procesos de funcionalización a nanopartículas, producción industrial y almacenamiento. Asimismo, es importante la estabilidad en entornos reductores para la expresión

en el citoplasma bacteriano y células eucariotas. En algunos casos, como para los nanoanticuerpos con aplicaciones terapéuticas o para ayudas diagnósticas con imágenes en humanos, se requiere una baja inmunogenicidad. Con el fin de reducir la inmunogenicidad la región marco puede someterse a procedimientos de humanización sustituyendo algunos aminoácidos que se encuentran en las cadenas pesadas de los anticuerpos humanos. Sin embargo, esto podría afectar la estabilidad de la región marco (Valdés-Tresanco et al., 2022).

El diseño de los CDRs se centra en la variabilidad, principalmente del CDR 3 que interactúa con mayor frecuencia con el antígeno y también es en más variable en su longitud y composición de aminoácidos. Por ejemplo, la longitud de los CDR 1 y 2 varia entre 5 y 8 aminoácidos, mientras que la longitud del CDR 3 varia entre 6 y 18 aminoácidos. Por esto, la estrategia más común en el diseño y construcción de las regiones hipervariables es establecer una longitud fija para los CDR 1 y 2, en cambio para el CDR 3 se sugiere variar las longitudes (Valdés-Tresanco et al., 2022).

En resumen, para el diseño y construcción de una biblioteca sintética es importante centrarse en la estabilidad de la región marco, mientras que para el diseño de los CDRs se requiere más variabilidad.

El uso de estas bibliotecas sintéticas aumenta la diversidad de nanoanticuerpos y de esta manera aumenta la probabilidad de encontrar anticuerpos con diferentes propiedades, siendo útiles para la selección de VHH provenientes de una misma biblioteca sintética frente a diferentes de antígenos.

5. Antígenos Tumorales

Las células cancerosas se desarrollan y proliferan rápidamente, llevando al paciente a un rápido avance de la enfermedad que resulta con un desenlace fatal. Se han implementado terapias basadas en anticuerpos monoclonales para el tratamiento de tumores sólidos. Sin embargo, los tratamientos se ven limitados principalmente por el gran tamaño y poca capacidad de penetrar en el tejido canceroso. En los últimos años el desarrollo de nanoanticuerpos a logrado superar los incovenientes de las terapias basadas en anticuerpos monoclonales. Las terapias actuales basadas en VHH funcionan como antagonistas o bloqueantes de receptores o antígenos que contribuyen a la proliferación, metástasis o angiogénesis del tumor.

El factor de crecimiento epidérmico (EGF) se produce principalmente de forma paracrina y su concentración en suero humano es muy variable, pero tiende a ser mayor en paciente con cáncer. Es uno de los ligandos más importantes del receptor del factor de crecimiento epidérmico (EGFR). Este receptor es una glicoproteína que pertenece a la familia de receptores de tirosina cinasa (RTK). Presenta un dominio de unión a ligando extracelular y un dominio de tirosina quinasa intracelular. La unión del EGF al dominio extracelular de la molécula receptora promueve su activación mediante dimerización y autofosforilación del dominio citoplasmático. La activación del receptor desencadena una cascada de señales para la síntesis de ADN y la proliferación celular (Roovers et al., 2007b). Una cantidad elevada de EGF más la sobreexpresión de EGFR en células de cáncer crean las condiciones para el crecimiento de algunos tumores

dependientes de EGF (Crombet Ramos et al., 2021). Por lo tanto, el EGFR y el EGF son considerados potenciales diana para la terapia del cáncer.

Actualmente, se desarrolló una nueva vacuna terapéutica compuesta por el EGF recombinante humano llamada CIMAvax-EGF. Esta vacuna se basa en un conjugado químico del EGF a la proteína P64 de *Neisseria meningitides*. CIMAvax-EGF induce la producción de anticuerpos neutralizantes que reconocen, "atrapan" el EGF y reduce su concentración tanto en el suero como en el microambiente tumoral. El éxito de los ensayos clínicos dirigidos a pacientes con cáncer de pulmón realizados con la vacuna anti-EGF CimaVax ponen en evidencia el EGF como objetivo importante para el tratamiento de tumores (Garcia Verdecia et al., 2008). Los nanoanticuerpos contra el EGF constituyen una nueva área de investigación por su capacidad de unirse al antígeno de interés EGF bloqueando la interacción con su receptor (Guardiola et al., 2022). Este bloqueo provocaría una disminución en la concentración disponible que EGF circulante en sangre, como consecuencia se inhibiría la transducción de señales y la proliferación celular (Garcia Verdecia et al., 2008; Gonzalez et al., 2003).

Otro antígeno importante en el desarrollo de cáncer es el factor de necrosis tumoral alfa TNFα como una citocina proinflamatoria. El TNFα es una citocina de 17 kDa con 157 aminoácidos, producido principalmente por macrófagos activados, linfocitos T y células asesinas naturales (NK), también en menor cantidad por células tumorales. Actúa a través de dos receptores: el receptor 2 del TNF y el receptor 1 del TNF. La mayoría de los tejidos y células expresan constitutivamente el receptor 1 de TNF (TNFR1) que, una vez unido al TNFα, desencadena la

formación del complejo de señalización del TNFR1. Además de su capacidad para inducir la muerte celular, también puede producir señales de supervivencia (Masola et al., 2022)(van Horssen et al., 2006). La unión del TNFα a su receptor inicia una cascada de señalización con activación de proteasas que conducen a la apoptosis mediante la activación de endonucleasas como EndoG, lo que resulta en la fragmentación del ADN. En el caso contrario, El TNFα actúa como uno de los principales mediadores de la inflamación dentro del ambiente tumoral mediante la activación de factores de transcripción como el factor nuclear B (NF-κB) que inducen la transcripción de genes antiapoptóticos, proliferativos y la transcripción de CXCL10 la cual promueve la migración celular (Wang et al., 2021).

Teniendo en cuenta la participación del TNFα en la progresión de tumores sólidos, podría ser una diana importante para la generación de nanoanticuerpos que bloqueen su actividad.

III. RESULTADOS PREVIOS DE NUESTRO GRUPO DE INVESTIGACIÓN

La biblioteca sintética de nanoanticuerpos basada en la tecnología de phage display, usada en esta investigación, se diseñó y construyó en el marco del proyecto NanoBioCáncer (Angélica Contreras et al., 2021).

1. Diseño de una Nueva Biblioteca Sintética de Genes de Nanoanticuerpos

En el diseño de una biblioteca sintética de nanoanticuerpos es importante tener en cuenta dos componentes de su estructura, la región marco y las regiones hipervariables, también conocida como regiones determinantes de complementariedad CDR.

La biblioteca sintética utilizada en el presente proyecto se construyó sobre un marco VHH universal del nanoanticuerpo cAbBCII10. En el diseño de los CDR1 y CDR2 se mantuvo la misma longitud fija que en cAbBCII10 y sólo se aleatorizaron los residuos con cadenas expuestas a la superficie 8 a.a. en el CDR 1 y 4 en el CDR 2. No se permitió la presencia de cisteínas en ninguna posición.

Para esta biblioteca la longitud establecida en el CDR3 fue de 10 aminoácidos (a.a.) y se seleccionaron las posiciones para aleatorizar con el objetivo de mantener la estabilidad. Los codones VRN y WMY se introdujeron en varias posiciones para favorecer las propiedades como la polaridad en las posiciones expuestas al solvente.

En total se aleatorizaron 22 posiciones en las secuencias de a.a. La variabilidad teórica por este diseño es del orden de 10^{18}.

En la Figura 4. Se muestra el diseño de la biblioteca a nivel de nucleótidos y estructura, así como el repertorio de a.a. correspondiente a cada uno de los codones degenerados empleados en el diseño. Los nanoanticuerpos tienen cuatro regiones marco y tres regiones hipervariables, en la Figura 4.A. se observa la estructura de la región marco altamente conservada del nanoanticuerpo cAbBCII10 (PDB: 3DWT) que incluye 2 láminas β. Los CDR 1, CDR 2 y CDR 3 están representados con color azul, verde y rojo respectivamente.

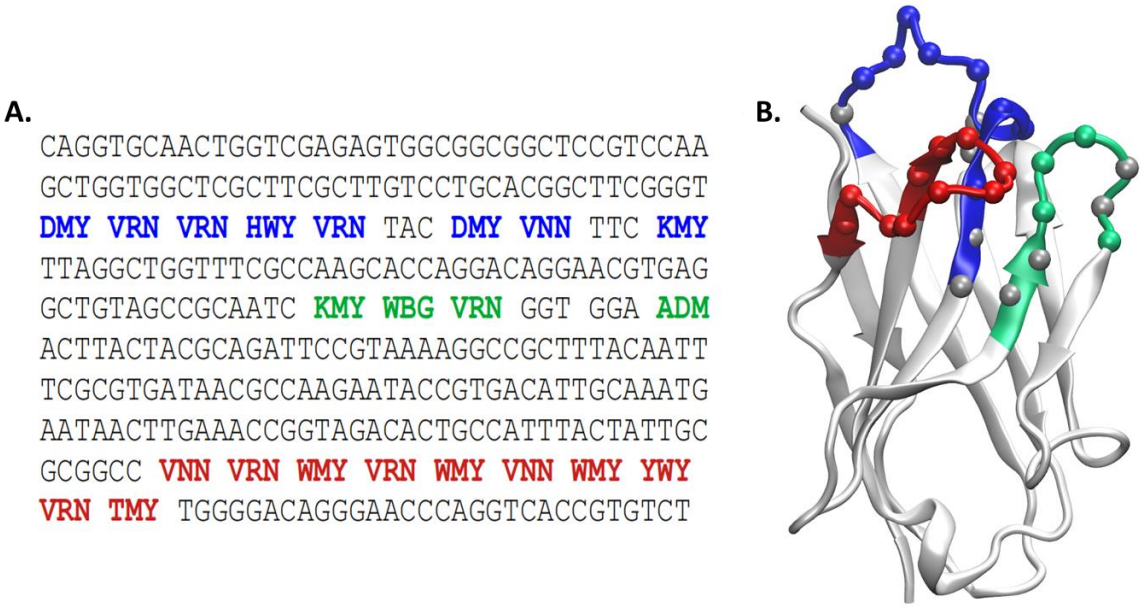

Figura 4. Diseño de la biblioteca sintética. (A.) Secuencia de nucleótidos con codones degenerados. Las secuencias CDR se resaltan en colores (azul, verde y rojo para CDRs 1, 2 y 3, respectivamente) y secuencia de nucleótidos de regiones marco en color gris; (B.) Modelo 3D de un nanoanticuerpo representativo de la biblioteca basado en la estructura cristalográfica de cAbBCII10 (PDB: 3DWT). Los CDRs están coloreados siguiendo el mismo esquema que en el panel (A.). Las esferas coloreadas en los carbonos alfa de las CDRs representan las posiciones

aleatorizadas, mientras que las esferas grises representan las posiciones de los CDRs que se mantuvieron fijas.

En la literatura internacional se encuentran una gran cantidad de reportes sobre bibliotecas inmunes. Sin embargo, en los últimos años se han reportado un número creciente de bibliotecas sintéticas, destacando los beneficios que traen estas bibliotecas al no requerir la inmunización ni manipulación de animales y el uso de una sola biblioteca para múltiples antígenos (Muyldermans, 2021b). En la revisión realizada por Liu B. y Yang D. se realiza una descripción general del diseño de la región marco, aleatorización de CDRs y antígenos de 8 bibliotecas sintéticas (B. Liu & Yang, 2022). En la biblioteca reportada por Yan J. *et* al. se utilizó la estructura del cAbBCII10 y sólo se aleatorizó el CDR 3, con este diseño y mediante la metodología de phage display se seleccionaron anticuerpos frente a dos antígenos diferentes (Yan et al., 2014).

2. Obtención de Biblioteca Sintética de Fagos Recombinantes

Los genes de la biblioteca se sintetizaron por la empresa GenScript (NJ, USA) y se clonaron en el vector fagémido pMAC. Este vector incluye una secuencia líder peIB que contiene un sitio de restricción NcoI en el extremo 3´, seguido de otros tres sitios de restricción únicos EcoRI, BamHI y NotI, luego un conector corto de serinas y glicinas (SGGGG), una etiqueta 6xHis, un codón de terminación ambar y finalmente la proteína pIII del fago M13KO7.

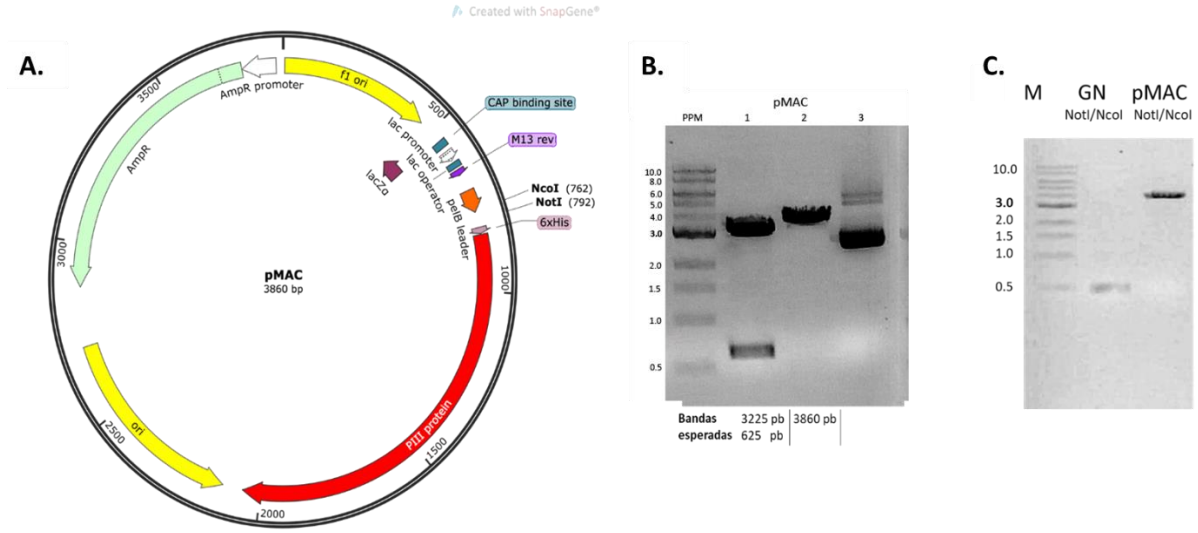

Figura 5. Chequeo con enzimas de restricción del plásmido pMAC y biblioteca de nanoanticuerpos. (A) Mapa del vector fagémido pMAC. (B) Chequeo de restricción del vector pMAC en gel de agarosa 0.8%. PPM: 1 kb DNA ladder (NEB), 1: pMAC digerido con NgoM IV (3225 pb y 625 pb), 2: pMAC digerido con Pvu II (3860 pb), 3: pMAC nativo (sin digerir). (C.) Gel de agarosa al 0,8 % que muestra el chequeo de restricción con las enzimas Not I/Nco I. PPM: Patrón de peso molecular 1 kb DNA ladder (NEB), 1: Digestión de las diferentes secuencias génicas que codifican los nano-anticuerpos, 2: Digestión del plásmido pMAC

El ensamblaje de la biblioteca génica y el vector pMAC (digeridos ambos con las enzimas de restricción Not I y Nco I Figura 5.) se llevó a cabo en 17 reacciones de ligazón mediante electroporación para aumentar la eficiencia de transformación en *E. coli* SS320. La transformación de la cepa SS320 con los genes de la biblioteca se corroboró mediante la siembra en medio sólido con el marcador de resistencia específico donde se observó el crecimiento de colonias aisladas. Bajo el precepto de que cada colonia bacteriana debería tener un fagémido con una secuencia de nanoanticuerpo distinta, se obtuvo una diversidad de la biblioteca de 1.5 x 10^8. Para evaluar la calidad de la biblioteca y su diversidad en comparación con el

diseño teórico se secuenciaron 100 clones elegidos al azar. Los resultados mostraron 76 clones con una secuencia de nanoanticuerpo correcta y se confirmó la diversidad obtenida al observar la variabilidad de aminoácidos en los CDRs, asi como los aminoácidos altamente conservados en las regiones marco (Figura 6.). Los resultados también mostraron 15 clones con desplazamiento del marco de lectura, 5 clones con secuencias de VHH sin CDR3, 3 clones con secuencias desconocidas arbitrarias y un clon con un vector fagémido vacío. A partir de estos resultados se obtuvo un estimado de 76% de clones correctos en la biblioteca, lo que mantiene su tamaño real en el mismo orden de magnitud determinado previamente (10^8).

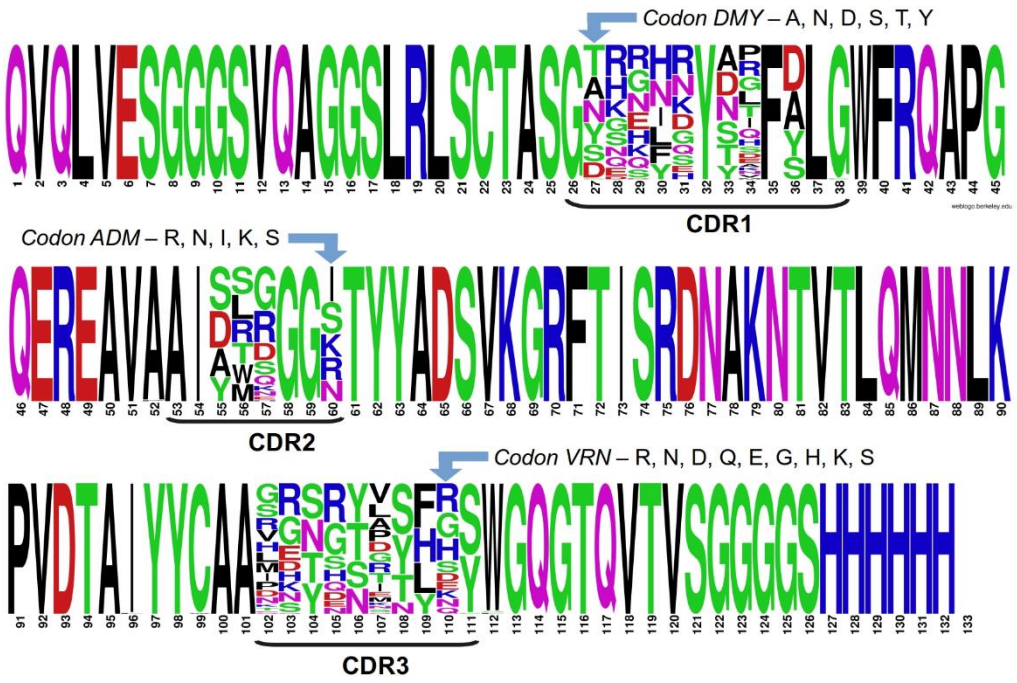

Figura 6. Evaluación de la diversidad de la biblioteca. Distribución de aminoácidos por posición de secuencia para el conjunto de 76 clones de nano-anticuerpos correctos, mostrados como logo de secuencias. Las posiciones marco y CDR fijas muestran su aminoácido conservado como una única letra grande. La variabilidad de aminoácidos encontrada en cada posición aleatoria se

representa como un apilado de letras, cada una de ellas con un tamaño proporcional a su frecuencia en el alineamiento múltiple. La estrecha correspondencia entre el diseño teórico y la diversidad experimental real se ilustra para tres posiciones de CDR (una para cada CDR).

IV. HIPOTESIS

La aplicación de dos estrategias de selección diferentes mediante la tecnología de presentación de nanoanticuerpos sobre la superficie de fagos filamentosos, permite la obtención de nanoanticuerpos específicos contra antígenos tumorales de una biblioteca sintética con una diversidad de 100 millones.

V. OBJETIVOS

1. OBJETIVO GENERAL:

Seleccionar nanoanticuerpos específicos contra dos antígenos tumorales a partir de la biblioteca sintética de nanoanticuerpos expresada sobre bacteriófagos.

2. OBJETIVOS ESPECÍFICOS

2.1. Seleccionar nanoanticuerpos contra el antígeno tumoral TNFα mediante una única ronda de selección con condiciones astringentes de lavado y elución.

2.2. Seleccionar nanoanticuerpos contra el antígeno tumoral EGF mediante tres rondas de enriquecimiento y eluciones consecutivas con diferentes métodos químicos y físicos.

VI. METODOLOGÍA

1. Generación de Biblioteca Sintética de Fagos Recombinantes

a. Producción del Fago Auxiliador M13KO7

Para la replicación del fago se infectaron células de *E. coli* TG1 ($D.O_{600}$ 0.4-0.6) con diluciones de M13KO7 de 10^{-6} hasta 10^{-12} y se incubaron durante 30 minutos a 37°C sin agitación. Posteriormente, se adicionó 100 µL y 10 µL de cada infección a placas con agar 2xYT (triptona 16 g/L, extracto de levadura 10 g/L, NaCl 5 g/L) suplementado con 50 µg/mL de kanamicina y se incubaron durante 20-24 horas a 37°C.

Pasado el tiempo de incubación, se tomó una colonia aislada para crecerla en caldo 2xYT suplementado con 50 µg/mL de kanamicina y se incubó 16-20 horas a 37°C y 250 rpm. Este cultivo se transfirió a un erlenmeyer de 1 L con 250 mL de 2xYT suplementado con 50 µg/mL de kanamicina y se incubó 16-20 horas bajo las mismas condiciones de temperatura y agitación.

b. Precipitación de Fagos

Se centrifugó el cultivo anterior a 10.000 rpm durante 10 minutos a 4°C. El sobrenadante obtenido se transfirió a un erlenmeyer con 0.2 volúmenes de PEG/NaCl (20% de polietilenglicol 8000 en NaCl 2.5 M) y se incubó durante 2 horas en hielo. Luego de precipitar los fagos se centrifugó 20 minutos a 15.650 x g, se descartó el sobrenadante, y el pellet de fagos se resuspendió en 15 mL de

tampón fosfato salino PBS (NaCl 137 mM, KCl 2.7 mM, Na_2HPO_4 10mM, KH_2PO_4 1.8 mM). Se realizó una segunda precipitación siguiendo el mismo protocolo. El pellet se resuspendió en 1-5 mL de PBS y se conservó a -80°C para su posterior uso y titulación.

c. Titulación de Fagos

Para titular la amplificación de los fagos se realizaron diluciones de 10^{-1} a 10^{-12}, se tomaron 100 µl de las ultimas diluciones de 10^{-6} hasta 10^{-12} y se les agregó a cada una 100 µL de *E. coli* 15597 ($D.O_{600}$ 0.4-0.6). Se incubaron durante 30 minutos a 37°C sin agitación. Posteriormente, se adicionó de cada infección 100 µL en placas con agar 2xYT suplementado con 50 µg/mL de kanamicina y se incubó durante 20-24 horas a 37°C. El título de partículas infectivas de fago se calculó a partir del número de colonias aisladas utilizando la siguiente fórmula:

Titulo (UFC/mL)= n° de colonias x 20/dilución

d. Amplificación de la Biblioteca Sintética de Fagos Recombinantes

Se inocularon en 500 µL de células procedentes de la biblioteca en 5 mL de caldo 2xYT suplementado con 100 µg/mL de ampicilina y se incubaron a 37°C y 250 rpm hasta alcanzar una $D.O_{600}$ de 0.4 a 0.6. Una vez alcanzada la densidad óptica deseada, las células se infectaron con el fago M13K07 MOI 20 y se incubaron 30 minutos a 37ºC sin agitación y 30 minutos a 50 rpm. Luego de centrifugar a 15.650

x g 10 minutos, el sobrenadante se descartó y el precipitado se resuspendió en 500 mL de caldo 2xYT suplementado con 100 µg/mL de ampicilina, kanamicina 50 µg/mL y 1 mM de IPTG para su crecimiento a 28ºC y 250 rpm durante 16-20 horas. Al día siguiente, el cultivo se centrifugó a 15.650 x g 10 minutos a 4ºC y se recuperó el sobrenadante. Se añadieron 100 mL de PEG/NaCl (20% Polietilenglicol 8000 en NaCl 2.5 M) al sobrenadante recuperado y se continuó el protocolo descrito anteriormente de precipitación y titulación de fagos.

e. Producción de la Biblioteca en E. coli *TG1*

Para la producción de la biblioteca en la cepa supresora de *E. coli* TG1, se adicionó 2.5 mL de un pre-cultivo crecido durante 16-20 horas a 37°C de TG1 a 300 mL de caldo 2xYT suplementado con 100 µg/mL de ampicilina. Este cultivo se incubó a 37°C y 250 rpm hasta alcanzar una $D.O_{600}$ de 1.0 a 1.5. Teniendo en cuenta que 1.0 $D.O_{600}$ del cultivo equivale a 8×10^8 UFC/mL, se realizó la infección adicionando los fagos de la biblioteca con multiplicidad de infección (MOI del inglés: *Multiplicity of infection*) de 58 y se incubó 30 minutos a 37ºC sin agitación y 30 minutos a 50 rpm. Posteriormente, se centrifugó el cultivo a 2000 x g durante 15 minutos a 4°C, se descartó el sobrenadante y el precipitado se resuspendió en 300 mL de caldo 2xYT suplementado con 100 µg/mL de ampicilina, el cual se incubó durante 16-20 horas a 28°C y 100 rpm. Al día siguiente, se agregaron 200 mL del cultivo crecido durante 16-20 horas a 600 mL de caldo 2xYT suplementado con 100 µg/mL de ampicilina y se incubó a 37°C y 250 rpm. Una vez alcanzó una $D.O_{600}$ de 2.0 se infectó con el fago auxiliador M13KO7 a un MOI de 20 y se

incubó 30 minutos a 37ºC sin agitación y 60 minutos a 50 rpm. Pasado el tiempo de infección se centrifugó a 2000 xg durante 15 minutos y el precipitado se resuspendió en 500 mL de caldo 2xYT suplementado con 100 µg/mL de ampicilina, kanamicina 50 µg/mL y 1 mM de IPTG. Finalmente, se incubó a 28°C y 250 rpm durante 16-20 horas.

Para concentrar y titular los fagos de la biblioteca se continuó el protocolo descrito anteriormente de precipitación y titulación de fagos.

2. Selección de Nanoanticuerpos Específicos Mediante Phage Display

*a. Selección de Nanoanticuerpos Específicos del Antígeno EGF Mediante Enriquecimiento por Afinidad (*Biopanning*)*

Se recubrieron 8 pocillos de ELISA con el antígeno EGF preparado en tampón carbonato pH 9.6 a 10 µg/mL durante 16-20 horas a 4°C (100 ul por porcillo), y se bloquearon con leche al 3% en PBS una hora a temperatura ambiente: Luego, se incubó 2 horas a temperatura ambiente con 100 µl de la biblioteca a 10^{10} partículas de fagos por pocillo diluidos en la misma solución de bloqueo preincubados durante 1 hora en agitación a temperatura ambiente. Al culminar el tiempo de incubación se descartaron los fagos no unidos de la biblioteca y se realizaron 20 lavados con 300 µl de PBS-Tween 20 al 0.1% y dos lavados adicionales con 300 µl de PBS.

Para eluir los fagos unidos al antígeno, se diseñó una serie de eluciones utilizando 4 tratamientos secuenciales: dos químicos bajo condiciones básicas y ácidas, uno

físico mediante ultrasonido y por último una elución agregando células TG1 directamente en los pocillos. La primera elución consistió en tratar a los pocillos con 100 uL de una solución de trietilamina 0,1 M pH 12.0 durante 10 min. Tras la incubación se colectaron los fagos eluidos y se neutralizó tanto la colecta como el pocillo con solución de tris-HCl 1M pH 7.5, seguido de dos lavados con PBS-Tween 0.1% y uno con PBS . La segunda elución se realizó con una solución de glicina 0,2 M pH 2.0 durante 10 min, se siguieron los mismos pasos descritos en la elución anterior y la neutralización se realizó con una solución de tris-HCl 1M pH 9.1 seguido de dos lavados con PBS-Tween 0.1% y uno con PBS. La tercera elución consistió en añadir 200 µL de PBS a los pocillos y someterlos a ultrasonido con una potencia 40 KHz, durante 30 minutos. Se colectaron los fagos eluidos mediante este tratamiento, seguido de dos lavados con PBS-Tween 0.1% y uno con PBS.

A continuación, la última elución consistió en adicionar células de *E. coli* TG1 en fase exponencial $D.O_{600}$ de 0.4 a 0.6 a los pocillos sometidos a los tres tratamientos anteriores. Los fagos colectados en las eluciones (glicina, trietilamina y ultrasonido) se sometieron al mismo tratamiento con *E. coli* TG1 $D.O_{600}$ de 0.4 a 0.6. Tras 30 minutos de incubación a 37°C, las células de *E. coli* infectadas se sembraron en placas de agar 2xYT suplementado con 100 µg/mL de ampicilina y se incubaron a 37 °C durante 16-20 horas. Culminado el tiempo de incubación se colectaron las células a partir de las placas, se re-suspendieron con ayuda de un asa de siembra en 10mL de caldo 2xYT suplementado con 100 µg/mL de ampicilina para dar continuación a las siguientes rondas de selección. Se tomaron 3-5 mL para conservar con glicerol al 20% y se almacenaron a -80°C.

b. Amplificación de las Rondas de Selección de Nanoanticuerpos Anti-EGF

Se agregaron 3-5 mL de las células procedentes de la colecta de cada ronda durante la selección de nanoanticuerpos específicos para el antígeno EGF a 50 mL de caldo 2xYT suplementado con 100 µg/mL de ampicilina y se incubaron a 37°C y 250 rpm durante 16-20 horas. Al día siguiente se refrescó el cultivo agregando la totalidad del cultivo (50 mL) en 500 mL de caldo 2xYT suplementado con 100 µg/mL de ampicilina y se incubó a 37°C y 250 rpm hasta alcanzar una $D.O_{600}$ de 2.0. Seguidamente, se realizó la infección con fago auxiliador (M13KO7) teniendo en cuenta una MOI de 20 y se incubó 30 minutos a 37°C sin agitación y 30 minutos a 50 rpm. Las células infectadas se centrifugaron a 2000 x g durante 15 minutos. El precipitado celular se resuspendió en 500 mL de caldo 2xYT suplementado con ampicilina al 100 µg/mL, kanamicina 50 µg/mL e IPTG 1 mM, y se crecieron a 28°C y 250 rpm, durante 16-20 horas. La precipitación y la titulación de los fagos recombinantes obtenidos se llevó a cabo siguiendo los procedimientos 1-b. y 1-c. en metodología.

A partir del material obtenido en la amplificación de la tercera ronda se realizó un ELISA de fagos.

c. Selección de Nanoanticuerpos Específicos del Antígeno TNFα

Se recubrieron 24 pocillos de ELISA con el antígeno TNFα diluido en tampón carbonato (50 mM carbonato/bicarbonato de sodio pH 9.6) a 10 µg/mL

durante 16-20 horas a 4°C (100 ul por porcillo), y se bloquearon con 300 µL de leche al 5% preparada en PBS durante 16-20 horas a 4°C. Luego, se incubó 2 horas a temperatura ambiente y 350 rpm con 100 µl de la biblioteca diluida en leche al 5% (10 µL de la biblioteca de fagos en 2.5 mL de leche al 5%). Al culminar el tiempo de incubación se descartaron los fagos no unidos de la biblioteca y se realizaron 20 lavados con 300 µl de PBS-Tween 20, cada uno durante 5 minutos, seguido de 4 lavados adicionales con glicina pH2.2 durante 5 minutos cada uno. Los pocillos se neutralizaron entre lavados con PBS durante 5 minutos. La recuperación de los fagos que siguen unidos al antígeno consistió en adicionar el mismo antígeno TNFα a una concentración por pocillo de 10 µg y se incubó una hora a temperatura ambiente y 300 rpm.

La elución colectada se usó para infectar células de *E. coli* TG1 $D.O_{600}$ de 0.4 a 0.6. y se incubaron 30 minutos a 37°C, las células TG1 infectadas se sembraron en placas de agar 2xYT suplementado con 100 µg/mL de ampicilina y se incubaron a 37 °C durante 16-20 horas.

3. Detección de Clones Positivos Mediante ELISA Grupal de Fagos

a. Recuperación de Fagos Recombinantes

Cada colonia individual se inoculó en un pocillo de placas de cultivo de 96 pocillos fondo en U que contenía 150 uL de caldo 2xYT suplementado con ampicilina al 100 µg/mL y se incubó a 37°C y 250 rpm, durante 16-20 horas. Al día siguiente se tomaron 25 uL de cada clon y se inocularon en grupos de 4 clones en

un mismo tuvo de 2 mL que contenía 400 uL de caldo 2xYT suplementado con ampicilina a 100 µg/mL. El volumen restante del cultivo se usó para conservar con glicerol al 20% a -80°C

b. Amplificación de Fagos Recombinantes

Con el propósito de analizar un mayor número de clones se formaron grupos de 4 clones para llevar a cabo la amplificación, para esto, se tomaron 25 uL de cultivo de cada clon individual y se agregaron a 400 uL de suplementado con ampicilina al 100 µg/mL, se incubaron a 37°C y 250 rpm hasta alcanzar una $D.O_{600}$ de 2.0. Seguidamente se infectaron 1 hora con el fago auxiliador M13KO7 teniendo en cuenta una MOI de 20. Luego de la infección, se centrifugó a 10.020 xg durante 10 min a 4°C. El precipitado celular se resuspendió en 650 uL de caldo 2xYT suplementado con ampicilina al 100 µg/mL, kanamicina 50 µg/mL e IPTG 1 mM, y se crecieron a 28°C y 250 rpm, durante 16-20 horas para la producción de los fagos recombinantes. Al día siguiente se centrifugaron a 10.020 xg durante 5 minutos y se colecto el sobrenadante para evaluarlo mediante ELISA de fagos.

c. ELISA de los Grupos de Fagos Anti-EGF

Para la detección de clones positivos, el protocolo se llevó a cabo en placas de ELISA de 96 pocillos. Las placas de ELISA se recubrieron con el antígeno de interés preparado en tampón carbonato pH 9.6 a 10 µg/mL durante 16-20 horas a 4°C (100 µl por porcillo). La evaluación se clones en la última ronda de selección

incluyó 2 placas adicionales, una recubierta con solución de bloqueo (leche) y otra con un nanoanticuerpo (9G8) que posee las etiquetas 6xHis y SV5, las mismas que están presentes en el antígeno recombinante EGF. Esto con el fin de eliminar clones que pudieran reconocer proteínas contenidas en la leche o las etiquetas 6xHis y SV5 presentes en el antígeno recombinante de interés EGF.

Cada pocillo se bloqueó con 300 µl de leche al 3% durante 1 hora a temperatura ambiente. Se añadieron 200 µl de los sobrenadantes correspondientes a los grupos de fagos, diluidos en solución de bloqueo. Estos sobrenadantes de fagos, fueron previamente incubados durante 30 minutos con leche al 3%. Luego de 2 horas de incubación con el sobrenadante de fagos, se añadió 100 µl/pocillo de anticuerpo anti-PVIII diluido 1:10.000 en leche al 3% y se incubó 1 hora a temperatura ambiente. A continuación, se añadió 100 µl/pocillo de anticuerpo anti-mouse conjugado con peroxidasa diluido 1:5000 en solución de bloqueo. Finalmente, se reveló mediante la adición de 100 µl de TMB (3,3',5,5' tetrametilbenzidina) y la reacción enzimática se detuvo a los 20-30 minutos adicionando 50 µl de ácido sulfúrico 2.5 M. La absorbancia se determinó a 490 nm con el lector de placas de ELISA BOECO BMR-100.

Todas las etapas de incubación se realizaron a temperatura ambiente. Al finalizar cada etapa, se realizaron 3 lavados con PBS-Tween 20 al 0.1%.

4. Detección de Clones Positivos Mediante ELISA Individual de Fagos

a. ELISA con los Clones Individuales de Fagos

Se comenzó con la amplificación de clones individuales obtenidos en el apartado 3-b. de metodología teniendo en cuenta que se tomaron 25 µL del cultivo de cada clon individual y se agregaron a 475 µL de suplementado con ampicilina al 100 µg/mL, se incubaron a 37°C y 250 rpm hasta alcanzar una $D.O_{600}$ de 2.0. y se continua el protocolo descrito anteriormente.

Los sobrenadantes obtenidos de cada clon individual se someten a la detección de clones positivos mediante ELISA de fagos, protocolo descrito en el apartado 3-c. de metodología.

Se consideraron como clones positivos para EGF, aquello con valores de D.O.450 ≥ 0,8, y una $D.O._{450}$ para leche o para la proteína no relacionada tres o más veces por debajo de los valores en EGF.

b. Electroforesis de Proteínas SDS-PAGE y Western Blot

La electroforesis se realizó en condiciones desnaturalizantes con SDS (docecilsulfato sódico) en gel de poliacrilamida con gel de resolución al 15% y gel concentrador al 6%. Las muestras analizadas, fueron previamente tratadas con tampón de carga reductor 6X a 96°C durante 10 minutos. Las muestras se cargaron en el gel contenido en la cámara de electroforesis (Cleaver scientific, UK) con tampón de tris-glicina y se usó la fuente de poder EC 300 XL de Thermo Scientific. Se corrió hasta que el azul de bromofenol alcanzó el borde inferior del gel, aplicando una corriente de 120 V y 375 mAmps.

Finalizada la electroforesis, se procedió a realizar transferencia de las proteínas en el equipo trans-blot SD semi-dry transfer cell. Para esto, la membrana de

nitrocelulosa y el gel se sumergieron en tampón de transferencia (tris 48 mM, glicina 39 mM, SDS 0,037%, metanol 20%) y se dejó transfiriendo durante 30 minutos a15 V, 0.7 A y 300 W. La membrana se bloqueó con leche al 5% durante 1 hora, se lavó 3 veces con PBS-Tween y se añadió el anticuerpos anti-His-HRP (1:5000) diluido en leche durante 16-20 horas a 4°C. Se lavó nuevamente y se agregó el sustrato diaminobencidina DAB hasta observar las bandas correspondientes. Para detener la reacción, se lavó con agua tipo I.

5. Secuenciación de los Clones

Una vez se identificaron los clones, se realizó extracción del ADN plasmídico utilizando el Kit GenElute Plasmid Miniprep de Sigma-Aldrich y siguiendo el protocolo recomendado por el fabricante. Al final del protocolo de extracción el ADN se eluyó en 60 ul de agua grado biología molecular y se cuantificó en el equipo NanoDrop One. El ADN obtenido se conservó a -20°C hasta su envío.

La secuenciación se solicitó con la empresa Macrogen mediante el método de Sanger usando el primer M13R de secuencia 5'-CAGGAAACAGCTATGAC-3' que hibrida sobre la secuencia del gen lacZ del plásmido. Con los resultados obtenidos, se analizaron las secuencias de las regiones marco y CDRs de los nanoanticuerpos con CLC Genomics Workbench v.21 (QIAGEN Aarhus, Denmarck).

VII. RESULTADOS Y DISCUSIÓN

Aunque la terapia basada en anticuerpos monoclonales se ha usado ampliamente en el tratamiento de pacientes con tumores sólidos, su gran tamaño y poca penetración en los tumores limitan la eficacia. Los nanoanticuerpos, son un novedoso desarrollo que puede superar estos inconvenientes (Verhaar et al., 2021). Su pequeño tamaño de ~15 kDa, estabilidad, fabricación y alta penetración en los tejidos, lo convierten en una herramienta prometedora para el tratamiento y diagnóstico de diferentes tipos de cáncer (Jovčevska & Muyldermans, 2020). Las terapias actuales basadas en VHH identifican antígenos o receptores que contribuyen al desarrollo del tumor, como por ejemplo el EGF y el TNFα son moléculas que favorecen la proliferación celular y supervivencia.

La identificación de nanoanticuerpos con especificidad hacia el antígeno depende en gran medida de la biblioteca. Las bibliotecas sintéticas se les atribuyen múltiples ventajas entre las cuales se destaca su diversidad de nanoanticuerpos, permitiendo la selección de VHH contra diferentes antígenos.

1. Producción de la Biblioteca Sintética de Fagos Recombinantes

La cepa de *E. coli* SS320 se utilizó para la inserción de los genes de la biblioteca clonados en el vector pMAC. Estas células son no supresoras, lo que hace necesario la producción de la biblioteca en células supresoras del codón de terminación UAG denominado ámbar (ej. TG1), ubicado antes de la proteína pIII.

De esta manera, se continua la lectura del ADN para la síntesis de los nanoanticuerpos fusionados a la proteína pIII del fago recombinante.

Se generaron bibliotecas de fagos recombinantes en células de E. coli TG1 siguiendo el protocolo descrito en el aparte de metodología sección 1. Con el objetivo de conservar la diversidad de la biblioteca anterior se realizó una infección adicionando los fagos de la biblioteca con un MOI de 58, teniendo en cuenta su diversidad y su titulación inicial de 3.6 x 10^{10} ufc/µl la MOI utilizada representa 120.000 veces la diversidad de la biblioteca. De esta manera el titulo obtenido para la biblioteca producida en células TG1 fue de 8,2 x 10^{10} UFC/mL. Se puede inferir que la biblioteca obtenida a partir de *E. coli* TG1 conserva su diversidad y cada clon está representado alrededor de 240 veces.

1. Precipitación del bacteriófago auxiliador M13KO7

Con el fin de tener disponibilidad suficiente del bacteriófago auxiliador M13KO7 para los requerimientos en los procedimientos que conlleva la selección de nano-anticuerpos contra los antígenos de interés, se llevó a cabo el protocolo de amplificación y purificación con PEG 20% /2.5 M NaCl (ver apartados 1-a. y 1-b. de metodología). Se obtuvieron lotes de fago M13KO7 con títulos entre 9,2 x 10^{12} UFC/mL y 3,2 x 10^{14} UFC/mL, valores similares e incluso mayores a los obtenidos por Carroll-Portillo et al. quienes utilizando PEG 6000 obtuvieron un título de 1.03 x 10^{12} UFC/mL mientras que con PEG 8000 el titulo obtenido fue de 7.83 x 10^{11} UFC/mL de fago M13 (Carroll-Portillo et al., 2021).

2. Selección de Fagos Recombinante Usando la Biblioteca Sintética

Se realizó la selección de fagos recombinantes contra los antígenos tumorales TNFα. La metodología se basó en prolongar el tiempo de los lavados y combinarlos con 4 lavados astringentes con glicina pH 2.2 durante 5 minutos cada uno. La elución usada fue por competencia, adicionando una concentración mayor (10 µg/pocillo) del antígeno de interés. Se realizó una única ronda y se seleccionaron el total de colonias obtenidas 97 colonias para la detección de clones positivos mediante ELISA siguiendo el protocolo descrito en el apartado de Metodología sección 4.

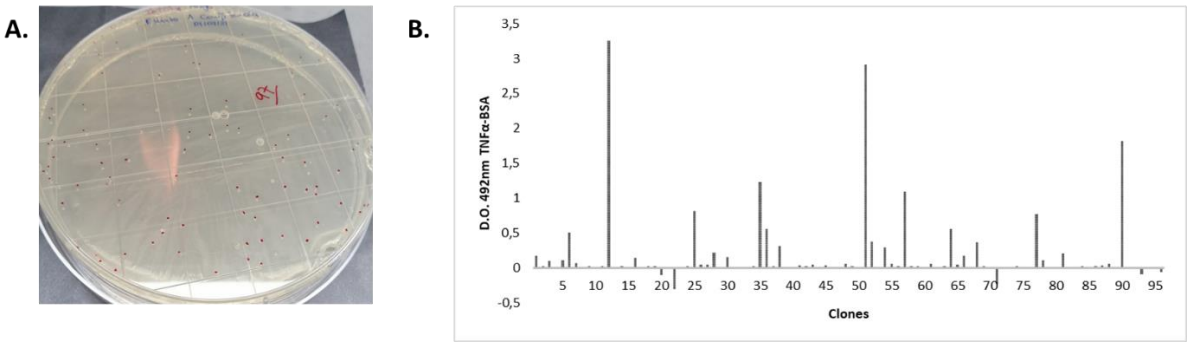

Figura 7. Selección de clones recombinantes contra el antígeno TNFα. A. colonias de fagos recombinantes obtenidos de la selección TNFα. Crecidas a 37°C durante 16-20 h en placas de agar 2xYT suplementadas con ampicilina a 100 µg/mL. B. Identificación de clones anti-TNFα mediante ELISA de fagos. Los valores de D.O. corresponden a la diferencia entre la señal obtenida del recubrimiento con antígeno EGF su respectiva señal de recubrimiento con Albumina de suero bovino BSA (solución de bloqueo) de cada clon.

De los 97 clones evaluados se seleccionaron 22 clones específicos de TNFα y fueron secuenciados 22. Además, con esta misma biblioteca de nanoanticuerpos sintética y utilizando el mismo método de selección se han obtenido clones de

fagos recombinantes contra otros antígenos: 24 de VEGF y 41 de GnGc, demostrando la funcionalidad de nuestra biblioteca de nanoanticuerpos

Las bibliotecas sintéticas son una plataforma multifuncional y permite la obtención de nanoanticuerpos contra diferentes antígenos con diversas aplicaciones (B. Liu & Yang, 2022). Recientemente la Administración de Alimentos y Medicamentos (FDA) aprobó el primer nanoanticuerpo para uso terapéutico: caplacizumab, para el tratamiento de la púrpura trombocitopénica trombótica adquirida y durante la pandemia del COVID-19, se han generado numerosos VHH contra el SARS-CoV-2 (Valdés-Tresanco et al., 2022). Los resultados obtenidos nos demuestran que la utilidad de esta biblioteca no se limita a la selección de nanoanticuerpos contra antígenos tumorales, su diversidad también puede ser usada para la selección de nanoanticuerpos contra proteínas de agentes infecciosos.

3. Selección de nanoanticuerpos contra el antígeno EGF.

Las condiciones de elución para la obtención de nanoanticuerpos varían ampliamente, siendo las soluciones ácidas las más utilizadas (Davydova, 2022). Los cambios en el pH desnaturalizan y rompen las interacciones no covalentes como las interacciones electrostáticas o de van der Waals entre el nanoanticuerpo y el antígeno de interés, lo que resulta en la liberación y recuperación de los fagos recombinantes (G. Yang et al., 2014). Para la obtención de nanoanticuerpos específicos contra el antígeno EGF se implementó una estrategia de selección diferente. Las variaciones consistieron en modificaciones en los lavados, las

eluciones y la cantidad de rondas, tal como se describe en la sección de Metodología 2-a.

Se realizaron un total de tres rondas, en cada una de las rondas se realizaron cuatro eluciones consecutivas aplicando 2 métodos químicos (glicina 0.2 M pH 2.2 y trietilamina 0.1 M pH 12), un método físico (ultrasonido) y por último una elución añadiendo *E. coli* TG1 directamente en los pocillos.

En cada ronda de selección se observa la obtención de colonias en cada una de las eluciones y se observó un incremento notable entre rondas como indicativo del enriquecimiento en clones que reconocen el EGF. En la Figura 8. se muestran se muestran las colonias en placas de agar 2xYT suplementado con 100 µg/mL de ampicilina obtenidas a partir de la primera ronda de selección. En la tercera ronda (Figura 10) es posible identificar un crecimiento abundante en los cuatro métodos de elución respecto al crecimiento que se presentó en la segunda ronda de selección (Figura 9).

Se ha reportado por varios autores que han implementado 3 o más rondas para identificar nanoanticuerpos específicos para un antígeno de interés un comportamiento similar. Por ejemplo, los resultados obtenidos por S. Naderi et al. (2020) quienes con su metodología de selección de nanoanticuerpos contra un inhibidor de la angiogénesis neutrofilia-1 (NPR-1) observaron un incremento de colonias en las rondas de selección (tercera y cuarta ronda) (Naderi et al., 2020).

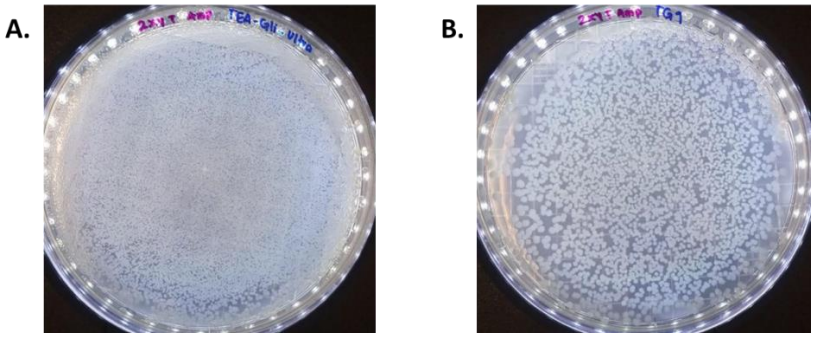

Figura 8. Clones de fagos recombinantes obtenidos en la primera ronda de selección EGF. Crecimiento a 37°C durante 16-20 h en placas de agar 2xYT suplementadas con ampicilina a 100 µg/mL. A: Células infectadas con la mezcla de fagos eluidos con Trietilamina, Glicina y Ultrasonido. B: Ultima elución con células de E. coli TG1 infectadas con lo fagos unidos a los pocillos sometidos a las tres eluciones.

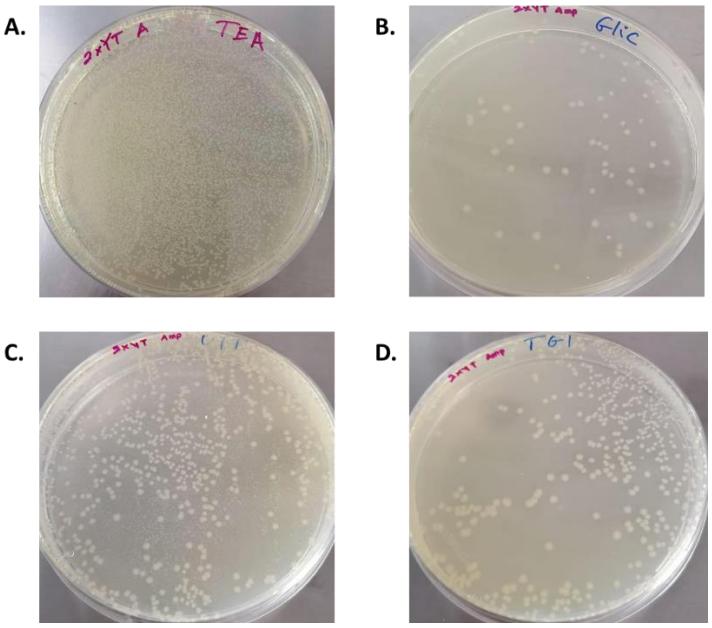

Figura 9. Clones de fagos recombinantes obtenidos en la segunda ronda de selección EGF. Crecimiento a 37°C durante 16-20 h en placas de agar 2xYT suplementadas con ampicilina a 100 µg/mL. A, B y C: Células infectadas con fagos eluidos de Trietilamina, Glicina y Ultrasonido respectivamente. D: Ultima elución con células de E. coli TG1 infectadas con lo fagos unidos a los pocillos sometidos a las tres eluciones.

En otras investigaciones que buscaban aislar nanoanticuerpos contra antígenos tumorales también en su estrategia de selección realizaron varias rondas consecutivas se selección en el biopanning. En el caso de la investigación R. Roshan *et* al. (2020), a partir de una biblioteca inmune realizaron 4 rondas de selección y elución con glicina pH2.2, observaron un incremento en el número de fagos unidos a partir de la tercera ronda, y lograron obtener nanoanticuerpos contra la molécula de adhesión de células epiteliales (EpCAM) (Roshan et al., 2021).

Al final de la tercera ronda de selección del antígeno EGF se eligieron al azar 95 colonias por cada elución (trietilamina, glicina, ultrasonido y TG1). Un total de 380 colonias se usaron para la detección de clones positivos mediante ELISA siguiendo el protocolo “detecciones clones positivos mediante ELISA” descrito en el apartado de Metodología sección 3.

Se realizaron dos métodos para estudio de clones positivos que permitieran la evaluación de un mayor número de clones: ELISA por grupos de fagos y ELISA individual de fagos. Los resultados obtenidos a partir del ELISA por grupos de fagos, permitió la identificación de 50 grupos, considerando el punto de cohorte D.O. mayor a 0,088 según la fórmula de BIOREBA AG y bajo fondo en leche (< a 0.3). Para algunos clones se obtienen valores negativos, lo que sugiere en estos clones un mayor reconocimiento por las proteínas presentes en la leche. Teniendo en cuenta nuestro criterio de selección más exigente ($D.O._{450nm} \geq 0.8$ para la unión con EGF y $D.O._{450nm}$ para la leche tres o mas veces menor que para el EGF), se identificaron 35 grupos, de los cuales se eligieron 24 grupos que equivalen a 96 clones y se dio continuidad con el análisis de clones de fagos recombinantes

mediante el ELISA individual de fagos (procedimiento descrito en la Metodología parte 4.). Los criterios de selección de clones positivos fueron los mismos y se descartaron los clones que mostraran reconocimiento por el nanoanticuerpo 9G8 que al tener las mismas etiquetas del antígeno EGF (6xHis y SV5) se usó para seleccionar clones que identificaran esta etiqueta.

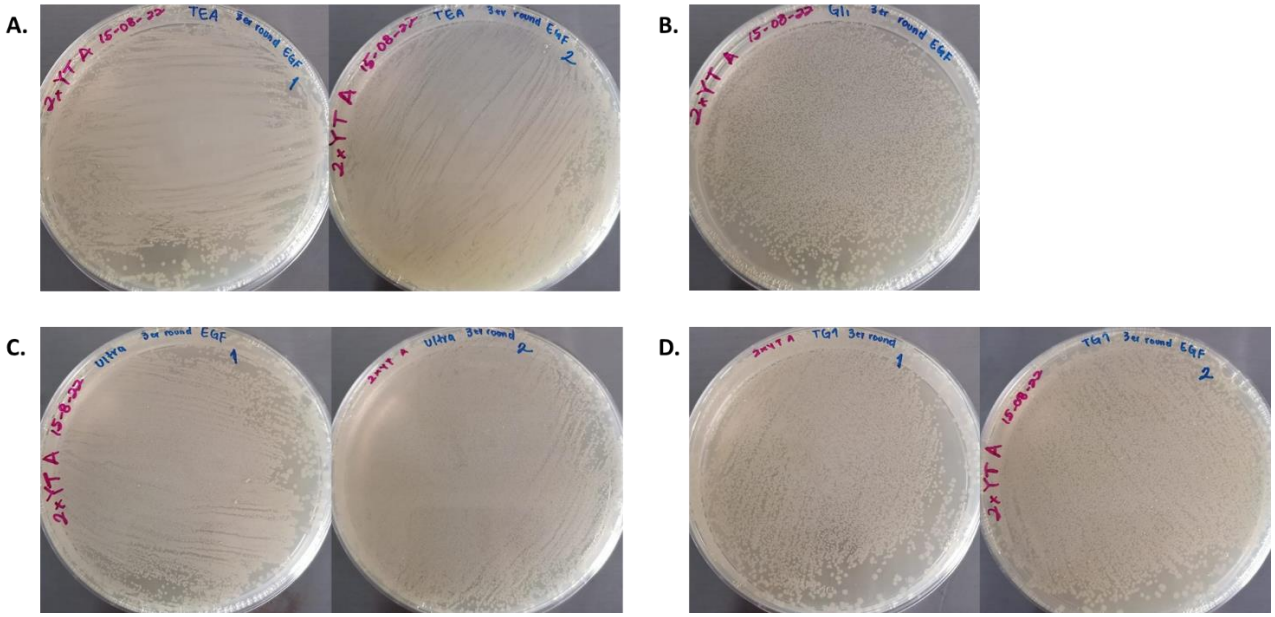

Figura 10. Clones de fagos recombinantes obtenidos en la tercera ronda de selección EGF. Crecimiento a 37°C durante 16-20 h en placas de agar 2xYT suplementadas con ampicilina a 100 µg/mL. A, B y C: Células infectadas con fagos eluidos de Trietilamina, Glicina y Ultrasonido respectivamente. D: Ultima elución con células de E. coli TG1 infectadas con lo fagos unidos a los pocillos sometidos a las tres eluciones.

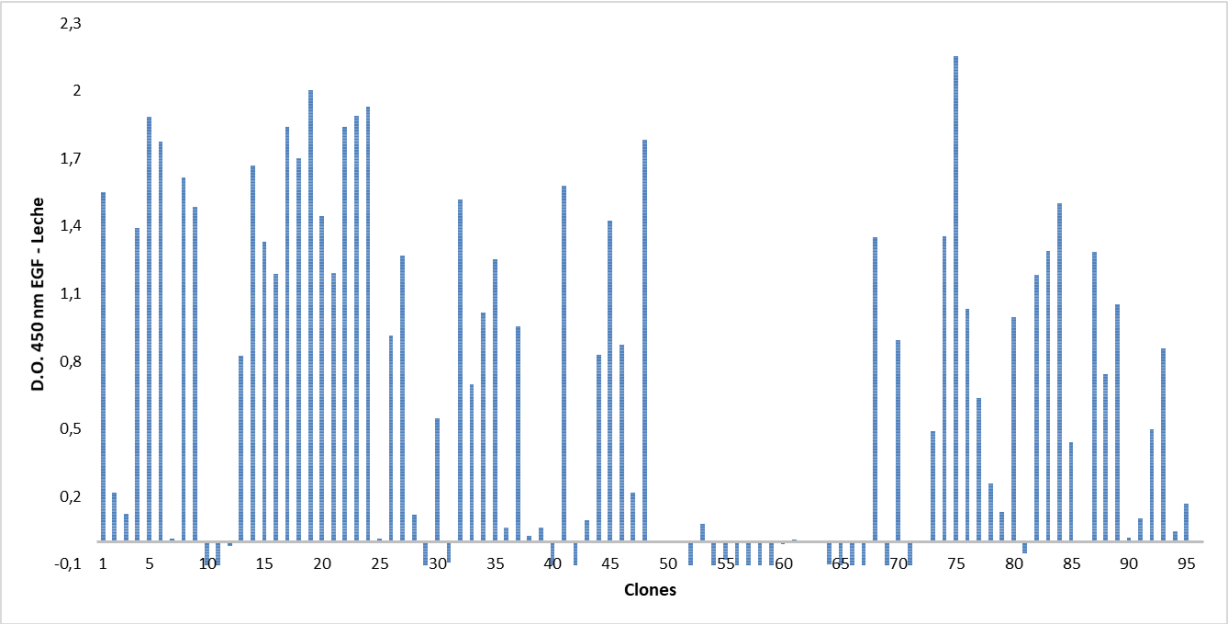

Figura 11. Identificación de grupos de clones anti-EGF mediante ELISA por grupo de fagos. Los valores de D.O. corresponden a la diferencia entre la señal obtenida del recubrimiento con antígeno EGF y su respectiva señal de recubrimiento con leche (solución de bloqueo) de cada clon.

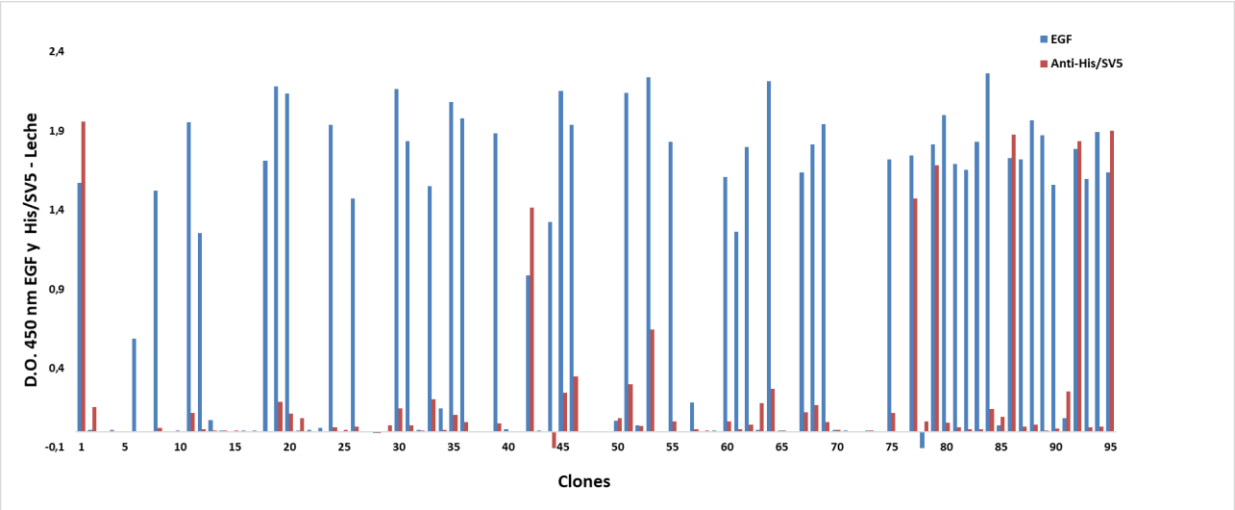

Figura 12. Identificación de clones anti-EGF mediante ELISA de fagos individual. Los valores de D.O. corresponden a la diferencia entre la señal obtenida del recubrimiento con antígeno EGF o VHH 9G8 y su respectiva señal de recubrimiento con leche (solución de bloqueo) de cada clon.

Se detectaron 38 clones que cumplieron con los 3 criterios de selección y se consideraron como clones de fagos recombinantes positivos, capaces de reconocer el antígeno EGF. También se identificaron 7 clones que presentaron reconocimiento similar por el antígeno EGF y por el nanoanticuerpo 9G8, por lo que se clasificaron como clones que reconocen las etiquetas presentes en ambas moléculas (anti-His/SV5). A continuación, en la Tabla 1. Se compilan los resultados obtenidos a partir del ELISA individual de fagos y se muestran los porcentajes por elución de clones positivos anti-EGF y clones anti-His/SV5.

En otra investigación al combinar diferentes estrategias de elución y varias rondas de enriquecimiento logran obtener anticuerpos prometedores contras haptenos libres con valores de KD en el rango de 10^{-8} M. Los anticuerpos que demostraron mejor afinidad fueron obtenidos cada uno de diferente elución, demostrando la efectividad del uso de diferentes estrategias de elución consecutivas (Tullila & Nevanen, 2017).

Los primeros nanoanticuerpos inhibidores de EGF fueron reportados por Guardiola S. et al. en 2018. Estos VHH fueron obtenidos a partir de una biblioteca inmune con una diversidad de 4.3×10^8 y su metodología de selección al igual que la descrita aquí consistió en la expresión de proteínas foráneas en la superficie de fagos filamentosos (phage display), realizando tres rondas de selección y a diferencia de nosotros, una única elución con trietilamina por ronda.

Tabla 1.

Resultados obtenidos tras la tercera ronda de biopanning en el ELISA individual de fagos con el antígeno EGF.

ELUCIÓN	CLONES EVALUADOS	CLONES ANTI-EGF	CLONES ANTI-His/SV5
Trietilamina	56	17	2
Glicina	20	9	0
Ultrasonido	4	1	0
E. coli TG1	16	11	5

Finalmente, seleccionaron al azar 47 colonias de la segunda y tercera ronda para su evaluación por ELISA. Entre las secuencias de clones positivos diferenciaron 6 nanoanticuerpos para continuar con estudios de afinidad (Guardiola et al., 2018). Estudios dirigidos a obtener nanoanticuerpos que inhiban la acción del EGF y por tanto la fosforilación y activación de su receptor (EGFR) son una alternativa frente a las terapias de cáncer dirigidas a EGFR, ya que se han encontrado la aparición de mutaciones que confieren resistencia a los medicamentos actualmente usados.

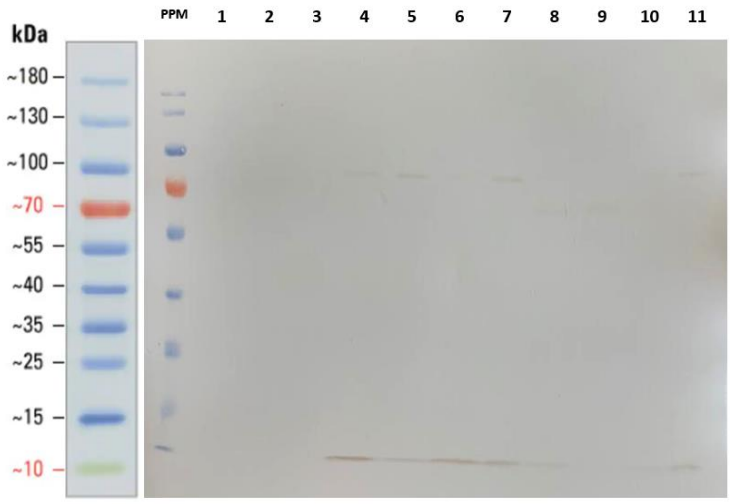

Figura 13. Análisis de expresión del nanoanticuerpo fusionado a la proteína 3 del fago M13. Se realizó SDS-PAGE en condiciones reductoras, seguido de la inmunotrasferencia Western Blot utilizando un anticuerpo anti-His-HRP (1:5000) diluido en leche 3%. Sobrenadantes de clones anti-EGF. Carril 1: sobrenadante de *E. coli* TG1; Carril 3: sobrenadante *E. coli* infectada con el fago M13; Carriles 4 al 11: sobrenadante de clones A8-1, G7-1, A11-2, B6-2, H10-3, F11-3, D6-4 y H1-4 respectivamente.

En la metodología de phage display el sistema más destacado y frecuente consiste en presentar las moléculas, que en este caso corresponden a nanoanticuerpos, a través de la fusión con la proteína pIII de la cápside del fago M13 en el extremo N-terminal (Georgieva & Konthur, 2011). La expresión del VHH fusionado a la pIII del fago se corroboró realizando un análisis de detección de la etiqueta 6xHis a través de un western blot, presentado en la Figura 13. Se observa la producción de los nanoanticuerpos fusionado a la pIII del fago recombinante en la región ~70 kDa. Las proteínas del fago pIII de 44.7 kDa y pVI de 12.4 kDa forman un complejo denominado “complejo de adsorción” que requiere condiciones desnaturalizantes más intensas para separarlas. Como

consecuencia, la suma de sus pesos moleculares es de 57.1 kDa y su migración en electroforesis de proteínas se da a una altura aproximada de ~60 kDa (GAILUS & RASCHED, 1994). De esta manera, teniendo en cuenta el peso molecular de los nanoanticuerpos ~15 kDa se esperaba observar una banda a la altura de los ~70 kDa como indicativo de su fusión con la proteína pIII.

Se observa una banda adicional más abajo ~15 kDa compatible con el peso molecular de los VHH sin fusionar a la proteína III. Identidad confirmada al ser revelado con el anticuerpo anti-His conjugado con HRP dirigido a la etiqueta 6xHis presente en el diseño de los nanoanticuerpos. En el diseño del fagémido esta incluido un codón de parada ámbar que en células supresoras como *E. coli* TG1 se continua la lectura del ADN para la síntesis de los nanoanticuerpos fusionados a la pIII del fago recombinante. Sin embargo, se ha reportado una baja eficiencia en la supresión de este codón, teniendo como resultado la producción de los VHH sin fusionar a la proteína del fago (Agafonov et al., 2005).

4. Análisis de Secuencias de Clones Seleccionados Contra los Antígenos de Interés

En la metodología de selección para nanoanticuerpos contra TNFα (descrita en el apartado de Metodología 2-c), se realiza una única ronda, de esta manera la probabilidad de elegir colonias diferentes entre sí es mayor porque se conserva la diversidad inicial de la biblioteca, sin las rondas que permiten el enriquecimiento en clones positivos. Como se observa en la Figura 14. los CDRs secuenciados de

los nanoanticuerpos contra TNFα muestran mayor diversidad entre los clones, se identifican 21 clones diferentes.

(a) TNF

Clone	CDR1	CDR2	CDR3
p1-D11	GTNRFSYTRFALG	AIAMQGGR	IQSSNLTHRY
p1-E10	....	....	....
p2-B5	.YK.ND.SP....	...WG...	.RYDYAY.DS
p2-B7	.A.KNR.AL....	...S....	RRT.TANYHS
p1-D9	..HQNR.DT....	...RG...	NRTQ.VN.QS
p1-B2	.NHDLR.AS....	..YWR..I	RGYG.RYLH.
p2-E2	..G.LR.AV.D..	..Y.R..I	VR.G.ASFN.
p2-B6	.ARNNG.NP....	..YWH..I	TR.KSRSYG.
p1-C8	..R.LQ.S.....	...SR...	PDTHTTNFG.
p2-B2	..EDYQ.S.....	..Y.H..S	PKYQ.TY.G.
p1-B3	.YR.NK.NT.Y..	...LG..S	PETNY.SFG.
p2-C3	..RENN.DG.D..	..STR...	HGYRYR.YG.
p1-G6	.DQ.I..S.....	..SSE..K	GRYH.VN...
1-D10	.NQ..R.YG....	..SSS..N	LRYNSI...S
p1-G3	.ARK.R.YA....	..S.N..N	TRTR.RSFG.
p1-B6	.YGNYR.NT.S..	..SSS..I	.G.KTAS..S
p1-E6	.DKKYK.S..S..	..SLD..I	VRTRYVSLES
p1-F8	.NREHH.YA.Y..	..YSH..S	NRYNSVS..S
p2-D4	.NQK.R.YV.Y..	..YRK..S	LR..YNS.K.
p1-G2	.YQ.HK.NH.Y..	..SRK..K	QRTESDNY.S
p2-C9	.YR.NG..V.D..	...SK..N	NKYR.PSFK.
p1-G7	.SRNNH.YT....	..SWG..K	LGYGYVSYG.

Figura 14. Comparación de las secuencias de aminoácidos de los CDRs de nanoanticuerpos obtenidos en la selección del antígeno TNFα. Los aminoácidos que coinciden con la secuencia del clon ubicado en la primera línea se representan con un punto (.).

Se analizaron y se compararon las secuencias de aminoácidos de 20 clones anti-EGF, 7 clones negativos y 6 clones con igual señal en el ELISA de fagos con el antígeno EGF y el VHH 9G8 considerados anti-His/SV5. Las secuencias aminoacídicas de cada uno de los nanoanticuerpos recombinantes anti-EGF se muestran en la Figura 15. Como se puede observar, de los nanoanticuerpos que reconocieron el EGF, 16 clones presentaron una similitud del 100% con el clon A11-2 independiente de la elución por la cual fueron obtenidos.

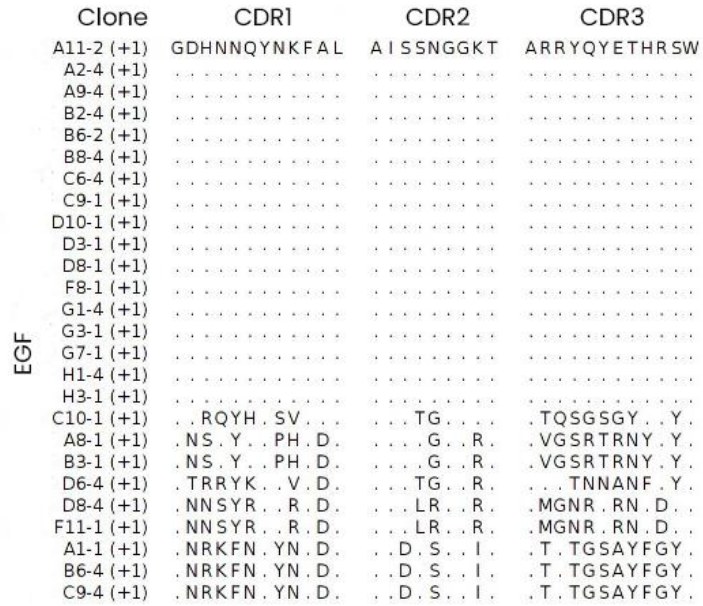

Figura 15. Comparación de las secuencias de aminoácidos de los CDRs de nanoanticuerpos obtenidos en la selección con el antígeno EGF. Los aminoácidos que coinciden con la secuencia del clon A11-2 se representan con un punto (.).

La metodología de selección utilizada para obtener nanoanticuerpos contra EGF incluía 4 métodos de elución consecutivos diferentes entre sí. Las condiciones de elución se basan en el mecanismo por el cual interactúan el ligando y la proteína. En este caso, al cambiar el pH se altera el estado de protonación en los residuos de aminoácidos que contienen grupos ácidos o básicos, cambiando la fuerza de las interacciones electrostáticas (Urh et al., 2009). Podría pensarse que los nanoanticuerpos presentarían diferentes propiedades de unión y por tanto diferencias en su secuencia según el método por el cual fueran eluidos (ácido, básico, físico y biológico), pero los resultados de la secuenciación demuestran que los VHH son iguales en su secuencia, aunque el tratamiento de elución por el cual fueron obtenidos fue diferente. Por ejemplo, el VHH C9-1, el A11-2 y el A2-4

eluidos con trietilamina, glicina y *E. coli* TG1 respectivamente tienen una secuencia 100% similar. Sin embargo, se obtuvieron 4 VHH diferentes: 2 de la primera elución con trietilamina, uno de glicina y uno recuperado con *E. coli* TG1, este último pudo ser recuperado después de aplicar las eluciones consecutivas (Figura 12).

Las rondas favorecen el enriquecimiento de fagos específicos del antígeno de interés, que luego en el proceso de amplificación se obtienen varias copias de un mismo clon, aumentando la probabilidad de ser seleccionado en la última ronda. Sin embargo, esto redujo la diversidad de clones al final de la metodología de selección de nanoanticuerpos contra EGF, obteniendo 4 clones positivos diferentes entre sí. El aumento en el número de lavados entre eluciones podría favorecer la identificación de nanoanticuerpos con diferencia de acuerdo al método de elución por el cual fueron seleccionados.

VIII. CONCLUSIONES

- La generación de nanoanticuerpos contra los antígenos EGF y TNFα, validan la nueva biblioteca sintética como una plataforma robusta y multifuncional para obtener nanoanticuerpos específicos contra diferentes antígenos de interés.
- La obtención de nanoanticuerpos positivos contra el EGF usando una metodología diferente a la inicial refuerza la gran versatilidad de esta poderosa herramienta en la obtención de potenciales biofármacos.
- -La metodología de elución que se emplea durante la realización de la técnica de Phage Display podría influir en la diversidad de secuencias de los fagos que reconocen el antígeno de interés.
- Por primera vez en Colombia se introdujo la metodología de bibliotecas sintéticas basadas en la expresión de proteínas sobre la superficie de fagos filamentosos.

IX. BIBLIOGRAFIA

Agafonov, D. E., Huang, Y., Grote, M., & Sprinzl, M. (2005). Efficient suppression of the amber codon in E. coli in vitro translation system. *FEBS Letters*, *579*(10), 2156–2160. https://doi.org/10.1016/j.febslet.2005.03.004

Alfaleh, M. A., Jones, M. L., Howard, C. B., & Mahler, S. M. (2017). Strategies for selecting membrane protein-specific antibodies using phage display with cell-based panning. In *Antibodies* (Vol. 6, Issue 3). MDPI. https://doi.org/10.3390/antib6030010

Angélica Contreras, M., Serrano-Rivero, Y., González-Pose, A., Salazar-Uribe, J., Rubio-Carrasquilla, M., Soares-Alves, M., Parra, N. C., Camacho-Casanova, F., Sánchez-Ramos, O., & Moreno, E. (2021). *Design and construction of a synthetic nanobody library: testing its potential with a single selection round strategy*. https://doi.org/10.3390/xxxxx

Arbabi-Ghahroudi, M. (2022). Camelid Single-Domain Antibodies: Promises and Challenges as Lifesaving Treatments. In *International Journal of Molecular Sciences* (Vol. 23, Issue 9). MDPI. https://doi.org/10.3390/ijms23095009

Bazan, J., Całkosiñski, I., & Gamian, A. (2012). Phage display: A powerful technique for immunotherapy. In *Human Vaccines and Immunotherapeutics* (Vol. 8, Issue 12, pp. 1817–1828). https://doi.org/10.4161/hv.21703

Carroll-Portillo, A., Coffman, C. N., Varga, M. G., Alcock, J., Singh, S. B., & Lin, H. C. (2021). Standard bacteriophage purification procedures cause loss in numbers and activity. *Viruses*, *13*(2). https://doi.org/10.3390/v13020328

Crombet Ramos, T., Santos Morales, O., Dy, G. K., León Monzón, K., & Lage Dávila, A. (2021). The Position of EGF Deprivation in the Management of Advanced Non-Small Cell Lung Cancer. In *Frontiers in Oncology* (Vol. 11). Frontiers Media S.A. https://doi.org/10.3389/fonc.2021.639745

Davydova, E. K. (2022). Protein Engineering: Advances in Phage Display for Basic Science and Medical Research. In *Biochemistry (Moscow)* (Vol. 87, pp. S146–S167). Pleiades journals. https://doi.org/10.1134/S0006297922140127

GAILUS, V., & RASCHED, I. (1994). The adsorption protein of bacteriophage fd and its neighbour minor coat protein build a structural entity. *European Journal of Biochemistry*, *222*(3), 927–931. https://doi.org/10.1111/j.1432-1033.1994.tb18941.x

Garcia Verdecia, B., Neninger, E., de La Torre, A., Leonard, I., Martínez, R., Viada, C., González, G., Mazorra, Z., Lage, A., & Crombet, T. (2008). Effective inhibition of the epidermal growth factor/epidermal growth factor receptor binding by anti-epidermal growth factor antibodies is related to better survival in advanced non-small-cell lung cancer patients treated with the epidermal growth factor cancer vaccine. *Clinical Cancer Research*, *14*(3), 840–846. https://doi.org/10.1158/1078-0432.CCR-07-1050

Georgieva, Y., & Konthur, Z. (2011). Design And Screening Of M13 phage display cDNA libraries. In *Molecules* (Vol. 16, Issue 2, pp. 1667–1681). https://doi.org/10.3390/molecules16021667

Gonzalez, G., Crombet, T., Torres, F., Catala, M., Alfonso, L., Osorio, M., Neninger, E., Garcia, B., Mulet, A., Perez, R., & Lage, R. (2003). Epidermal growth

factor-based cancer vaccine for non-small-cell lung cancer therapy. *Annals of Oncology*, *14*(3), 461–466. https://doi.org/10.1093/annonc/mdg102

Greenberg, A. S., Avila, D., Hughes, M., Hughes, A., McKinney, E. C., & Flajnik, M. F. (1995). A new antigen receptor gene family that undergoes rearrangement and extensive somatic diversification in sharks. *Nature*, *374*, 168–173.

Guardiola, S., Sánchez-Navarro, M., Rosell, R., Giralt, E., & Codony-Servat, J. (2022). Anti-EGF nanobodies enhance the antitumoral effect of osimertinib and overcome resistance in non-small cell lung cancer (NSCLC) cellular models. *Medical Oncology*, *39*(12). https://doi.org/10.1007/s12032-022-01800-1

Guardiola, S., Varese, M., Sánchez-Navarro, M., Vincke, C., Teixidó, M., García, J., Muyldermans, S., & Giralt, E. (2018). Blocking EGFR Activation with Anti-EGF Nanobodies via Two Distinct Molecular Recognition Mechanisms. *Angewandte Chemie - International Edition*, *57*(42), 13843–13847. https://doi.org/10.1002/anie.201807736

Hamers-Casterman, C., Atarhouch, T., Muyldermans, S., Robinson, G., Hamers, C., Bajyana Songa, E., Bendahman, N., & Hamers, R. (1993). Naturally occurring atibodies devoid of light chains. *Nature*, *363*, 446–448.

Hay, I. D., & Lithgow, T. (2019). Filamentous phages: masters of a microbial sharing economy. *EMBO Reports*, *20*(6). https://doi.org/10.15252/embr.201847427

Hoey, R. J., Eom, H., & Horn, J. R. (2019). Structure and development of single domain antibodies as modules for therapeutics and diagnostics. In *Experimental Biology and Medicine* (Vol. 244, Issue 17, pp. 1568–1576). SAGE Publications Inc. https://doi.org/10.1177/1535370219881129

Jovčevska, I., & Muyldermans, S. (2020). The Therapeutic Potential of Nanobodies. In *BioDrugs* (Vol. 34, Issue 1, pp. 11–26). Adis. https://doi.org/10.1007/s40259-019-00392-z

Khong Nguyen, V., Desmyter, A., & Muyldermans, S. (2001). Functional Heavy-Chain Antibodies in Camelidae. *ADVANCES IN IMMUNOLOGY*, *79*.

Kinoshita, S., Nakakido, M., Mori, C., Kuroda, D., Caaveiro, J. M. M., & Tsumoto, K. (2022). Molecular basis for thermal stability and affinity in a VHH: Contribution of the framework region and its influence in the conformation of the CDR3. *Protein Science*, *31*(11). https://doi.org/10.1002/pro.4450

Könning, D., Zielonka, S., Grzeschik, J., Empting, M., Valldorf, B., Krah, S., Schröter, C., Sellmann, C., Hock, B., & Kolmar, H. (2017). Camelid and shark single domain antibodies: structural features and therapeutic potential. In *Current Opinion in Structural Biology* (Vol. 45, pp. 10–16). Elsevier Ltd. https://doi.org/10.1016/j.sbi.2016.10.019

Liu, B., & Yang, D. (2022). Easily Established and Multifunctional Synthetic Nanobody Libraries as Research Tools. In *International Journal of Molecular Sciences* (Vol. 23, Issue 3). MDPI. https://doi.org/10.3390/ijms23031482

Liu, Y., & Huang, H. (2018). Expression of single-domain antibody in different systems. In *Applied Microbiology and Biotechnology* (Vol. 102, Issue 2, pp. 539–551). Springer Verlag. https://doi.org/10.1007/s00253-017-8644-3

Lyu, M., Shi, X., Liu, X., Liu, Y., Zhu, X., Liao, L., Zhao, H., Sun, N., Wang, S., Chen, L., Fan, L., Xu, Q., Zhu, Q., Gao, K., Chen, H., Zhu, Y., Li, Z., Guo, W., Zheng, Y., … Liu, Y. (2022). Generation and Screening of Antigen-Specific Nanobodies from Mammalian Cells Expressing the BCR Repertoire Library

Using Droplet-Based Microfluidics. *Analytical Chemistry*, *94*(22), 7970–7980. https://doi.org/10.1021/acs.analchem.2c00865

Masola, V., Greco, N., Tozzo, P., Caenazzo, L., & Onisto, M. (2022). The role of SPATA2 in TNF signaling, cancer, and spermatogenesis. *Cell Death and Disease*, *13*(11). https://doi.org/10.1038/s41419-022-05432-1

McCafferty, J., Griffiths, A. D., Winter, G., & Chiswell, D. J. (1990). Phage antibodies: filamentous phage displaying antibody variable domains. *Nature*, *348*, 552–554.

McMahon, C., Baier, A. S., Pascolutti, R., Wegrecki, M., Zheng, S., Ong, J. X., Erlandson, S. C., Hilger, D., Rasmussen, S. G. F., Ring, A. M., Manglik, A., & Kruse, A. C. (2018). Yeast surface display platform for rapid discovery of conformationally selective nanobodies. *Nature Structural and Molecular Biology*, *25*(3), 289–296. https://doi.org/10.1038/s41594-018-0028-6

Moreno, E., Valdés-Tresanco, M. S., Molina-Zapata, A., & Sánchez-Ramos, O. (2022). Structure-based design and construction of a synthetic phage display nanobody library. In *BMC Research Notes* (Vol. 15, Issue 1). BioMed Central Ltd. https://doi.org/10.1186/s13104-022-06001-7

Muyldermans, S. (2021a). A guide to: generation and design of nanobodies. In *FEBS Journal* (Vol. 288, Issue 7, pp. 2084–2102). Blackwell Publishing Ltd. https://doi.org/10.1111/febs.15515

Muyldermans, S. (2021b). A guide to: generation and design of nanobodies. In *FEBS Journal* (Vol. 288, Issue 7, pp. 2084–2102). Blackwell Publishing Ltd. https://doi.org/10.1111/febs.15515

Naderi, S., Roshan, R., Ghaderi, H., Behdani, M., Mahmoudi, S., Habibi-Anbouhi, M., Shokrgozar, M. A., & Kazemi-Lomedasht, F. (2020). Selection and characterization of specific nanobody against neuropilin-1 for inhibition of angiogenesis. *Molecular Immunology*, *128*, 56–63. https://doi.org/10.1016/j.molimm.2020.10.004

Nagano, K., & Tsutsumi, Y. (2021). Phage display technology as a powerful platform for antibody drug discovery. In *Viruses* (Vol. 13, Issue 2). MDPI AG. https://doi.org/10.3390/v13020178

Ortega-Portilla, P. A., Cancino-Villeda, L., Coronado-Aceves, E. W., & Espitia-Pinzón, C. (2021). Nanoanticuerpos: desarrollo biotecnológico y aplicaciones. *TIP Revista Especializada En Ciencias Químico-Biológicas*, *24*. https://doi.org/10.22201/fesz.23958723e.2021.398

Pedreáñez, A., Mosquera-Sulbarán, J., Muñóz, N., Tene, D., & Robalino, J. (2021a). Nanoantibodies: Small molecules, big possibilities. *Biotechnologia*, *102*(3), 321–336. https://doi.org/10.5114/bta.2021.108724

Pedreáñez, A., Mosquera-Sulbarán, J., Muñóz, N., Tene, D., & Robalino, J. (2021b). Nanoantibodies: Small molecules, big possibilities. *Biotechnologia*, *102*(3), 321–336. https://doi.org/10.5114/bta.2021.108724

Roovers, R. C., Laeremans, T., Huang, L., de Taeye, S., Verkleij, A. J., Revets, H., de Haard, H. J., & van Bergen En Henegouwen, P. M. P. (2007a). Efficient inhibition of EGFR signalling and of tumour growth by antagonistic anti-EGFR Nanobodies. *Cancer Immunology, Immunotherapy*, *56*(3), 303–317. https://doi.org/10.1007/s00262-006-0180-4

Roovers, R. C., Laeremans, T., Huang, L., de Taeye, S., Verkleij, A. J., Revets, H., de Haard, H. J., & van Bergen En Henegouwen, P. M. P. (2007b). Efficient inhibition of EGFR signalling and of tumour growth by antagonistic anti-EGFR Nanobodies. *Cancer Immunology, Immunotherapy*, *56*(3), 303–317. https://doi.org/10.1007/s00262-006-0180-4

Roshan, R., Naderi, S., Behdani, M., Cohan, R. A., Ghaderi, H., Shokrgozar, M. A., Golkar, M., & Kazemi-Lomedasht, F. (2021). Isolation and characterization of nanobodies against epithelial cell adhesion molecule as novel theranostic agents for cancer therapy. *Molecular Immunology*, *129*, 70–77. https://doi.org/10.1016/j.molimm.2020.10.021

Salema, V., & Fernández, L. Á. (2017). Escherichia coli surface display for the selection of nanobodies. In *Microbial Biotechnology* (Vol. 10, Issue 6, pp. 1468–1484). John Wiley and Sons Ltd. https://doi.org/10.1111/1751-7915.12819

Shamir, Y., & Goldbourt, A. (2022). Atomic-Resolution Structure of the Protein Encoded by Gene v of fd Bacteriophage in Complex with Viral ssDNA Determined by Magic-Angle Spinning Solid-State NMR. *Journal of the American Chemical Society*. https://doi.org/10.1021/jacs.2c09957

Sidhu, S. S. (2001). Engineering M13 for phage display. In *Biomolecular Engineering* (Vol. 18). www.elsevier.com/locate/geneanabioeng

Smith, G. P. (1985). Filamentous fusion phage: novel expression vectors that display cloned antigens on the virion surface. *Science*, *228*, 1315–1317. http://science.sciencemag.org/

Smith, G. P. (2019). Phagen-Display: Einfache Evolution in der Petrischale (Nobel-Vortrag). *Angewandte Chemie*, *131*(41), 14566–14576. https://doi.org/10.1002/ange.201908308

Smolarek, D., Bertrand, O., & Czerwinski, M. (2012). Variable fragments of heavy chain antibodies (VHHs): a new magic bullet molecule of medicine? *Postepy Hig Med Dosw*, *66*, 348–358. www.phmd.pl

Tullila, A., & Nevanen, T. K. (2017). Utilization of multi-immunization and multiple selection strategies for isolation of hapten-specific antibodies from recombinant antibody phage display libraries. *International Journal of Molecular Sciences*, *18*(6). https://doi.org/10.3390/ijms18061169

Ul Haq, I., Chaudhry, W. N., Akhtar, M. N., Andleeb, S., & Qadri, I. (2012). Bacteriophages and their implications on future biotechnology: A review. In *Virology Journal* (Vol. 9). https://doi.org/10.1186/1743-422X-9-9

Urh, M., Simpson, D., & Zhao, K. (2009). Chapter 26 Affinity Chromatography. General Methods. In *Methods in Enzymology* (Vol. 463, Issue C, pp. 417–438). Academic Press Inc. https://doi.org/10.1016/S0076-6879(09)63026-3

Valdés-Tresanco, M. S., Molina-Zapata, A., Pose, A. G., & Moreno, E. (2022). Structural Insights into the Design of Synthetic Nanobody Libraries. In *Molecules* (Vol. 27, Issue 7). MDPI. https://doi.org/10.3390/molecules27072198

van Horssen, R., ten Hagen, T. L. M., & Eggermont, A. M. M. (2006). TNF-α in Cancer Treatment: Molecular Insights, Antitumor Effects, and Clinical Utility. *The Oncologist*, *11*(4), 397–408. https://doi.org/10.1634/theoncologist.11-4-397

Verhaar, E. R., Woodham, A. W., & Ploegh, H. L. (2021). Nanobodies in cancer. In *Seminars in Immunology* (Vol. 52). Academic Press. https://doi.org/10.1016/j.smim.2020.101425

Wang, Z., Ao, X., Shen, Z., Ao, L., Wu, X., Pu, C., Guo, W., Xing, W., He, M., Yuan, H., Yu, J., Li, L., & Xu, X. (2021). Tnf-α augments cxcl10/cxcr3 axis activity to induce epithelial-mesenchymal transition in colon cancer cell. *International Journal of Biological Sciences*, *17*(11), 2683–2702. https://doi.org/10.7150/ijbs.61350

Yang, E. Y., & Shah, K. (2020). Nanobodies: Next Generation of Cancer Diagnostics and Therapeutics. In *Frontiers in Oncology* (Vol. 10). Frontiers Media S.A. https://doi.org/10.3389/fonc.2020.01182

Yang, G., Velgos, S. N., Boddapati, S. P., & Sierks, M. R. (2014). Probing Antibody-Antigen Interactions. *Microbiology Spectrum*, *2*(1). https://doi.org/10.1128/microbiolspec.aid-0010-2013

Yan, J., Li, G., Hu, Y., Ou, W., & Wan, Y. (2014). Construction of a synthetic phage-displayed Nanobody library with CDR3 regions randomized by trinucleotide cassettes for diagnostic applications. *Journal of Translational Medicine*, *12*(1). https://doi.org/10.1186/s12967-014-0343-6

ANEXOS

Los resultados presentados en este trabajo de tesis se integraron en la elaboración de dos artículos científicos y un artículo adicional que incluye resultados adicionales durante el tiempo de desarrollo de la maestría.

ANEXO 1. Angélica Contreras M, Serrano-Rivero Y, González-Pose A, **Salazar-Uribe J**, Rubio-Carrasquilla M, Soares-Alves M, et al. (2023). Design and construction of a synthetic nanobody library: testing its potential with a single selection round strategy. Publicado en la revista Molecules.

ANEXO 2. Serrano-Rivero Y, **Salazar-Uribe J**, Rubio-Carrasquilla M, Camacho-Casanova F, Sánchez-Ramos O, González-Pose A, et al. (2023). Selecting nanobodies specific for the epidermal growth factor from a synthetic nanobody library. Publicado en la revista Molecules.

ANEXO 3. Cruz-Pacheco, A. F., Monsalve, Y., Serrano-Rivero, Y., **Salazar-Uribe, J.**, Moreno, E., & Orozco, J. (2023). Engineered synthetic nanobody-based biosensors for electrochemical detection of epidermal growth factor receptor. Chemical Engineering Journal, 465.

ANEXO 1.

molecules

MDPI

Article

Design and Construction of a Synthetic Nanobody Library: Testing Its Potential with a Single Selection Round Strategy

María Angélica Contreras [1,†], Yunier Serrano-Rivero [2,†], Alaín González-Pose [2], Julieta Salazar-Uribe [2], Marcela Rubio-Carrasquilla [2], Matheus Soares-Alves [1], Natalie C. Parra [1], Frank Camacho-Casanova [1], Oliberto Sánchez-Ramos [1,*] and Ernesto Moreno [2,*]

[1] Pharmacology Department, School of Biological Sciences, University of Concepcion, Concepcion 4070386, Chile; mcontrerasv@udec.cl (M.A.C.); malves@udec.cl (M.S.-A.); natparra@udec.cl (N.C.P.); fcamacho@udec.cl (F.C.-C.)
[2] Faculty of Basic Sciences, University of Medellin, Medellin 050026, Colombia; 0905yunierserrano@gmail.com (Y.S.-R.); agonzalezp@udemedellin.edu.co (A.G.-P.); julieta.salazaru@gmail.com (J.S.-U.); marcelaru@yahoo.com (M.R.-C.)
* Correspondence: osanchez@udec.cl (O.S.-R.); emoreno@udemedellin.edu.co (E.M.)
† These authors contributed equally to this work.

Abstract: Nanobodies (Nbs) are single domain antibody fragments derived from heavy-chain antibodies found in members of the Camelidae family. They have become a relevant class of biomolecules for many different applications because of several important advantages such as their small size, high solubility and stability, and low production costs. On the other hand, synthetic Nb libraries are emerging as an attractive alternative to animal immunization for the selection of antigen-specific Nbs. Here, we present the design and construction of a new synthetic nanobody library using the phage display technology, following a structure-based approach in which the three hypervariable loops were subjected to position-specific randomization schemes. The constructed library has a clonal diversity of 10^8 and an amino acid variability that matches the codon distribution set by design at each randomized position. We have explored the capabilities of the new library by selecting nanobodies specific for three antigens: vascular endothelial growth factor (VEGF), tumor necrosis factor (TNF) and the glycoprotein complex (GnGc) of Andes virus. To test the potential of the library to yield a variety of antigen-specific Nbs, we introduced a biopanning strategy consisting of a single selection round using stringent conditions. Using this approach, we obtained several binders for each of the target antigens. The constructed library represents a promising nanobody source for different applications.

Keywords: nanobody; synthetic library; phage display; CDR randomization; biopanning; tumor necrosis factor; vascular endothelial growth factor; Andes virus

Citation: Contreras, M.A.; Serrano-Rivero, Y.; González-Pose, A.; Salazar-Uribe, J.; Rubio-Carrasquilla, M.; Soares-Alves, M.; Parra, N.C.; Camacho-Casanova, F.; Sánchez-Ramos, O.; Moreno, E. Design and Construction of a Synthetic Nanobody Library: Testing Its Potential with a Single Selection Round Strategy. *Molecules* **2023**, *28*, 3708. https://doi.org/10.3390/molecules28093708

Academic Editor: Jahir Orozco Holguín

Received: 20 March 2023
Revised: 18 April 2023
Accepted: 18 April 2023
Published: 25 April 2023

1. Introduction

Nanobodies (Nbs) are single domain antibody fragments derived from heavy-chain antibodies, lacking the light chain present in classical immunoglobulins [1]. These special antibodies are found in members of the Camelidae family, which includes camels, dromedaries, llamas and alpacas. Nbs have several important advantages as compared to antibodies and their fragments, such as their small size (~15 kDa) and high thermal stability (median melting temperature (Tm) ~67 °C [2]). These tiny proteins have found multiple applications in many different areas, from basic research—for example, as affinity capture reagents and crystallization chaperones [3])—to the clinics, with more than 40 clinical trials reported for different Nb-based products in the ClinicalTrials.gov web repository maintained by the National Institutes of Health (https://clinicaltrials.gov) and two Nbs approved for clinical use: one in the United States [4] and another one in Japan [5]. Such application versatility is due in large part to the single-domain structure of Nbs, which

makes them easy to engineer and integrate into many different constructs. Notably, Nbs can achieve high affinities in spite of their smaller binding region displaying only three hypervariable loops [6].

Nbs are obtained mostly from immune libraries generated by animal immunization [6]. During the last few years, however, synthetic libraries with different designs are gaining ground as reliable Nb sources, offering important advantages in terms of cost and speed [7]. Two key features define a synthetic Nb library: framework selection and the design of the complementarity-determining regions (CDRs). A few recent works have relied on both sequence and structural data to define the CDR positions to be randomized, as well as the sets of amino acids (aa) to be introduced at those positions [8–14], including a recent report by our group [15].

A first, comprehensive work in designing and validating a synthetic Nb library was reported in 2016 by Moutel and coworkers [8] using as scaffold an in-house developed framework. They kept CDRs 1 and 2 with a constant length (7 aa each), randomizing each position in a way that resembles the natural diversity observed for these two CDRs. For CDR3, four different CDR3 lengths were introduced (9, 12, 15 and 18 aa) and all the positions were randomized, allowing all amino acids except cysteine. Two years later, McMahon and coworkers [9] reported the structure-based design and construction of a yeast-displayed library in which the amino acid variability in CDRs 1 (7 aa) and 2 (5 aa) recapitulates the natural diversity observed in a set of over 90 Nb crystal structures available at that time. CDR3 was constructed with different lengths (7, 11 and 15 aa), fully randomizing every position. That same year (2018), Zimmermann et al. [10] reported the design and construction of a ribosome-displayed library composed of three sub-libraries with different CDR3 lengths, using two different frameworks. Their design was based on a structure-based analysis of Nb crystal structures, finding that Nbs with a short CDR3 (6 aa) show a concave shape, those with an intermediate length (12 aa) show a protrusion, and those with a longer loop (16 aa) display a convex surface. CDR randomization focused on achieving an optimal balance between charged, polar, aromatic, and non-polar amino acids to keep a moderate hydrophobicity on the binding site surface. In a more recent (2021) report, Chen et al. [14] constructed a ribosome-displayed library using four CDR3 lengths (6, 9, 10 and 13 aa) and fully randomizing each CDR position. Several other synthetic nanobody libraries have been reported during the last few years following similar design strategies, as recently reviewed [7]. Library sizes range from 10^8–10^{10} for phage-displayed libraries, and up to 10^{12} when using ribosome display [7].

An important issue to consider in Nb library design is the length of CDR3. It has been shown that nanobodies can recognize clefts and cryptic epitopes in proteins that are less accessible to conventional antibodies [16–18]. This important capability is due to the compact prolate shape of Nbs together with their usually long CDR3 loop that folds over the framework region, generating a convex paratope. In several cases, this effect may be enhanced by a protruding loop structure. Such convex–concave Nb–antigen interface provides an interaction surface as large as that of a two-domain antibody paratope, while interacting with a smaller section of the antigen [16]. As observed by Zimmermann and coworkers [10] from the analysis of a large number of nanobody crystal structures, medium length CDR3 loops (10–12 aa) adopt an extended, protruding conformation that can be inserted into a receptor cavity.

Here, we describe the design and construction of a new synthetic nanobody library with a 10 amino acid-long CDR3, in which the three hypervariable loops were subjected to position-specific randomization schemes. The design follows a structure-based approach that seeks to maintain the high stability shown by the original framework-donor nanobody and increase the number of functional variants within the combinatorial space of mutations. As scaffold, we used the framework region from the camelid nanobody cAbBCII10 [19]. This "universal" framework has been shown to be highly stable (Tm = 68 °C [20]), capable of accepting many different CDRs [21], and has been used for the construction of several Nb libraries [15,22–24]. The capabilities of the new library were explored by selecting

nanobodies specific for three therapeutically relevant antigens: tumor necrosis factor (TNF), vascular endothelial growth factor (VEGF) and the glycoprotein complex (GnGc) of Andes virus. To test the potential of the library to yield a variety of antigen-specific Nbs, we introduced a biopanning strategy consisting of a single selection round using stringent conditions, aiming to wash out the weaker binders. By applying this strategy, we obtained several binders for each of the target antigens. For one of the obtained anti-TNF clones, we constructed a recombinant fusion protein that incorporates an albumin binding domain and confirmed the functionality of the two binding modules.

2. Results

2.1. Structure-Based Library Design

The design of this library follows a rationale similar to the approach described in a previous work by our group [15]. The amino acid sequence of the framework region was taken from the camelid nanobody cAbBCII10 [19]—a universal scaffold used for the construction of several Nb libraries [15,22–24]. The design of the CDRs relied on the analysis of the crystal structure of the parent cAbBCII10 nanobody (entry 3DWT in the Protein Data Bank [25]), focusing on the structural role played by individual residues in defining CDR conformation or exposing their side chains for antigen binding. The principles followed in the design of CDRs 1 and 2 are explained in detail in [15]. Briefly, the lengths of these two CDRs were kept as in the original cAbBCII10. Furthermore, the amino acids whose sidechains are packaged against framework residues in the 3D structure, as well as those found to be highly conserved in nanobody sequences, were kept as in the parent nanobody. This way we intended to preserve as much as possible the structural stability of the library mutants. CDR residues with surface-exposed side chains were subjected to tailored randomization by introducing degenerate codons in the gene sequence [26]. The allowed codons did not include cysteines and were carefully chosen to restrict the presence of hydrophobic amino acids at these solvent-exposed positions.

For this library, we chose a 10-long CDR3, which for most of the resulting nanobody variants should create a "concave" binding site topology with an "upright"-oriented and protruding CDR3 loop. This represents an important difference as compared with our previously constructed library, carrying a 14 aa-long CDR3 that bends over the framework flank, creating a "convex" topology [15]. Codons VRN and WMY were introduced at several positions to favor the presence of polar/charged amino acids, while the relatively high probability of Gly in the VRN codon may favor a conformational diversity. The highly variable VNN codon was also used. For the C-terminal part of CDR3 (the last two residues), we took into account the amino acid frequencies observed at these positions in the crystal structures of nanobodies with short CDR3 loops, which show that Ser and Tyr are the most frequent aa at the C-terminal end (position "n"), while polar residues are frequent at position "n − 1" (our own data). For the framework region, codon usage was optimized for bacterial expression. Figure 1 shows the library design at the amino acid, nucleotide and structural levels, as well as the amino acid repertoire corresponding to each of the degenerate codons employed in the design.

A total of 22 sequence positions were randomized. The theoretical variability resulting from this tailored design (calculated by multiplying the numbers of the different amino acids coded at each randomized position) is in the order of 10^{18}. This huge number, however, is in practice drastically reduced in the next two construction steps: firstly, by the actual number of genes that are synthesized and, secondly, by the number of bacteria that become transformed in the process of library construction, as explained below.

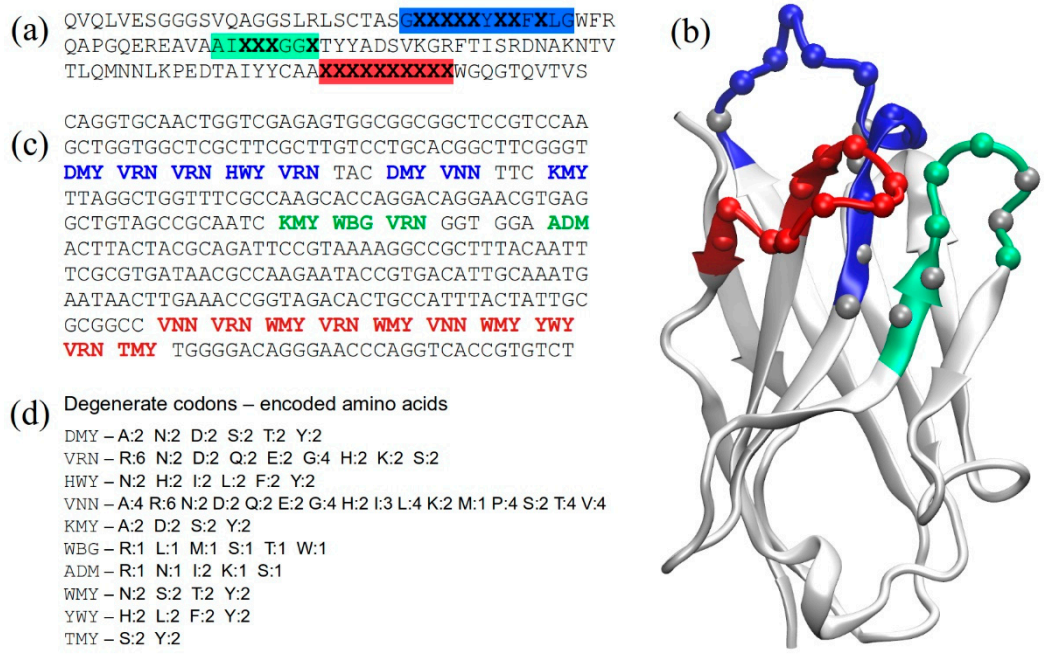

Figure 1. Library design. (**a**) Sequence design at the amino acid level. Positions chosen for randomization are shown as "X" in bold. The CDR sequences are highlighted in colors (blue, green and red for CDRs 1, 2 and 3, respectively), while the framework region is shown in light gray; (**b**) 3D model of a representative library nanobody based on the cAbBCII10 crystal structure (PDB: 3DWT). CDRs are colored following the same code as in panel (**a**). The colored spheres at the alpha carbons in CDRs represent the randomized positions, while gray spheres represent CDR positions that were kept fixed. (**c**) Nucleotide sequence with degenerate codons, colored by CDR; (**d**) degenerate codons used in library design and their encoded amino acids, showing also the numbers of resulting codons for each amino acid type.

2.2. Library Construction

The randomized genes were synthesized by GenScript (Piscataway, NJ, USA) and cloned as described in Methods into our ad hoc-designed pMAC phagemid vector [15] (see Figure S1). The amount of synthetic genes used for cloning (4 µg) corresponds roughly to 10^{13} individual molecules, that is, five orders of magnitude lower than the theoretical library variability. The pMAC vector employed for cloning includes a pelB leader containing a *NcoI* restriction site at its 3′ end, followed by three other unique restriction sites (*EcoRI*, *BamHI* and *NotI*, in this order). To avoid unnecessary N-terminal and/or C-terminal additions to the recombinant nanobodies, we used the outer *NcoI* and *NotI* sites for cloning. Then, the phagemid codes a short linker (SGGGG), a 6xHis tag, an amber stop codon and, finally, the M13 PIII protein. The amber codon allows the expression of recombinant nanobodies directly from recombinant library plasmids using a non-amber suppressor *E. coli* strain [27], and the obtained nanobodies can then be purified by affinity chromatography using the His tag. The library of recombinant phagemids was transformed by electroporation into SS320 *E. coli* cells as described in Methods.

The library size, which corresponds to its diversity, since with a very high probability each transformed bacterium acquired a unique nanobody gene, was assessed by colony-forming units (CFU) counting. The estimated size was 1.5×10^8. Phage titration by CFU counting yielded a phage concentration of 3.6×10^{10} cfu/µL.

2.3. Assessing Library Quality and Diversity

One hundred randomly picked library clones were sequenced to evaluate the quality of the constructed library and its diversity, as compared to the theoretical design. From these clones, 76 contained a correct nanobody sequence, 15 showed a reading frame shift,

5 clones contained nanobody sequences with no CDR3, 3 clones yielded arbitrary unknown sequences and 1 clone contained an empty phagemid vector. From these results we obtain an estimate of 76% correct clones in the library, which keeps its actual size in the same order of magnitude previously determined (10^8).

Figure 2 shows a sequence logo obtained from the alignment of the 76 correct nanobody sequences. All the randomized positions show an amino acid variability in correspondence with the gene library design, as illustrated in the figure for three CDR positions. Furthermore, and in spite of the relatively limited number of sequenced clones, even the highly variable positions (e.g., for codons VNN and VRN) show a large diversity, matching the expected repertoire of amino acids. For example, between 14 and 16 different residues, out of 16 possible amino acids, are found at the three positions (34, 102 and 107) coded with the VNN triplet.

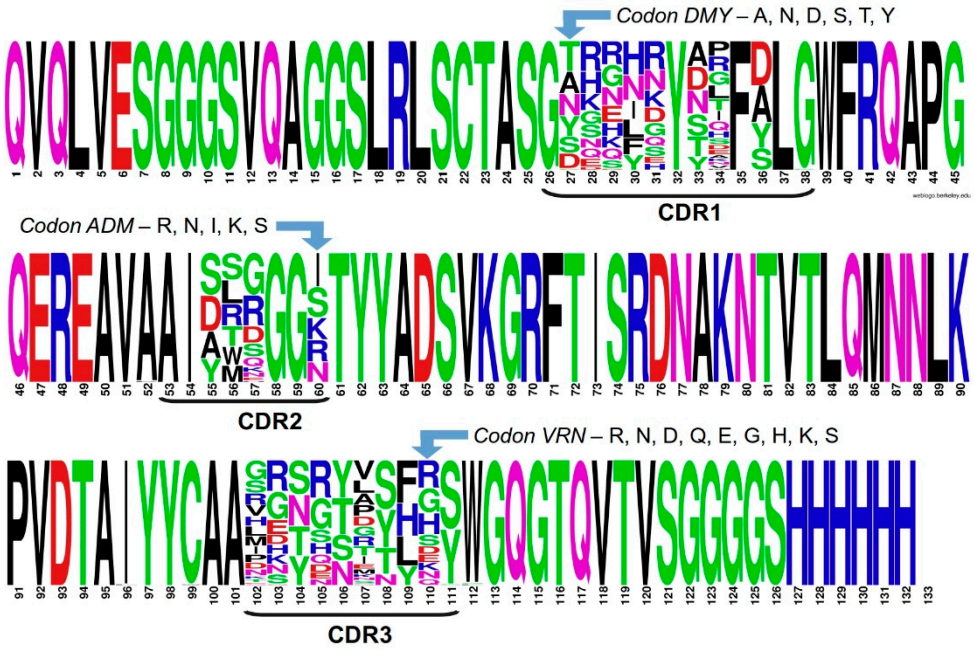

Figure 2. Amino acid distribution per sequence position for the ensemble of 76 correct nanobody clones, shown as a sequence logo. The framework and fixed CDR positions display their conserved amino acid as a single big letter. The amino acid variability found at each randomized position is represented as a stack of letters, each of them with a size that is proportional to its frequency in the multiple alignment. The close match between the theoretical design and the actual experimental diversity is illustrated for three CDR positions (one for each CDR).

2.4. Library Screening

The capability of the library to yield specific binders was tested for three protein antigens: tumor necrosis factor (TNF), vascular endothelial growth factor (VEGF) and the glycoprotein complex (GnGc) of Andes virus. Both TNF and VEGF, as well as their receptors, are relevant therapeutic targets in cancer and autoimmune diseases, and several monoclonal antibodies targeting these molecules have been used in the clinics for several years [28–30]. Furthermore, several nanobodies specific for VEGF have been reported [31], and very recently (Sept/2022) a trivalent anti-TNF nanobody called ozoralizumab was approved in Japan for the treatment of rheumatoid arthritis [5]. Regarding the viral GnGc antigen, to our knowledge no nanobodies specific for this molecule have been yet reported.

2.4.1. Selection of Antigen-Specific Binders in a Single Round

Here we decided to implement a screening procedure based on a single selection round using stringent conditions, aiming at a quick enrichment of the selected phages with the strongest binders in only one selection step, and also as a way of probing the

capabilities of the newly designed library. Before elution, we applied four serial washes with glycine-HCl pH 2.2, a buffer commonly used for elution in phage display biopannings. No phage collection was carried out in this step since the aim of these stringent washes was to remove a large part of the phages that would bind with weaker affinity. In a subsequent, final step, the wells were incubated with a relatively high concentration of the antigen (10 µg/well, 10-fold the amount used for coating) to recover the bound recombinant phages by binding competition against the coated and soluble antigens.

For each antigen, the whole eluted phage sample was used to infect *E. coli* TG1 bacteria, which were seeded on 2xYT/ampicillin plates. The numbers of obtained colonies were 97, 1404 and 1656 for TNF, VEGF and GnGc, respectively. We then proceeded to select individual clones to produce recombinant phages and analyze their ability to bind to their corresponding antigens. For TNF, we tested all the 97 obtained clones, whereas for both VEGF and GnGc we randomly picked 180 clones. Figure 3 shows the results from the binding experiments. Notably, we obtained a high number of positive clones in only one selection round, for the three antigens, several of them showing high OD signals.

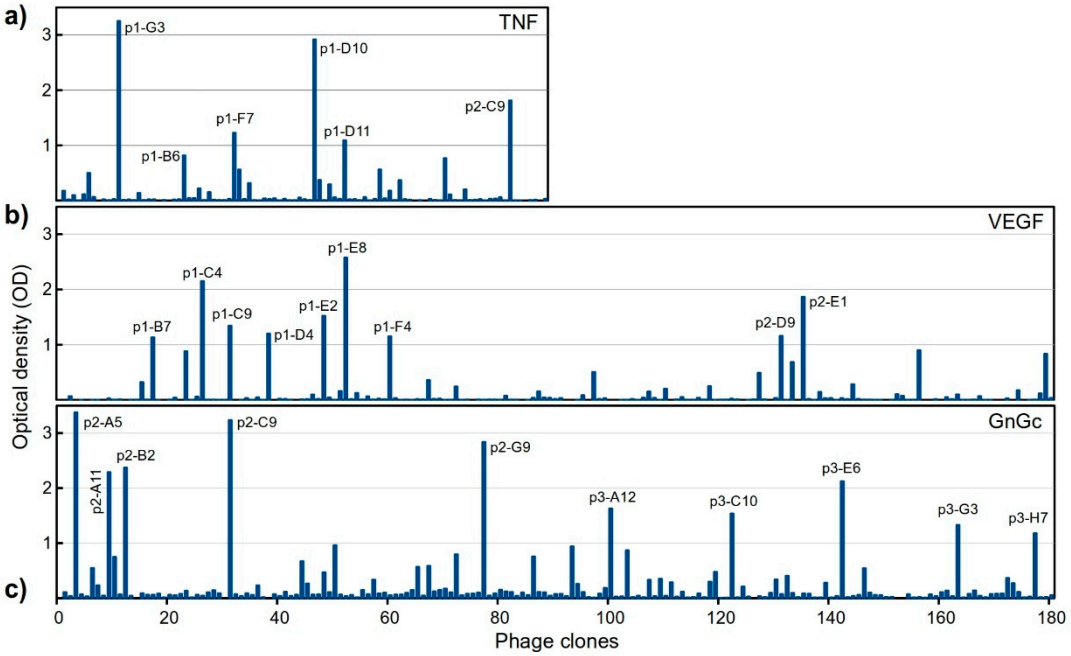

Figure 3. Binding of individual phage clones to their antigens, as measured by ELISA, (**a**) TNF, (**b**) VEGF, (**c**) GnGc. The optical density (OD) values for each clone corresponds to antigen binding with subtracted binding to BSA. For a few clones showing a negative value for this difference, the OD was set to 0 in the graph. The X-axis scale (clone numbers) is common for the three panels. Clones with high binding signal (OD > 1) are labeled, matching their IDs in Figure 4.

2.4.2. Sequencing of Selected Groups of Phage Clones

We decided to sequence all the clones showing OD values above 0.15, for the three antigens, resulting in 28, 24 and 44 clones for TNF, VEGF and GnGc, respectively. In practice, we obtained the sequences for 22, 22 and 34 clones, respectively, since a few of the samples could not be correctly sequenced. Nonetheless, we obtained the sequences for practically all of the best binders shown in Figure 3, with the exception of the anti-TNF clone p1-F7 and the anti-GnGc clone p2-C9.

As shown in Figure 4, for the three antigens we obtained sets of unique different binders (with only one identical pair of anti-TNF clones) as a consequence of performing a single selection round, without further binding clone enrichment. In the three cases, no common sequence motifs are evident from the alignment, for any of the CDRs, which sug-

gests that these clones have different binding modes, likely recognizing different epitopes on the antigen surface.

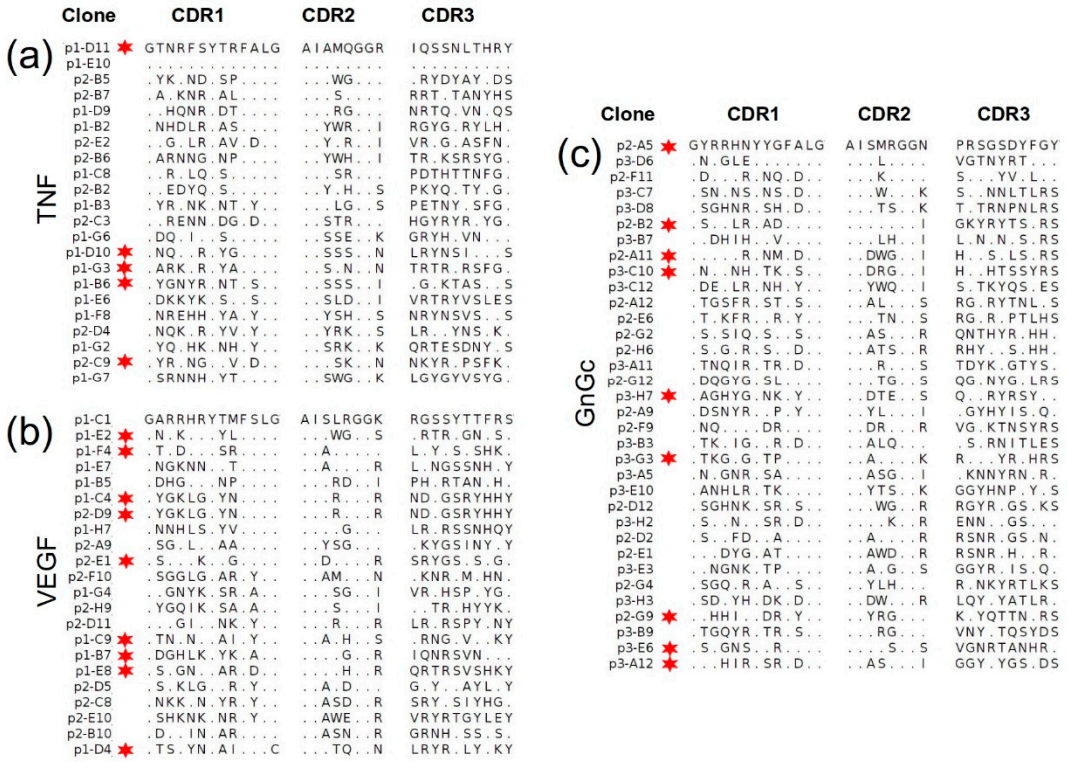

Figure 4. Alignments of CDR sequences obtained for groups of clones selected from the biopannings against the following: (**a**) TNF (22 clones); (**b**) VEGF (22 clones) and (**c**) GnGc (34 clones). Dots indicate the presence of the same amino acid as in the first sequence in the alignment. Red stars denote a high binding signal by ELISA (OD > 1), matching their labels in Figure 3.

2.5. Design and Expression of a Recombinant Fusion Protein with an Anti-TNF Nb

A known drawback for the therapeutic use of nanobodies is their short half-life in serum due their small size. Several strategies can be followed to prolong the Nb half-life, one of them being the genetic fusion or chemical conjugation to a molecule capable of binding to serum albumin [32]. Here, we decided to construct a fusion protein (NbB6-ABD) composed of an anti-TNF Nb and an albumin binding domain (ABD) from the *Streptococcus* sp. G protein, which shows high specificity and affinity for human serum albumin (HSA), with a dissociation constant (KD) in the nanomolar order [33,34] (Figure 5a). The anti-TNF clone p1-B6 was selected for this purpose. Although this clone is not among the strongest binders (OD = 0.9), it was chosen because of its very low background signal to BSA and skim milk (data not shown). In addition to the 46 aa constituting the ABD domain, six additional aa (AVDANS) of the protein were included at the N-terminal end since they are packed with the ABD domain in its crystal structure. A c-Myc tag was included between the nanobody and ABD, separated by short linkers. An *EcoRI* restriction site inserted right after the Nb sequence allows switching the Nb binder to target any antigen of interest. The gene coding for the fusion protein was cloned into the pET22b plasmid, which adds a C-terminal His tag, as shown in Figure 5a.

For binding assays, the fusion protein was biotinylated as described in Methods. Figure 5b shows the ELISA results for the binding to TNF and HSA. The ABD domain kept its binding capability to HSA (Figure 5b, right panel). For the binding of the nanobody domain to TNF, a titration ELISA [35] was performed in order to estimate the dissociation constant, obtaining a KD = $(1.48 \pm 0.35) \times 10^{-7}$ M. This is quite an encouraging result, taking into account that this was an initial test for this fusion protein design, using one of

the obtained anti-TNF clones, which was not among the strongest binders in the phage-based ELISAs.

a)

(*NcoI*) QVQLVESGGGSVQAGGSLRLSCTASGYGNYRYNTFSLGWFRQAPGQEREAVAAISSSG
GITYYADSVKGRFTISRDNAKNTVTLQMNNLKPVDTAIYYCAAIGSKTASHRSWGQGTQVTVSS
EFGGGSEQKLISEEDLGGSGGSAVDANSLAEAKVLANRELDKYGVSDYYKNLINNAKTVEGVKA
LIDEILAALPGGSGGS (*XhoI*) HHHHHH*

b)

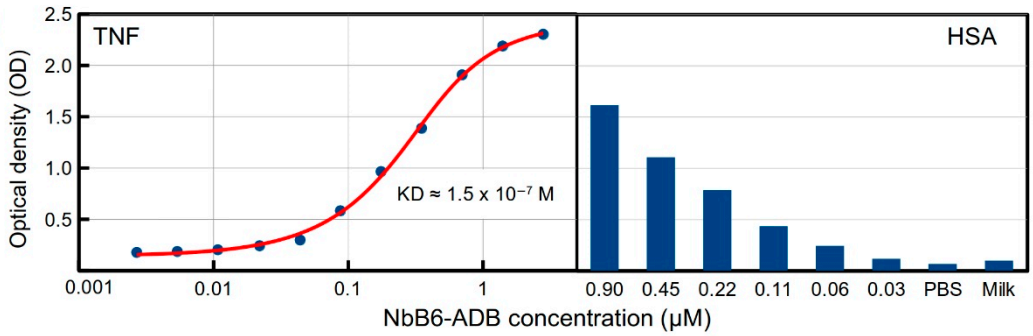

Figure 5. (**a**) Amino acid (aa) sequence of the NbB6-ABD fusion protein. Legend: White background—anti-TNF nanobody clone p1-B6; green—the two aa coded by an inserted *EcoRI* restriction site; gray—spacers (linkers); cyan—c-Myc tag; yellow—albumin binding domain; orange—6xHis tag. The *NcoI* and *XhoI* restriction sites were used for cloning into the pET22b vector, which adds the C-terminal histidine tag. (**b**) Binding of NbB6-ABD to TNF (**left chart**) and to HSA (**right chart**) as measured by ELISA. (**Left chart**): Negative control (not shown)—BSA coating: OD = 0.11. The red fitting curve for TNF binding was used for KD estimation. (**Right chart**): The Y-axis scale is the same as for the left chart; negative controls—PBS (instead of NbB6-ABD) and skim milk. For both antigens, we used the maximum tested NbB6-ABD concentration for the BSA/milk negative control. Experiments were performed in duplicates.

3. Discussion

We have constructed a new synthetic nanobody library following a tailored, structure-based design. Synthetic libraries are nonspecific and therefore seek to recreate a large clonal variability to increase the probability of obtaining good binders. For this reason, synthetic libraries must be large, at least 10^8 in size, preferably larger [6,7]. Most of the reported synthetic, phage-displayed nanobody libraries have sizes in the order of 10^9, as recently reviewed [7]. The clonal diversity of our library is in the order of 10^8, that is, at the lower limit of the accepted range. This level of diversity, however, proved to be enough to produce a high rate of specific clones against three different, relevant therapeutic targets. In this regard, we believe that the library's CDR design creates a high-quality repertoire of binding paratopes that may, to a certain extent, counteract the relatively smaller size of the library.

As scaffold for the library, we chose a well-proven framework—from the cAbBCII10 Nb—that has been shown to support CDR loops of different lengths [21]. This is an important base point in the design to ensure that most of the inserted CDR sequences yield functional nanobodies. As a basis for the CDR design, firstly we carefully analyzed the structural role played by each aa in CDRs 1 and 2 in the parental cAbBCII10 Nb. A first rule applied here was to keep fixed every aa whose sidechain is buried in the structure, as well as those aa found to be highly or relatively conserved in nanobody sequences, or thought to be important in holding CDR conformation in cAbBCII10. This approach differs from the all-position randomization strategies followed in many reported libraries [7], e.g., in [8,11,13,14].

A few recent reports, however, incorporate structure-based strategies to select the positions in CDRs 1 and 2 to be randomized. For example, McMahon and coworkers [9] selected four positions in CDR1 and one in CDR2, based on their large variability in a set of

analyzed Nb sequences. All these positions were fully randomized (avoiding Cys and Met). Zimmerman et al. [10] selected five residues in CDR1 and also in CDR2 for randomization, using three different mixtures of nucleotide triplets. The most used mixture coded for 18 aa (excluding Cys and Pro). CDR residues contributing to the Nb hydrophobic core were kept fixed, as in our library. By difference with these designs, here we used 10 different degenerate codons instead of triplets, tailoring the use of these codons at a position level. The amino acid repertoires resulting from these codons vary from 2 to 16 aa, with most of the sets having only 4 or 6 aa. Even so, the theoretical diversity is huge, in the order of 10^{18}.

Although the cAbBCII10 Nb has been shown to accept CDR1 loops of different lengths [21], in this library we kept the full length of the parental CDR1, randomizing 8 out of its 13 positions. In contrast, only 4 positions were randomized in CDR2. Therefore, most of the variability in the library comes from CDR1 and CDR3, which in a modeled structure (Figure 1) form a shallow concave surface between them. We speculate that this shape would be likely fitting for binding to relatively small globular proteins and slightly concave surface patches on proteins in general. Furthermore, the protruding CDR3 might bind to protein cavities.

The new library was tested against three protein antigens of therapeutic relevance: TNF, VEGF and GnGc (a viral antigen). To evaluate its capabilities, we decided to apply a selection strategy consisting in applying stringent washing conditions, followed by competitive elution, aiming to retrieve mostly strong binders in a single screening step. For stringent washing (repeated four times) we used glycine-HCl pH 2.2—a commonly used elution buffer in phage display biopannings [36]. This way, many phages that otherwise would be collected for a second biopanning round were discarded. Subsequently, the wells were incubated with a relatively high concentration of antigen (100 μg/mL) to recover bound recombinant phages by binding competition against the coated antigens. Such competitive phage elution is also a common procedure used to collect phages with high affinity for their target molecule [6,37].

Stringent washes are very often used before the elution step, but in general, such stringency consists in increasing the washing time, number of washes and/or Tween 20 concentration [6,37–39], as well as decreasing the antigen concentration in each subsequent selection round [6,40,41]. There are few reports, however, in which a glycine-HCl solution was used as a wash buffer. Lunder et al. [42], for example, implemented several protocols that included four glycine-HCl (0.2 M, pH 2.2) washings and then eluted the phages that remained bound to the antigen by direct infection with *E. coli*, ultrasound or competition. On the other hand, although using several selection-amplification rounds enriches the library in clones specific for the target molecule, it may also have a negative effect by reducing the diversity of the finally obtained clones [37].

Here, applying stringent washes and without further enrichment rounds, we were able to obtain a significant number of clones with high, specific binding signals by ELISA, with a positivity of 13–29%. For TNF, we obtained 97 clones, all of which were tested individually. For VEGF and GnGc the number of clones was much higher—around 1400 and 1600, respectively—of which we tested only 180 in each case. Notably, all the positive clones, for the three antigens, corresponded to unique sequences (with the only exception of a pair of clones for TNF), with no evident common motifs. Since for VEGF and GnGc we tested only about 12% of the total number of clones, we would expect about a 10-fold higher number of positive clones for these two antigens, most of them most likely with unique sequences.

Finally, we tested the functionality of one of the obtained anti-TNF nanobodies, in a format of a recombinant fusion protein that incorporates an albumin binding domain—a strategy used to prolong the half-life in serum of therapeutic Nbs [32]. A similar solution was employed in the design of the anti-TNF nanobody trimer ozoralizumab (approved for clinical use in Japan), which consists of two anti-human TNF Nbs and an anti-human serum albumin Nb [5]. The estimated dissociation constant for TNF was in the order of 10^7 M, which is an encouraging result considering that the anti-TNF clone chosen for

this construction showed a moderate OD signal in the phage ELISA. This design can be also extended to multimeric Nb constructions, using Nbs targeting the same antigen in a non-competitive manner to synergically increase the affinity, as with ozoralizumab.

For future development of this library, we plan to include other CDR3 lengths to enrich its conformational variability. We are also exploring other selection strategies involving different stringent conditions and numbers of selection rounds.

4. Materials and Methods

4.1. In Silico Design and Analyses

Several bioinformatics tools were used along the design process and sequence analyses. The program VMD [43] was employed for visualization and analyses of nanobody structures. The Degenerate Codon Designer online tool (https://www.novoprolabs.com/tools/degenerate-codon-designer, NovoPro, Shanghai, China, last accessed on 20 January 2023) was used for codon analyses. The CLC Genomics Workbench v.21 (QIAGEN Aarhus, Aarhus, Denmark) was employed for sequence analyses.

4.2. Library Construction

The nanobody gene library was synthesized by GenScript (NJ, USA) following the theoretical design. The genes were flanked with the restriction sites *NotI* and *NcoI* for cloning in the pMAC phagemid vector [15]. After cloning (using 4 µg of both the gene library and pMAC), the recombinant plasmids were transformed by electroporation (voltage 2.5 kV, resistance 200 Ω, capacitance 25 µF) in the *E. coli* strain SS320, previously transduced with the helper phage M13KO7 (New England Biolabs, Ipswich, MA, USA).

Transformed bacteria were recovered in SOC medium for (i) determining library diversity by seeding serial dilutions in plates containing solid 2xYT medium supplemented with 100 µg/mL ampicillin, and (ii) amplifying the recombinant phage library in 2xYT medium containing 100 µg/mL ampicillin, 50 µg/mL kanamycin, 1 mM isopropyl β-D-1-thiogalactopyranoside (IPTG) by incubating 20 h at 30 °C and 185 rpm. Phage library was precipitated from the supernatant with 0.2 volumes of a solution containing PEG/NaCl (20% polyethylene glycol 8000 and 2.5 M NaCl) at 4 °C for two hours, and aliquoted in 10% glycerol until further use [44,45].

4.3. Library Screening

Antigens. Recombinant TNF [46], VEGF [47] and GnGc [48] antigens were produced and purified in-house, at the Pharmacology Department, University of Concepcion, as previously described.

Polystyrene high-binding microtiter plates (Costar) were coated with 100 µL of the antigen (TNF, VEGF or GnGc) at 10 µg/mL (24 wells per antigen for TNF and GnGc, 12 wells for VEGF), and incubated overnight at 4 °C. After two washes with phosphate buffered saline (PBS), wells were blocked with 5% skim milk (Sigma-Aldrich, Burlington, MA, USA) in PBS (300 µL/well) overnight at 4 °C. Wells were washed twice with PBS plus 0.05% Tween 20 and incubated at room temperature (RT) for two hours with 100 µL of library phages (in a quantity 500 times bigger than the library diversity) diluted in 5% skim milk. PBS plus 0.1% Tween 20 was used to perform twenty washes (250 µL/well) of five minutes each. Four additional 5 min washes were made with glycine-HCl (0.2 M, pH 2.2), and subsequently neutralized with PBS pH 7.2 for five minutes. Afterwards, recombinant phages were obtained by competitive elution with 100 µg/mL (100 µL/well) of the antigen of interest (TNF, VEGF or GnGc) for one hour at RT and 300 rpm. The E. coli strain TG1 in exponential phase of growing was transduced with the elution and incubated at 37 °C overnight in 2xYT plates supplemented with 100 µg/mL ampicillin and 2% glucose. Deep well plates were used to amplify individual clones in a final volume of 0.5 mL. Individual phage-infected colonies were picked and used to produce phagemid particles in a 96-well plate scale to test their target recognition [49].

4.4. Binding Assays to Detect Positive Phage Clones

Polystyrene high-binding microtiter plates (Costar) were coated with 100 µL of the antigens (TNF, VEGF or GnGc) at 5 µg/mL and incubated overnight at 4 °C. After washing with PBS, wells were blocked with 3% BSA in PBS (250 µL/well) for two hours at 37 °C. Supernatants of individual clones, previously amplified, were added to the plate (50 µL of supernatant plus 50 µL BSA 3%) for one hour at 37 °C. After three washes with PBS-0.1% Tween 20, the anti-M13 antibody conjugated to horseradish peroxidase (GE Healthcare, Chicago, IL, USA) diluted 1:5000 in BSA 1% plus PBS-0.05% Tween 20 was added for one hour at 37 °C. Plates were washed with PBS 0.1% Tween 20 and the reaction was developed with a solution of o-phenylenediamine dihydrochloride (Sigma-Aldrich) and hydrogen peroxide as substrate, and stopped with 2.5 M sulfuric acid. The absorbance was measured in a Synergy/HTX multi-mode reader (BioTek Instruments, Winooski, VT, USA) at 492 nm.

4.5. Sanger Sequencing

Recombinant phagemids from selected TG1 clones were purified using the GenElute Plasmid Miniprep Kit (Sigma-Aldrich) and sequenced by Macrogen (Seoul, Korea) using the standard M13R primer. Sequences were analyzed using the CLC Genomics Workbench v. 21 (QIAGEN Aarhus, Aarhus, Denmark).

4.6. Production of Recombinant Fusion Protein

The sequence of the ABD from the *Streptococcus* sp. G protein was taken from the PDB structure 1GJS [34]. The gene coding the chimeric protein Nb-TNFB6-ABD was synthesized and cloned into the plasmid pET22b, using the *NcoI* and *XhoI* restriction sites, by GenScript (USA). The production of NbB6-ABD was carried out in two 1L Erlenmeyers containing 500 mL each of SMM9 medium, 0.05% yeast extract (Oxoid, Basingstoke, UK), and 100 µg/mL ampicillin. After inducing the gene expression with 25 µM IPTG, the culture was stirred at 100–120 rpm and incubated at 28 °C for 18 h in a shaker-incubator (ES-20/80, BOECO, Hamburg, Germany). Next, the culture was centrifuged at 10,000× *g* for 15 min at 4 °C, the pellet was re-suspended in half-diluted SMM9, and then subjected to five freeze/thaw rounds.

Soluble NbB6-ABD was obtained in the supernatant after centrifugation at 10,000× *g* for 15 min at 4 °C. The presence of the soluble fusion protein was verified by sodium dodecyl sulphate-polyacrylamide gel electrophoresis (SDS-PAGE) and Western blot.

For SDS-PAGE, protein samples were diluted in a buffer with beta-mercaptoethanol and run in 15% polyacrylamide and 3% stacking gels. Western blot assay was performed using a 0.2 µm PVDF transfer membrane (Thermo Fisher Scientific, Waltham, MA, USA) in a semi-dry transfer system Trans-Blot® Turbo™ (Bio-Rad, USA) at 0.3 A and 25 V for 30 min. After blocking with 5% skim milk in PBS, the membrane was incubated with the HRP anti-6xHis tag rabbit polyclonal antibody (ab1187, Abcam, Boston, MA, USA) diluted 1:5000 in the blocking buffer. The reaction was visualized using a DAB substrate kit (Thermo Fisher Scientific, USA).

Protein purification was performed by immobilized metal affinity chromatography (IMAC) by adding 5 mM imidazole to the equilibrium buffer (150 mM NaCl, 10 mM Na2HPO4, pH 7.7) and the initial sample diluted in the same EB. Wash and elution was done in EB by adding 25 mM and 250 mM imidazole, respectively. All fractions were monitored using the purification system BioLogic LP (BioRad, Hercules, CA, USA). Imidazole from the elution sample was removed by diafiltering against PBS (Sigma-Aldrich, Burlington, MA, USA) in 5 kDa Spin-X® UF concentrators (Corning, Corning, NY, USA). Samples were analyzed by SDS-PAGE and Western blot as described above. NbB6-ABD purity was estimated using the analytical tool of the iBright 750 Imaging System (Thermo Fisher Scientific, USA), and its concentration was determined using a Pierce BCA Protein Assay Kit (Thermo Fisher Scientific, USA).

For biotinylation of NbB6-ABD, 50 µL of Na_2CO_3/$NaHCO_3$ buffer (500 mM, pH 9.6) were mixed with 900 µL of the fusion protein (1.1 mg/mL). Next, 50 µL of biotin (H1759,

Sigma-Aldrich, USA) prepared at 10 mg/mL in dimethyl sulfoxide (Merck, Rahway, NJ, USA) was slowly added at a rate of 10 µL/min and mixed. The amounts used correspond to an 80:1 biotin/NbB6-ABD molar ratio. The reaction was incubated for 6 h at room temperature (RT) under stirring. Free biotin was removed by dialysis (88244, Thermo Fisher Scientific, Waltham, MA, USA) against 4 L of 1X PBS overnight at RT.

4.7. Binding Assay for the Fusion Protein

Binding of biotinylated NbB6-ABD to TNF and HSA was determined by ELISA, using streptavidin-HRP (DY998, Biotechne R&D Systems, USA) for detection. Plate wells (2592, Corning, USA) were coated with 1µg of TNF or HSA in carbonate buffer pH 9.6 overnight at 4 °C, then washed three times with 0.3 mL of PBS 1X 0.1% Tween 20 (PBST) and blocked with 3% BSA or 5% milk in 1X PBS for 1 h at room temperature. Wells were then washed three times with 0.3 mL PBST and incubated for 1h at RT with 100 µL of different concentrations of the biotinylated protein. Wells were again washed three times with 0.3 mL PBST and incubated for 1 h at RT with 100 µL streptavidin-HRP (1:200, DY998, Biotechne R&D Systems, USA). They were then washed four times with 0.3 mL PBST, revealed with 100 µL of 3,3′,5,5,5′-Tetramethylbenzidine (TMB) (DY999, Biotechne R&D Systems, USA), and stopped with 50 µL of 2N H2SO4. Binding signals were read at 450 nm in a plate reader (BOECO, Germany). KD estimation was carried out followed the method and fitting function described in [35]. Linear regression analysis using this function was performed using the MyCurveFit web server (https://mycurvefit.com/, last accessed on 20 March 2023).

Supplementary Materials: The following supporting information can be downloaded at: https://www.mdpi.com/article/10.3390/molecules28093708/s1, Figure S1: Map of the designed pMAC phagemid vector.

Author Contributions: Conceptualization, O.S.-R. and E.M.; methodology, M.A.C., A.G.-P., Y.S.-R., M.R.-C., F.C.-C., O.S.-R. and E.M.; investigation, M.A.C., Y.S.-R., A.G.-P., J.S.-U., M.R.-C., M.S.-A., N.C.P., F.C.-C., O.S.-R. and E.M.; writing—original draft preparation, M.A.C., A.G.-P., Y.S-R., J.S.-U., M.S.-A. and E.M.; writing—review and editing, M.A.C., A.G.-P., M.R.-C., N.C.P., F.C.-C., O.S.-R. and E.M.; supervision, project administration and funding acquisition, O.S.-R. and E.M. All authors have read and agreed to the published version of the manuscript.

Funding: This research was funded by MINCIENCIAS, MINEDUCACIÓN, MINCIT and ICETEX through the Program NanoBioCancer (Cod. FP44842-211-2018, project number 58676). M.A.C., F.C.-C. and O.S.-R. thank the University of Concepción for its support. A.G.-P. and E.M. thank the support from the University of Medellin.

Institutional Review Board Statement: Not applicable.

Informed Consent Statement: Not applicable.

Data Availability Statement: The data presented in this study are contained in the article tables and supplementary materials.

Conflicts of Interest: The authors declare no conflict of interest.

Sample Availability: Not applicable. The phagemids and molecules used in this work were either purchased or produced in limited amount only to perform the reported experiments.

References

1. Hamers-Casterman, C.; Atarhouch, T.; Muyldermans, S.; Robinson, G.; Hammers, C.; Songa, E.B.; Bendahman, N.; Hammers, R. Naturally Occurring Antibodies Devoid of Light Chains. *Nature* **1993**, *363*, 446–448. [CrossRef] [PubMed]
2. Valdés-Tresanco, M.S.; Valdés-Tresanco, M.E.; Molina-Abad, E.; Moreno, E. NbThermo: A New Thermostability Database for Nanobodies. *Database* **2023**, baad021. [CrossRef] [PubMed]
3. Hassanzadeh-Ghassabeh, G.; Devoogdt, N.; De Pauw, P.; Vincke, C.; Muyldermans, S. Nanobodies and Their Potential Applications. *Nanomedicine* **2013**, *8*, 1013–1026. [CrossRef] [PubMed]
4. Morrison, C. Nanobody Approval Gives Domain Antibodies a Boost. *Nat. Rev. Drug. Discov.* **2019**, *18*, 485–487. [CrossRef]
5. Keam, S.J. Ozoralizumab: First Approval. *Drugs.* **2023**, *83*, 87–92. [CrossRef]

6. Muyldermans, S. A Guide to: Generation and Design of Nanobodies. *FEBS. J.* **2021**, *288*, 2084–2102. [CrossRef]
7. Valdés-Tresanco, M.S.; Molina-Zapata, A.; Pose, A.G.; Moreno, E. Structural Insights into the Design of Synthetic Nanobody Libraries. *Molecules* **2022**, *27*, 2198. [CrossRef]
8. Moutel, S.; Bery, N.; Bernard, V.; Keller, L.; Lemesre, E.; de Marco, A.; Ligat, L.; Rain, J.-C.; Favre, G.; Olichon, A.; et al. NaLi-H1: A Universal Synthetic Library of Humanized Nanobodies Providing Highly Functional Antibodies and Intrabodies. *Elife* **2016**, *5*, e16228. [CrossRef]
9. McMahon, C.; Baier, A.S.; Pascolutti, R.; Wegrecki, M.; Zheng, S.; Ong, J.X.; Erlandson, S.C.; Hilger, D.; Rasmussen, S.G.F.; Ring, A.M.; et al. Yeast Surface Display Platform for Rapid Discovery of Conformationally Selective Nanobodies. *Nat. Struct. Mol. Biol.* **2018**, *25*, 289–296. [CrossRef]
10. Zimmermann, I.; Egloff, P.; Hutter, C.A.; Arnold, F.M.; Stohler, P.; Bocquet, N.; Hug, M.N.; Huber, S.; Siegrist, M.; Hetemann, L.; et al. Synthetic Single Domain Antibodies for the Conformational Trapping of Membrane Proteins. *Elife* **2018**, *7*, e34317. [CrossRef]
11. Sevy, A.M.; Chen, M.-T.; Castor, M.; Sylvia, T.; Krishnamurthy, H.; Ishchenko, A.; Hsieh, C.-M. Structure- and Sequence-Based Design of Synthetic Single-Domain Antibody Libraries. *Protein. Eng. Des. Selection.* **2020**, *33*, gzaa028. [CrossRef]
12. Zimmermann, I.; Egloff, P.; Hutter, C.A.J.; Kuhn, B.T.; Bräuer, P.; Newstead, S.; Dawson, R.J.P.; Geertsma, E.R.; Seeger, M.A. Generation of Synthetic Nanobodies against Delicate Proteins. *Nat. Protoc.* **2020**, *15*, 1707–1741. [CrossRef]
13. Zhao, Y.; Wang, Y.; Su, W.; Li, S. Construction of Synthetic Nanobody Library in Mammalian Cells by DsDNA-Based Strategies. *Chem. BioChem.* **2021**, *22*, 2957–2965. [CrossRef]
14. Chen, X.; Gentili, M.; Hacohen, N.; Regev, A. A Cell-Free Nanobody Engineering Platform Rapidly Generates SARS-CoV-2 Neutralizing Nanobodies. *Nat. Commun.* **2021**, *12*, 5506. [CrossRef]
15. Moreno, E.; Valdés-Tresanco, M.S.; Molina-Zapata, A.; Sánchez-Ramos, O. Structure-Based Design and Construction of a Synthetic Phage Display Nanobody Library. *BMC. Res. Notes.* **2022**, *15*, 124. [CrossRef]
16. De Genst, E.; Silence, K.; Decanniere, K.; Conrath, K.; Loris, R.; Kinne, J.; Muyldermans, S.; Wyns, L. Molecular Basis for the Preferential Cleft Recognition by Dromedary Heavy-Chain Antibodies. *Proc. Natl. Acad. Sci. USA* **2006**, *103*, 4586–4591. [CrossRef]
17. Uchański, T.; Pardon, E.; Steyaert, J. Nanobodies to Study Protein Conformational States. *Curr. Opin. Struct. Biol.* **2020**, *60*, 117–123. [CrossRef]
18. Shi, Z.; Li, X.; Wang, L.; Sun, Z.; Zhang, H.; Chen, X.; Cui, Q.; Qiao, H.; Lan, Z.; Zhang, X.; et al. Structural Basis of Nanobodies Neutralizing SARS-CoV-2 Variants. *Structure* **2022**, *30*, 707–720.e5. [CrossRef]
19. Conrath, K.E.; Lauwereys, M.; Galleni, M.; Matagne, A.; Frère, J.-M.; Kinne, J.; Wyns, L.; Muyldermans, S. β-Lactamase Inhibitors Derived from Single-Domain Antibody Fragments Elicited in the *Camelidae*. *Antimicrob. Agents. Chemother.* **2001**, *45*, 2807–2812. [CrossRef]
20. Dumoulin, M.; Conrath, K.; Van Meirhaeghe, A.; Meersman, F.; Heremans, K.; Frenken, L.G.J.; Muyldermans, S.; Wyns, L.; Matagne, A. Single-Domain Antibody Fragments with High Conformational Stability. *Protein. Sci.* **2002**, *11*, 500–515. [CrossRef]
21. Saerens, D.; Pellis, M.; Loris, R.; Pardon, E.; Dumoulin, M.; Matagne, A.; Wyns, L.; Muyldermans, S.; Conrath, K. Identification of a Universal VHH Framework to Graft Non-Canonical Antigen-Binding Loops of Camel Single-Domain Antibodies. *J. Mol. Biol.* **2005**, *352*, 597–607. [CrossRef] [PubMed]
22. Wei, G.; Meng, W.; Guo, H.; Pan, W.; Liu, J.; Peng, T.; Chen, L.; Chen, C.-Y. Potent Neutralization of Influenza A Virus by a Single-Domain Antibody Blocking M2 Ion Channel Protein. *PLoS ONE* **2011**, *6*, e28309. [CrossRef] [PubMed]
23. Yan, J.; Li, G.; Hu, Y.; Ou, W.; Wan, Y. Construction of a Synthetic Phage-Displayed Nanobody Library with CDR3 Regions Randomized by Trinucleotide Cassettes for Diagnostic Applications. *J. Transl. Med.* **2014**, *12*, 343. [CrossRef] [PubMed]
24. Chi, X.; Liu, X.; Wang, C.; Zhang, X.; Li, X.; Hou, J.; Ren, L.; Jin, Q.; Wang, J.; Yang, W. Humanized Single Domain Antibodies Neutralize SARS-CoV-2 by Targeting the Spike Receptor Binding Domain. *Nat. Commun.* **2020**, *11*, 4528. [CrossRef]
25. Vincke, C.; Loris, R.; Saerens, D.; Martinez-Rodriguez, S.; Muyldermans, S.; Conrath, K. General Strategy to Humanize a Camelid Single-Domain Antibody and Identification of a Universal Humanized Nanobody Scaffold. *J. Biol. Chem.* **2009**, *284*, 3273–3284. [CrossRef]
26. Cornish-Bowden, A. Nomenclature for Incompletely Specified Bases in Nucleic Acid Sequences: Rcommendations 1984. *Nucleic Acids Res.* **1985**, *13*, 3021–3030. [CrossRef]
27. Hoogenboom, H.R.; Griffiths, A.D.; Johnson, K.S.; Chiswell, D.J.; Hudson, P.; Winter, G. Multi-Subunit Proteins on the Surface of Filamentous Phage: Methodologies for Displaying Antibody (Fab) Heavy and Light Chains. *Nucleic Acids Res.* **1991**, *19*, 4133–4137. [CrossRef]
28. van Loo, G.; Bertrand, M.J.M. Death by TNF: A Road to Inflammation. *Nat. Rev. Immunol.* **2022**, *15*, 1–15. [CrossRef]
29. Leone, G.M.; Mangano, K.; Petralia, M.C.; Nicoletti, F.; Fagone, P. Past, Present and (Foreseeable) Future of Biological Anti-TNF Alpha Therapy. *J. Clin. Med.* **2023**, *12*, 1630. [CrossRef]
30. Ghalehbandi, S.; Yuzugulen, J.; Pranjol, M.Z.I.; Pourgholami, M.H. The Role of VEGF in Cancer-Induced Angiogenesis and Research Progress of Drugs Targeting VEGF. *Eur. J. Pharmacol.* **2023**, 175586. [CrossRef]
31. Arezumand, R.; Alibakhshi, A.; Ranjbari, J.; Ramazani, A.; Muyldermans, S. Nanobodies As Novel Agents for Targeting Angiogenesis in Solid Cancers. *Front. Immunol.* **2017**, *8*, 1746. [CrossRef]
32. Dennis, M.S.; Zhang, M.; Meng, Y.G.; Kadkhodayan, M.; Kirchhofer, D.; Combs, D.; Damico, L.A. Albumin Binding as a General Strategy for Improving the Pharmacokinetics of Proteins. *J. Biolo. Chem.* **2002**, *277*, 35035–35043. [CrossRef]

33. Jonsson, A.; Dogan, J.; Herne, N.; Abrahmsen, L.; Nygren, P.-A. Engineering of a Femtomolar Affinity Binding Protein to Human Serum Albumin. *Protein Eng. Des. Sel.* **2008**, *21*, 515–527. [CrossRef]
34. Johansson, M.U.; Frick, I.-M.; Nilsson, H.; Kraulis, P.J.; Hober, S.; Jonasson, P.; Linhult, M.; Nygren, P.-Å.; Uhlén, M.; Björck, L.; et al. Structure, Specificity, and Mode of Interaction for Bacterial Albumin-Binding Modules. *J. Biol. Chem.* **2002**, *277*, 8114–8120. [CrossRef]
35. Eble, J.A. Titration ELISA as a Method to Determine the Dissociation Constant of Receptor Ligand Interaction. *J. Vis. Exp.* **2018**, *15*, 57334. [CrossRef]
36. Lakzaei, M.; Rasaee, M.J.; Fazaeli, A.A.; Aminian, M. A Comparison of Three Strategies for Biopanning of Phage-scFv Library against Diphtheria Toxin. *J. Cell. Physiol.* **2019**, *234*, 9486–9494. [CrossRef]
37. Jaroszewicz, W.; Morcinek-Orłowska, J.; Pierzynowska, K.; Gaffke, L.; Węgrzyn, G. Phage Display and Other Peptide Display Technologies. *FEMS Microbiol. Rev.* **2022**, *46*, fuab052. [CrossRef]
38. Scarrone, M.; González-Techera, A.; Alvez-Rosado, R.; Delfin-Riela, T.; Modernell, Á.; González-Sapienza, G.; Lassabe, G. Development of Anti-Human IgM Nanobodies as Universal Reagents for General Immunodiagnostics. *New Biotechnol.* **2021**, *64*, 9–16. [CrossRef]
39. Roshan, R.; Naderi, S.; Behdani, M.; Cohan, R.A.; Ghaderi, H.; Shokrgozar, M.A.; Golkar, M.; Kazemi-Lomedasht, F. Isolation and Characterization of Nanobodies against Epithelial Cell Adhesion Molecule as Novel Theranostic Agents for Cancer Therapy. *Mol. Immunol.* **2021**, *129*, 70–77. [CrossRef]
40. Kazemi-Lomedasht, F.; Behdani, M.; Bagheri, K.P.; Habibi-Anbouhi, M.; Abolhassani, M.; Arezumand, R.; Shahbazzadeh, D.; Mirzahoseini, H. Inhibition of Angiogenesis in Human Endothelial Cell Using VEGF Specific Nanobody. *Mol. Immunol.* **2015**, *65*, 58–67. [CrossRef]
41. Wu, M.; Tu, Z.; Huang, F.; He, Q.; Fu, J.; Li, Y. Panning Anti-LPS Nanobody as a Capture Target to Enrich Vibrio Fluvialis. *Biochem. Biophys. Res. Commun.* **2019**, *512*, 531–536. [CrossRef] [PubMed]
42. Lunder, M.; Bratkovič, T.; Urleb, U.; Kreft, S.; Štrukelj, B. Ultrasound in Phage Display: A New Approach to Nonspecific Elution. *Biotechniques* **2008**, *44*, 893–900. [CrossRef] [PubMed]
43. Humphrey, W.; Dalke, A.; Schulten, K. VMD: Visual Molecular Dynamics. *J. Mol. Graph.* **1996**, *14*, 33–38. [CrossRef] [PubMed]
44. Tonikian, R.; Zhang, Y.; Boone, C.; Sidhu, S.S. Identifying Specificity Profiles for Peptide Recognition Modules from Phage-Displayed Peptide Libraries. *Nat. Protoc.* **2007**, *2*, 1368–1386. [CrossRef]
45. Chen, G.; Sidhu, S.S. Design and Generation of Synthetic Antibody Libraries for Phage Display. In *Monoclonal Antibodies: Methods and Protocols*; Ossipow, V., Fischer, N., Eds.; Humana Press: Totowa, NJ, USA, 2014; pp. 113–131.
46. Contreras, M.A.; Macaya, L.; Neira, P.; Camacho, F.; González, A.; Acosta, J.; Montesino, R.; Toledo, J.R.; Sánchez, O. New Insights on the Interaction Mechanism of RhTNFα with Its Antagonists Adalimumab and Etanercept. *Biochem. J.* **2020**, *477*, 3299–3311. [CrossRef]
47. Parra, N.C.; Mansilla, R.; Aedo, G.; Vispo, N.S.; González-Horta, E.E.; González-Chavarría, I.; Castillo, C.; Camacho, F.; Sánchez, O. Expression and Characterization of Human Vascular Endothelial Growth Factor Produced in SiHa Cells Transduced with Adenoviral Vector. *Protein J.* **2019**, *38*, 693–703. [CrossRef]
48. Beltrán-Ortiz, C.E.; Starck-Mendez, M.F.; Fernández, Y.; Farnós, O.; González, E.E.; Rivas, C.I.; Camacho, F.; Zuñiga, F.A.; Toledo, J.R.; Sánchez, O. Expression and Purification of the Surface Proteins from Andes Virus. *Protein. Expr. Purif.* **2017**, *139*, 63–70. [CrossRef]
49. Baek, H.; Suk, K.; Kim, Y.; Cha, S. An Improved Helper Phage System for Efficient Isolation of Specific Antibody Molecules in Phage Display. *Nucleic. Acids. Res.* **2002**, *30*, e18. [CrossRef]

ANEXO 2.

molecules

MDPI

Article

Selecting Nanobodies Specific for the Epidermal Growth Factor from a Synthetic Nanobody Library

Yunier Serrano-Rivero [1,†], Julieta Salazar-Uribe [1,†], Marcela Rubio-Carrasquilla [1], Frank Camacho-Casanova [2], Oliberto Sánchez-Ramos [2], Alaín González-Pose [1,*] and Ernesto Moreno [1,*]

[1] Faculty of Basic Sciences, University of Medellin, Medellin 050026, Colombia; 0905yunierserrano@gmail.com (Y.S.-R.); julieta.salazaru@gmail.com (J.S.-U.); marcelaru@yahoo.com (M.R.-C.)
[2] Pharmacology Department, School of Biological Sciences, University of Concepcion, Concepcion 4070386, Chile; fcamacho@udec.cl (F.C.-C.); osanchez@udec.cl (O.S.-R.)
* Correspondence: agonzalezp@udemedellin.edu.co (A.G.-P.); emoreno@udemedellin.edu.co (E.M.)
† These authors contributed equally to this work.

Abstract: The epidermal growth factor (EGF) is one of the most critical ligands of the EGF receptor (EGFR), a well-known oncogene frequently overexpressed in cancerous cells and an important therapeutic target in cancer. The EGF is the target of a therapeutic vaccine aimed at inducing an anti-EGF antibody response to sequester this molecule from serum. However, strikingly, very few investigations have focused on EGF immunotargeting. Since the use of nanobodies (Nbs) for EGF neutralization may be an effective therapeutic strategy in several types of cancer, in this study, we decided to generate anti-EGF Nbs from a recently constructed, phage-displaying synthetic nanobody library. To our knowledge, this is the first attempt to obtain anti-EGF Nbs from a synthetic library. By applying a selection strategy that uses four different sequential elution steps along with three rounds of selection, we obtained four different EGF-specific Nb clones, and also tested their binding capabilities as recombinant proteins. The obtained results are very encouraging and demonstrate the feasibility of selecting nanobodies against small antigens, such as the EGF, from synthetic libraries.

Keywords: epidermal growth factor; nanobody; synthetic library; phage display

Citation: Serrano-Rivero, Y.; Salazar-Uribe, J.; Rubio-Carrasquilla, M.; Camacho-Casanova, F.; Sánchez-Ramos, O.; González-Pose, A.; Moreno, E. Selecting Nanobodies Specific for the Epidermal Growth Factor from a Synthetic Nanobody Library. *Molecules* **2023**, *28*, 4043. https://doi.org/10.3390/molecules28104043

Academic Editor: Jahir Orozco Holguín

Received: 24 March 2023
Revised: 8 May 2023
Accepted: 9 May 2023
Published: 12 May 2023

1. Introduction

The human epidermal growth factor (EGF) is a small protein of 53 amino acids, whose fold is structured by three disulfide bonds. It demonstrates potent biological activity in vitro and in vivo by stimulating cell and organ proliferation [1]. Furthermore, the EGF is one of the most critical ligands of the EGF receptor (EGFR) [2], a well-known oncogene frequently overexpressed in cancerous cells, causing cell-cycle deregulation, exacerbated angiogenesis, apoptosis blockade, and tumoral cell migration [3]. It was found very early that EGF detection in carcinomas is closely related to high levels of malignancy [4]. Indeed, EGF signaling is essential for tumor-cell growth for several types of cancer [5,6], and it is linked to the epithelial–mesenchymal transition, in which epithelial cells are transformed into fibroblast-like phenotypes with high motility and invasive properties, contributing to cancer metastasis [7,8]. Therefore, along with the EGFR, the EGF is also considered a potential target for cancer therapy.

The prevention of cancer using our own immune system against self-antigens is possible due to the observed natural self-reactivity of immune cells against autologous antigens [9]. In the case of the EGF, a self-antibody response against this molecule would diminish the serum availability of EGF, thus reducing EGFR activation and, in consequence, cancer-cell proliferation. Following this active therapeutic approach, a novel anti-EGF vaccine named CIMAvax-EGF was developed. This vaccine is based on a chemical conjugate of EGF and the protein P64k from Neisseria meningitidis, adjuvanted with Montanide ISA

51 VG [10]. The main function of this immunogen is to break the EGF's self-tolerance, inducing an anti-EGF antibody response, which dramatically reduces the EGF concentration in serum [11]. More than 10 clinical trials have been completed with the therapeutic cancer vaccine CIMAvax-EGF, including phase II, III, and IV trials, demonstrating safety, long-term immunogenicity and a significant effect on survival, with several patients achieving long-term survival after vaccination [10].

An alternative, passive-therapy-based approach for sequestering EGF would involve different antibody formats, particularly, nanobodies (Nbs), which are single-domain antibody fragments derived from the heavy chain antibodies found in camelids [12]. Nbs have several advantageous properties over classical antibodies: small size, high stability and solubility, and easy tailoring for multiple applications. Furthermore, they can achieve high affinities despite the fact that their monomeric binding region displays only three hypervariable loops. Nbs have become a relevant class of biomolecules with multiple applications, especially as diagnostic tools and promising therapeutic agents in cancer and other diseases [13]. They are obtained mostly from immune libraries, constructed from animal immunization with the target antigen [14]. In recent years, however, synthetic nanobody libraries have gained ground as alternative Nb sources, offering several advantages, such as lower costs and faster results [15]. As these libraries are not generated for a specific antigen, they can be used for the selection of nanobodies against numerous antigens, including those with high toxicity or low immunogenicity [15].

A successful example of the use of nanobodies to sequester a circulating cytokine is ozoralizumab—a trivalent anti-TNF nanobody, which was recently approved in Japan for the treatment of rheumatoid arthritis [16]. Strikingly, despite the proven potential of EGF as a cancer target, there are very few investigations focused on EGF immunotargeting. A recent work by Guardiola et al. reported the generation of anti-EGF Nbs using an immune library from alpaca, and showed their ability to block EGFR phosphorylation and produce antitumor effects in vitro [17,18]. To our knowledge, these were the only anti-EGF nanobodies reported before the present study.

Since the use of Nbs for EGF neutralization may be an effective therapeutic strategy in several types of cancer, in this study, we decided to generate anti-EGF nanobodies from our recently constructed synthetic nanobody library, based on the phage-display platform [19]. After three selection rounds, each of which used four different serial elution methods, we obtained about forty positive recombinant phage clones. Twenty of these clones were sequenced, resulting in four different amino-acid sequences. These three distinct nanobodies were produced in BL21 (DE3) and purified by ion exchange (IEC) and immobilized metal affinity (IMAC) chromatography, and their ability to bind to EGF was demonstrated.

2. Results and Discussion

2.1. Design and Production of a Recombinant EGF Protein

Firstly, we designed and produced, in-house, a recombinant EGF (rEGF) protein with two tags (SV5 and 6xHis) that confer a more versatile functionality to this molecule (Figure 1a). The rEGF gene was cloned into the bacterial expression vector pET22b (Figure 1b) under the control of strong bacteriophage T7 transcriptional and translational signals, which allow the production of large amounts of recombinant proteins upon induction. The inclusion of the PelB-signal peptide before the rEGF gene allows secretion into the periplasmic compartment, in order to obtain a protein of interest that is soluble after bacterial lysis. The bacterial system (*E. coli* BL21 (DE3)) successfully produced the rEGF, as expected (Figure 1c). After cell lysis, a rEGF fraction remained soluble (Figure 1d), and it was successfully purified by IMAC and IEC (Figure 1e). Although part of the recombinant protein was lost in the different chromatographic steps, we were able to obtain a sufficient amount, with more than 90% purity. The biological activity of the rEGF was assessed in vitro using the human cell line A431, characterized by high EGFR overexpression [20]. The cells were treated with different rEGF concentrations, ranging from 100 pm to 100 nM. Similarly as found in early studies with EGF [21], the lowest applied rEGF concentration

(100 pM) stimulated cell growth in cultures with a low concentration (0.5%) of fetal bovine serum (FBS). This effect vanished with higher rEGF concentrations. On the other hand, the expected inhibitory effect of high rEGF concentrations (10 and 100 nM) [21] was markedly observed in A431 cells cultured with 5% FBS (Figure 1f). Having proven the functionality of the in-house-produced rEGF (hereafter called EGF), we proceeded to select EGF binders from our synthetic nanobody library.

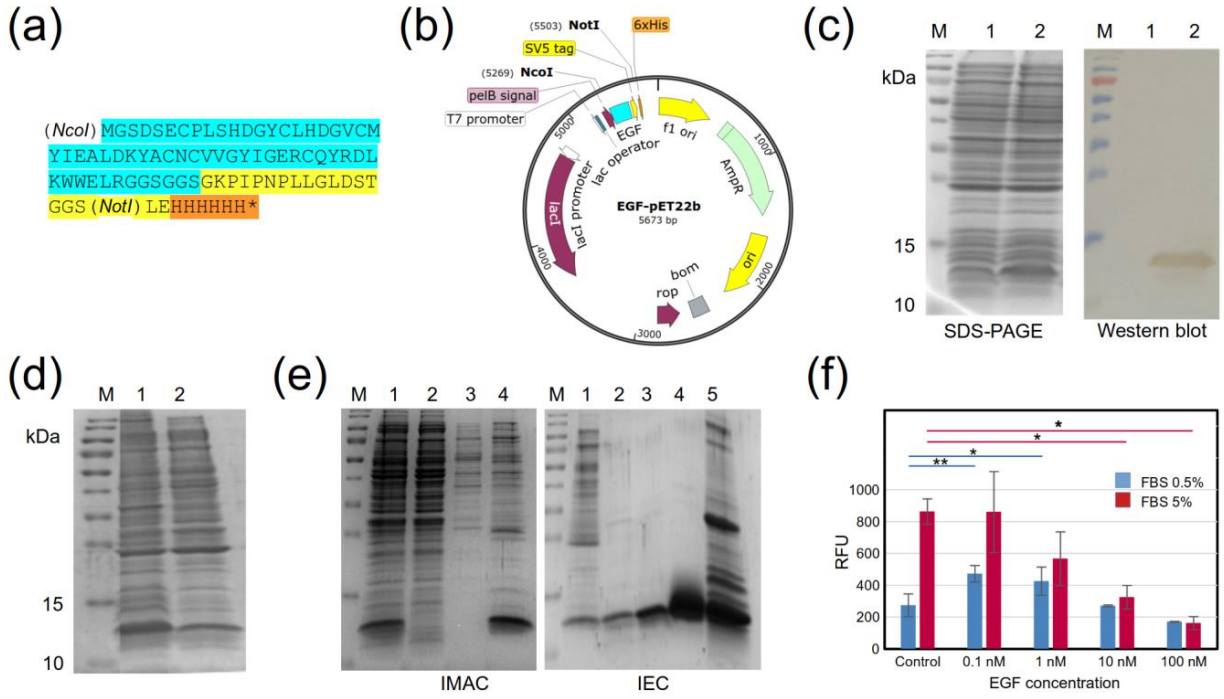

Figure 1. Production of (rEGF) in *E. coli*. (**a**) Amino-acid sequence of rEGF with C-terminal tags: cyan—EGF, yellow—SV5 tag, orange—6xHis tag. (**b**) Scheme of the pET22b-rEGF expression vector. (**c**) SDS-PAGE and Western blot of the production of rEGF in BL21 (DE3). The rEGF was identified using an anti-His tag monoclonal antibody conjugated to HRP. M: molecular-weight marker, Trident Prestained Protein Ladder GTX50875 (GeneTex, USA), 1: untransformed BL21, 2: BL21 transformed with pET22b-rEGF. (**d**) SDS-PAGE of the rEGF-soluble fraction obtained by cell lysis using several freezing/thawing rounds. M: molecular-weight marker, 1: total fraction of BL21 transformed with pET22b-hEGF, 2: soluble fraction of BL21 transformed with pET22b-hEGF. (**e**) SDS-PAGE of the rEGF-purification process. Left panel: first purification stage by IMAC. M: molecular-weight marker, 1: initial sample, 2: unbound proteins, 3: wash (40 mM imidazole), 4: elution (250 mM imidazole). Right panel: second purification stage with IEC. M: molecular-weight marker, 1: initial sample from IMAC elutions, 2, 3, and 4: unbound proteins, 5: elution from the anionic exchanger Bio-Scale Mini Macro-Prep High Q Cartridge (BioRad, Hercules, CA, USA). (**f**) In vitro evaluation of rEGF biological activity in A431 cells. Two FBS concentrations were used: (0.5%—blue bars; and 5%—red bars). Measurements were performed in triplicate. Stars indicate statistically significant differences between experimental conditions (* $p < 0.05$, ** $p < 0.005$).

2.2. Selection of EGF-Binding Phages

As a small protein, EGF presents a relatively small surface area for antibody/nanobody recognition, which presents a challenge in obtaining nanobodies from a synthetic library. We decided to implement a screening procedure based on three selection rounds, each of which was composed of four different types of elution, performed sequentially, using the following: (i) triethylamine (TEA—1), (ii) glycine-HCl (Gly—2), (iii) ultrasound (UltS—3), and (iv) the addition of the TG1 strain to previously washed wells (TG1—4). The aim was to recover binders with different physico-chemical properties that would not be eluted with TEA (a commonly used elution buffer), followed by binders not eluted either with Gly, and

so on. After each round, the phages collected from each elution were pulled together for amplification, except for the final round, in which the phages from the different elutions were amplified separately.

The use of successive rounds of selection against the antigen of interest is intended to increase the proportion of antigen-specific phages [14,22]. As in this study, Guardiola et al. performed three selection rounds to obtain EGF-specific phages from an alpaca immune library [17]. In most cases, the phages bound to the target molecule were collected using a single method, which can either be triethylamine (e.g., [17,23–25]), glycine [26–28], ultrasound (albeit to a lesser extent, such as in [29,30]) and, rarely, infection by the direct addition of cells to the wells [29]. The use of a single elution method may limit phage collection, losing a fraction of phages that remain strongly bound to the immobilized target molecule in the wells. In contrast, in our study, we used four sequential elutions, recovering significant amounts of phages in each of them.

With the aim of optimizing the screening of clones by ELISA for binding to EGF, we first tested groups of selected clones, each of which consisted of four individual clones (all belonging to the same elution). We evaluated 17, 15, 16, and 16 groups from the TEA, Gly, UltS, and TG1 elutions, respectively. A plate blocked with skimmed milk was included to identify mock-phages. Thus, this assay allowed us to select groups with a high EGF binding signal and low background. Figure 2a shows the ELISA results from this screening. Following the criterion defined in the Methods, a total of 24 positive groups were obtained, which were distributed as follows: TEA-14, Gly-5, UltS-1, and TG1-4. Subsequently, the individual clones from these 24 groups were tested in the same way (Figure 2b), with one important addition. As the recombinant EGF molecule has a C-terminal tail containing SV5 and His tags, we added a third plate coated with a non-related protein with the same C-terminal tail, to discard anti-tag phages. Of the 96 individual clones, 38 met the positivity criteria, and they were distributed by elution, as follows: TEA-16, Gly-1, UltS-1, and TG1-11. A few of these clones, mostly from the TG1 elution, also showed strong anti-tag binding (Figure 2b).

2.3. Sequences of Selected Clones

Most of the EGF-positive phage clones (21 clones, discarding only a few weaker binders), as well as several of the C-tail tag binders were sent for sequencing. Figure 3 shows the sequences obtained for the CDRs (the framework is common to all the nanobodies derived from the library). The 21 EGF-positive clones corresponded to only four unique Nb sequences, and 17 of the clones were identical. These results are comparable to those obtained by Guardiola et al., who recovered six different anti-EGF clones from an immune library [17].

The use of four different elutions for binder recovery yielded intriguing results. The group of 17 identical clones was composed of phages from three elutions (TEA-8; Gly-2; TG1-7); the identical A8-1/B3-1 pair of clones and the single C10-1 clone were obtained from the TEA elution, whereas the single clone, D6-4, was recovered from the TG1 elution. The mixed origin of the repeated clones obtained after the third selection round might have been associated with the pulling of the four elutions from rounds 1 and 2 for amplification and subsequent inputs for rounds 2 and 3, respectively. On the other hand, the unique D6-4 clone was the result of the sequential application of the four types of elution; otherwise, it would not have been recovered. The five anti-tag phage clones in fact corresponded to two unique Nb sequences. In future screenings, it would be interesting, and possibly more productive, to keep each elution separately through all the selection rounds.

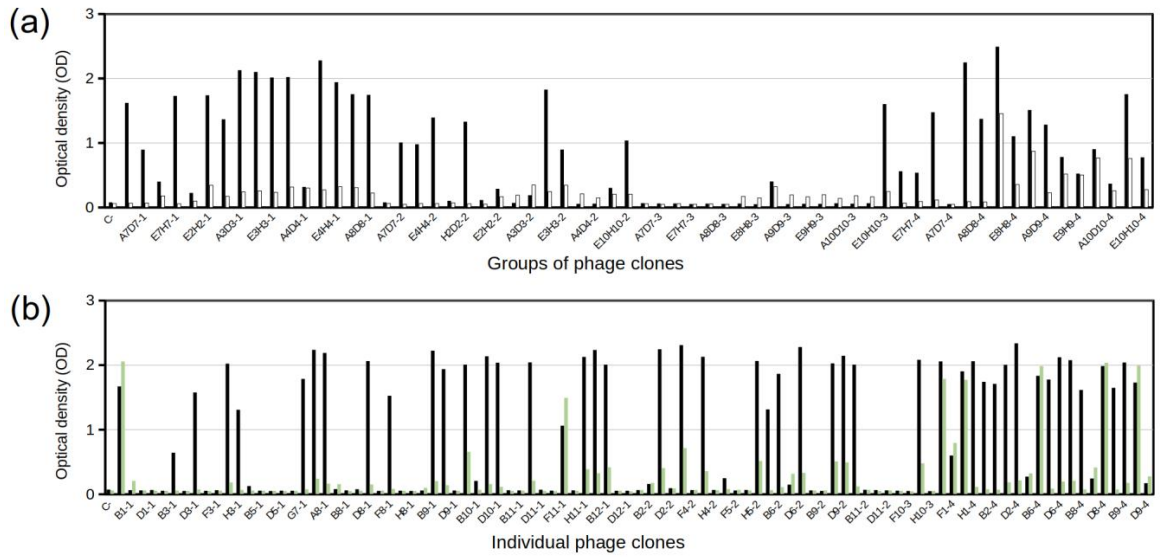

Figure 2. ELISA screening of selected phage clones for binding to EGF. (**a**) Identification of phage groups that bind to EGF (black bars). White bars correspond to background (milk) signals. (**b**) Positive phage groups were individualized and re-screened. Green bars correspond to binding to an unrelated nanobody with the same C-terminal tail as the recombinant EGF. Positivity was defined as $OD_{450nm} \geq 0.8$ for EGF binding, and an OD_{450nm} for milk or an unrelated tagged protein three or more times lower than for EGF. The last number in clone names refers to the type of elution: 1—TEA, 2—Gly, 3—UltS—3, 4—TG1.

Clone		CDR1	CDR2	CDR3
A11-2		SGDHNNQYNKFALG	AISSNGGK	ARRYQYETHRS
A2-4	★	. . . . .	. . . . .	. . . . .
C9-1		. . . . .	. . . . .	. . . . .
C10-1	★	. . . RQYH . SV . . .	. . . TG . . .	. TQSGSGY . . Y
A8-1	★	. . NS . Y . . PH . D . .	. . . . G . . R	. VGSRTRNY . Y
B3-1		. . NS . Y . . PH . D . .	. . . . G . . R	. VGSRTRNY . Y
D6-4	★	. . TRRYK . . V . D . .	. . . TG . . R	. . . TNNANF . Y
D8-4	Tag	. . NNSYR . . R . D . .	. . . LR . . R	. MGNR . RN . D .
F11-1		. . NNSYR . . R . D . .	. . . LR . . R	. MGNR . RN . D .
A1-1		. . NRKFN . YN . D . .	. . D . S . . I	. T . TGSAYFGY
B6-4	Tag	. . NRKFN . YN . D . .	. . D . S . . I	. T . TGSAYFGY
C9-4		. . NRKFN . YN . D . .	. . D . S . . I	. T . TGSAYFGY

Framework sequence:
QVQLVESGGGSVQAGGSLRLSCTAS<u>XXXXXXXXXXXXXX</u>WFRQAPGQEREAVA<u>XXXXXXXXX</u>T
YYADSVKGRFTISRDNAKNTVTLQMNNLKPEDTAIYYCAA<u>XXXXXXXXXXX</u>WGQGTQVTVS

Figure 3. CDR amino-acid sequences of selected clones. Red stars are for EGF binders, while "Tag" in blue is for tag-positive clones. Dots indicate the presence of the same amino acid as in the first sequence in the alignment. The first group of three clones (A11-2, A2-4, and C9-1), from different elutions, are representative of the group of 17 identical clones. The common framework sequence supporting the library is from the camelid nanobody cAbBCII10 [31]). CDRs are underlined, with their amino acids represented with "X".

2.4. Production of the Four Recombinant Anti-EGF Nanobodies

The four anti-EGF Nbs with different sequences (clones A8-1, A11-2, C10-1, and D6-4) were expressed as recombinant proteins by cloning their genes into pET22b and producing

them in *E. coli* BL21 (DE3), which is a commonly used system for nanobody production, with a high level of success [32–34]. The recombinant-protein production behaved similarly for the four nanobodies. Upon the induction with IPTG, a majority protein band of approximately 16 kDa was observed in the four induced cultures, while it was absent in the negative control. A Western blot corroborated the observation that all four bands corresponded to recombinant nanobodies (Figure 4a). The design incorporating the signal-peptide PelB allowed the secretion of the produced proteins into the bacterial periplasm, producing a large amount of soluble protein. After production, the four nanobodies were purified by combining two chromatographic methods: ion-exchange chromatography (IEC) followed by immobilized metal-affinity chromatography (IMAC). Usually, a single IMAC purification step is not sufficient to obtain Nbs with a high degree of purity; therefore, at least one additional molecular exclusion or IEC is also used [35], being the combination of IMAC and molecular exclusion chromatography the most commonly used method for Nb purification [25,34,36]. Here, we decided to first carry out an IEC step, which removed more than 50% of the contaminating proteins, followed by IMAC, which yielded recombinant Nbs with about 90% purity (Figure 4b).

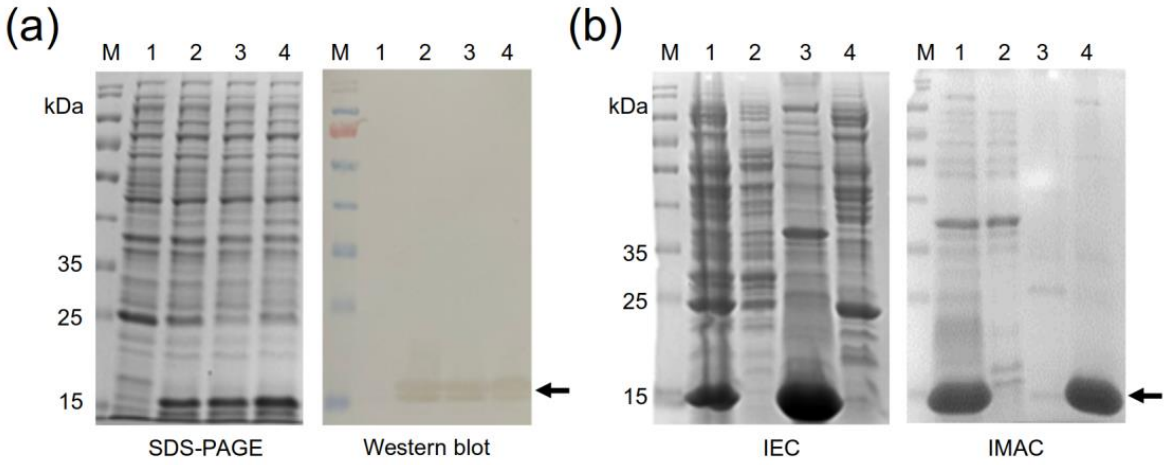

Figure 4. Production and purification of anti-EGF nanobodies. (**a**) SDS-PAGE and Western blot of nanobody production in BL21 (DE3). M: molecular-weight marker, PageRuler Prestained Protein Ladder (Thermo Fisher Scientific, USA), 1: untransformed BL21; BL21 transformed with (2) pET22b-NbA8-1, (3) pET22b-NbA11-2, and (4) pET22b-NbD6-4. The nanobodies were identified using an anti-His tag monoclonal antibody conjugated to HRP. (**b**) SDS-PAGE of the nanobody-purification process. Left panel: first purification stage by IEC. M: molecular-weight marker, 1: initial sample, 2: unbound proteins, 3: elution from the anionic exchanger, Bio-Scale Mini Macro-Prep High Q Cartridge (BioRad, USA), 4: elution from the cationic exchanger CM Sepharose Fast Flow (GE Healthcare, USA). Right panel: second purification stage by IMAC. M: molecular-weight marker, 1: initial sample from IEC, 2: unbound proteins, 3: wash (40 mM imidazole), 4: elution (250 mM Imidazole). Arrow heads indicate the protein bands corresponding to nanobodies A8-1, A11-2, and D6-4.

2.5. Binding Assays for Selected Recombinant Anti-EGF Nanobodies

The recognition of the EGF by the recombinant nanobodies was assessed by indirect ELISA. In a first attempt, we intended to use the SV5 tag in the recombinant EGF molecule for detection, by coating the wells with the recombinant nanobodies, adding the recombinant EGF and then an HRP-conjugated anti-SV5 antibody. This approach, however, yielded very weak signals. We speculate that with such a small molecule as a nanobody, adsorption on a plastic surface would reduce the binding-site availability or affect the conformation of the flexible CDR3 loop.

Since no other tag was available for detection (the His tag is common in both nanobodies and the EGF), we decided to biotinylate the recombinant nanobodies, taking advantage of the three lysine residues found in the framework region. With this method, we

successfully detected the expected nanobody–antigen-binding signals, and assessed the dissociation constant (KD) for the two best binders from a titration ELISA [37] (Figure 5). The nanobodies A8-1 and D6-4 showed very similar binding strengths, with KD in the order of 10^{-7} M, while the Nbs A11-2 y C10-1 showed a weaker binding (their KD values could not be assessed).

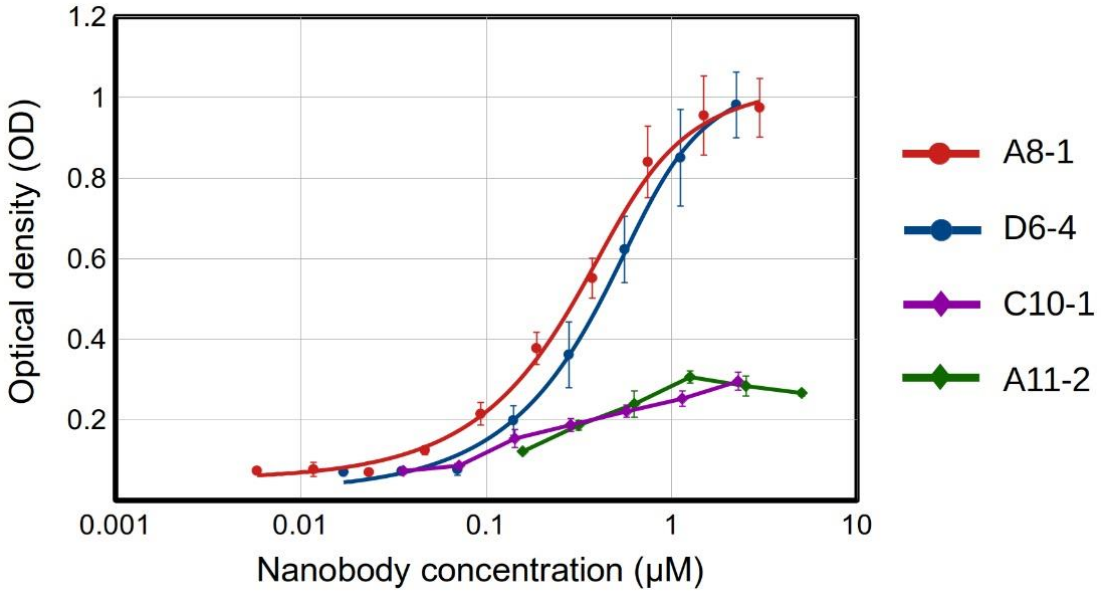

Figure 5. Binding of recombinant nanobodies to EGF by indirect ELISA. Biotinylated nanobodies were detected with streptavidin conjugated to HRP. The red and blue fitting curves were used for KD estimation, for clones A8-1 (KD = $(2.4 \pm 0.7) \times 10^{-7}$ M) and D6-4 (KD = $(3.7 \pm 0.8) \times 10^{-7}$ M), respectively. Negative controls (not shown)—BSA coating: OD = 0.11. For all Nbs, we used the maximum tested concentration for the negative controls. Experiments were performed in triplicates.

It is worth noting that while the clone A8-1 has no lysine in its CDRs, D6-4 shows a lysine in CDR1. This lysine could have been affected in the biotinylation procedure, thus abolishing or diminishing the binding capabilities of a fraction of the nanobody molecules. Therefore, the KD for the clone D6-4 might, in fact, be better. The other two clones also displayed lysine residues in their CDRs (two in A11-2, one in CDRs 1 and 2, and one in C10-1 in CDR2), which may have partially affected their binding to EGF. The impairment of the binding capacity of antibodies after biotinylation has been described, and it might be counteracted by establishing an adequate biotin:antibody ratio [38]. The incorporation of biotin into histidine, serine, threonine, and tyrosine residues has also been observed [39]. At least two of these residues are present in the CDRs of the four anti-EGF Nbs, and their possible biotinylation might have exerted a negative effect on the EGF recognition.

Despite these possible drawbacks, the affinities estimated for the clones A8-1 and D6-4 were similar to those measured by Guardiola et al. for five out of their six anti-EGF nanobodies, which showed KD values in the 10^{-7} molar order, while only one clone yielded a KD in the 10^{-8} M order [17]. That is, the anti-EGF nanobodies selected in this work from a synthetic library were comparable in terms of affinity to those obtained from an immunized alpaca. It is worth noting that these KD values are in the same order as the KD of the EGF–EGFR complex, which, in different studies using surface plasmon resonance (SPR) has been found to be within the range of 100–400 nM [40–42]. Notably, two of the anti-EGF Nbs obtained by Guardiola et al. were capable of inhibiting the binding of EGF to its receptor and EGFR phosphorylation, with IC50 constants in the micromolar order [17]. They also inhibited cell viability in tumor cells resistant to the EGFR-tyrosine-kinase inhibitor, osimertinib [18].

In this study, we applied a sequential astringent elution method for selecting specific anti-EGF Nb clones from the library, in which the triethylamine solution (suffix 1) was the first elution applied and the addition of TG1 cells (suffix 4) was the last. Therefore, it is reasonable to expect that the nanobodies obtained from the last elution should have a higher binding capacity. Paradoxically, our best binder was obtained from the first elution. This interesting outcome suggests that the nature of the molecular interactions governing nanobody–antigen binding determine the type of elution that detaches the nanobody from the immobilized antigen.

2.6. Concluding Remarks

In this study, we obtained four EGF-binding nanobodies from a synthetic library, applying a selection strategy that used four different sequential elution steps along three rounds of selection. To our knowledge, this was the first attempt to obtain anti-EGF nanobodies from a synthetic library. Notably, two of the obtained nanobodies showed KD values similar to those obtained for the Nbs derived from an immune library. It has been shown that it is possible to obtain high-affinity binders from synthetic libraries [15,43]. However, the fact that EGF is a small protein, offering a relatively small surface area for antibody/nanobody recognition, represents a major challenge. Thus, the obtained results are very encouraging. The next step will be to test the neutralizing capabilities of the obtained nanobodies. In future anti-EGF biopannings, as well as in those for other small proteins, we plan to use a different antigen-presentation system, in which the EGF is completely exposed for nanobody recognition, by, for example, using a biotinylated tag for anchoring to a streptavidin base [44]. In this way, we expect to increase the probability of obtaining high-affinity binders from the synthetic library.

3. Materials and Methods

3.1. Synthetic Library Production

The synthetic nanobody library was designed and constructed by our group as described in [19]. In this study, the library previously cloned into the phagemid pMAC and transformed in the *E. coli* strain SS320 was amplified into the amber suppressor, *E. coli* strain TG1. For this purpose, 300 mL of 2xYT medium containing 100 µg/mL ampicillin was inoculated with the TG1 strain and grown at 37 °C, and at 250 rpm, until an OD_{600nm} of 1.5. The phage library previously obtained in SS320 bacteria was used to transduce TG1 cells at a multiplicity of infection (MOI) of 58 at 37 °C for one hour (30 min static and 30 min at 50 rpm). After spinning at 2000× *g* for 15 min at 4 °C and discarding supernatant, the pellet was resuspended in 300 mL of 2xYT medium with 100 µg/mL ampicillin and incubated at 28 °C, 100 rpm, overnight. Next, 200 mL of the previous culture was added to a final volume of 800 mL of 2xYT medium with 100 µg/mL ampicillin and cultured at 37 °C, 250 rpm until an OD_{600nm} of 2. The culture was transduced with the helper phage M13K07 at a MOI of 25 at 37 °C for one hour (30 min static and 30 min at 50 rpm), and spined at 2000× *g* for 15 min at 4 °C. The pellet was diluted in 500 mL of 2xYT medium containing 100 µg/mL ampicillin, 50 µg/mL kanamycin, and 1 mM isopropyl β-D-1-thiogalactopyranoside (IPTG) for library amplification. After calculating library diversity, recombinant phages were concentrated by precipitation with PEG/NaCl (20% polyethylene glycol 8000 and 2.5 M NaCl) and aliquoted in 10% glycerol.

3.2. Production and Purification of a Recombinant EGF Protein

The gene coding the EGF was synthesized and cloned into the pET22b-expression vector (pET22b-EGF) by GenScript (Piscataway, NJ, USA). After transforming chemically competent BL21 (DE3), two inocula of 5 mL, each grown at 37 °C and at 250 rpm, overnight, in 2xYT medium with 100 µg/mL ampicillin were added to two Erlenmeyers of 1 L containing 500 mL each of Saline Minimal Medium M9 (SMM9) (45 mM Na_2HPO_4 (Sigma-Aldrich, Burlington, MA, USA), 22 mM KH_2HPO_4 (Sigma, Burlington, MA, USA), 19 mM NH_4Cl (Merck, Rahway, NJ, USA), 8,4 mM NaCl (Sigma-Aldrich, Burlington, MA, USA)),

0.05% yeast extract (Oxoid, Basingstoke, UK), and 100 µg/mL ampicillin. After reaching an OD_{600nm} of 0.5, the gene expression was induced with 25 µM IPTG, and cultures were incubated at 28 °C and at 100 rpm, overnight. Next, cultures were centrifuged at 10,000× *g* for 15 min at 4 °C, and the pellet was resuspended in buffer A (150 mM NaCl, 15 mM Na_2HPO_4, pH 7,4) and subjected to five freeze/thaw rounds for cell lysis. Soluble rEGF was obtained in the supernatant after spinning at 10,000× *g* for 15 min at 4 °C. The presence of soluble EGF was verified by sodium dodecyl sulphate–polyacrylamide gel electrophoresis (SDS-PAGE) and Western blot.

For SDS-PAGE, protein samples were diluted in a buffer with beta-mercaptoethanol and run in 15% polyacrylamide and 3% stacking gels. Western blot assay was performed in a 0.2-µm PVDF-transfer membrane (Thermo Fisher Scientific, Waltham, MA, USA) and a semi-dry transfer system Trans-Blot® Turbo™ (Bio-Rad, Hercules, CA, USA) at 0.3 A and 25 V for 30 min. After blocking with 5% skimmed milk in PBS, the membrane was incubated with the HRP anti-6X His tag rabbit polyclonal antibody (ab1187, Abcam, Boston, MA, USA) diluted 1:5000 in the blocking buffer. The reaction was visualized using a DAB substrate kit (Thermo Fisher Scientific, Waltham, MA, USA).

The rEGF was purified in two chromatographic stages. (i) The lysis supernatant containing rEGF was purified by immobilized metal-affinity chromatography (IMAC) by adding 5 mM imidazole to buffer A as equilibrium buffer and the initial sample. After loading the sample, the HisPur Ni-NTA Spin Column (Thermo Fisher Scientific, Waltham, MA, USA) was washed with 25 mM imidazole, and protein was eluted with 250 mM imidazole. Samples, washing, and elution were prepared in buffer A. (ii) For ion-exchange chromatography (IEC), a serial connection of two columns was used. One column featured the weak cation-exchanger CM Sepharose Fast Flow (GE Healthcare, Chicago, IL, USA), and the other was a pre-packed column with the anion exchanger, Bio-Scale Mini Macro-Prep High Q Cartridge (BioRad, Hercules, CA, USA). Both were equilibrated with buffer B (50 mM NaCl, 7 mM Na_2HPO_4 (Sigma-Aldrich, Burlington, MA, USA), 83 mM imidazole, pH 8). Samples from IMAC were diluted three times in water and loaded into these columns. After column equilibration with the same buffer B, the anion exchanger was eluted with buffer C (500 mM NaCl, 7 mM Na_2HPO_4, pH 5), and the cation exchanger was eluted with the same buffer C at pH 10. The pH of buffers for IEC was carefully adjusted according to the theoretical isoelectric point of rEGF, calculated using Prot-Pi (https://www.protpi.ch/Calculator/ProteinTool (accessed on 10 March 2023)). All fractions were monitored using the purification system, BioLogic LP (BioRad, Hercules, CA, USA). Samples containing the rEGF were diafiltered against PBS (Sigma, USA) in Spin-X® UF concentrators of 5 kDa (Corning, Corning, NY, USA), and analyzed by SDS-PAGE and Western blot, as described above. The rEGF purity was estimated using the analytical software of the iBright 750 Imaging System (Thermo Fisher Scientific, Waltham, MA, USA), and its concentration was determined using the Pierce BCA Protein Assay Kit (Thermo Fisher Scientific, Waltham, MA, USA).

3.3. Biological Activity of Recombinant EGF

The EGF activity was determined by an in vitro assay using the A431 cell line. Ninety-six-well plates (2592, Corning, Corning, NY, USA) were used for seeding 2500 cells/well in DMEM plus 0.5% or 5% fetal bovine serum (FBS), which were treated with different EGF concentrations (0.1 nM, 1 nM, 10 nM, and 100 nM) for four days. No EGF was added to negative control. Cell viability was measured with AlamarBlue Cell Viability Reagent (Invitrogen, Waltham, MA, USA) in a Varioskan LUX Multimode Microplate Reader (Thermo Fisher Scientific, Waltham, MA, USA).

3.4. Selection of EGF-Binding Phages

Polystyrene high-binding microtiter plates (Costar) were coated with 100 µL of the EGF antigen at 10 µg/mL (eight wells) and incubated overnight at 4 °C. After three washes with phosphate-buffered saline (PBS) plus 0.1% Tween 20 (PBST), wells were blocked with

3% skimmed milk (Sigma-Aldrich, Burlington, MA, USA) in PBS (300 µL/well) for one hour. Wells were washed three times with PBST and incubated at room temperature (RT) for two hours with 100 µL of five-hundred times the library diversity diluted in 0.7% skimmed milk. The PBST was used to perform twenty washes (300 µL/well). Two additional washes were conducted with PBS. Recombinant phage collection was undertaken through sequential steps of four types of elution following neutralization. (i) Triethylamine elution: 0.1 M triethylamine, pH 12.0 (100 µL/well), for 10 min at RT, followed by neutralization with Tris-HCl 1 M pH 7.5 (100 µL/well) for 5 min at RT. (ii) Glycine elution: 0.2 M glycine, pH 2.0 (100 µL/well), for 10 min at RT, followed by neutralization with Tris-HCl 1 M pH 9.1 (100 µL/well) for 5 min at RT. (iii) Ultrasound elution: after adding 100 µL/well of PBS, wells were subjected to ultrasound (40 MHz of potency for 30 min). During the first three elutions, wells were washed twice with PBST and once with PBS (300 µL/well each). (iv) TG1 strain elution: addition of the *E. coli* strain, TG1, in exponential phase of growing (100 µL/well). This elution was performed after the three elutions described above. Simultaneously, the *E. coli* strain, TG1, was transduced with the three elutions and incubated at 37 °C for 30 min. Elutions were seeded in 2xYT plates plus 100 µg/mL ampicillin and incubated at 37 °C, and at 250 rpm, overnight.

3.5. Enrichment of Positive Phages

Three biopanning rounds were carried out to enrich the phage pull in EGF binders. For the first round, all colonies from plates obtained from the four elutions were gathered in 15 mL of 2xYT medium with 100 µg/mL ampicillin, and 5 mL was used to inoculate 50 mL of the same medium, which was incubated at 37 °C, and at 250 rpm, overnight. Next, the culture was diluted 10 times (500 mL) and grown until a OD_{600nm} of 2 was reached. Transduction with the helper phage M13KO7 was performed at a multiplicity of infection (MOI) of 20 at 37 °C for one hour (30 min static and 30 min at 50 rpm). Transduced bacteria were spun at 2000× *g* for 15 min and diluted in 500 mL of 2xYT medium with 100 µg/mL ampicillin, 50 µg/mL kanamycin, and 1 mM IPTG for the amplification of recombinant phages at 28 °C, and at 250 rpm, overnight. Amplified phages were concentrated as previously described, for further testing against EGF. The second and third biopanning rounds were conducted in the same way, with a small variation in the final culture volume, from 500 mL to 200 mL.

3.6. Indirect ELISA for Detecting Positive Phage Clones

Polystyrene high-binding microtiter plates (Corning, Corning, NY, USA) were coated with 100 µL of EGF at 5 µg/mL and incubated overnight at 4 °C. After washing three times with PBS-0.1% Tween 20 (PBST), wells were blocked with 3% skimmed milk in PBS (300 µL/well) for one hour at RT. Supernatants of individual clones, previously amplified, were added to the plate (200 µL of supernatant) for two hours at RT. The M13KO7 phage was used as negative control. Three washes with PBST were performed, and the anti-M13 antibody (G8P) diluted 1:5000 in 3% skimmed milk was added for one hour at RT, followed by an anti-mouse antibody conjugated with horseradish peroxidase at the same dilution, time, and temperature. Plates were washed three times with PBST, and the reaction was visualized with a TMB kit solution (Thermo Fisher Scientific, Waltham, MA, USA). The reaction was stopped with 2.5 M sulphuric acid, and the absorbance was measured in a microplate reader (ES-20/80, BOECO, Hamburg, Germany) at 450 nm. Plates coated with a recombinant anti-EGFR antibody [45] (carrying the same SV5 and 6xHis tags as the recombinant EGF) at 10 µg/mL and with 3% skimmed milk were used to elude the backgrounds of recombinant phages against the SV5 and histidine tags. Positivity was considered for an OD_{450nm} signal $\geq$ 0.8 for EGF, and for a signal from milk or the non-related protein that was three or more times lower than for EGF.

3.7. Sequencing

The DNA from clones in TG1 were purified using the GenElute Plasmid Miniprep Kit (Sigma-Aldrich, Burlington, MA, USA) and sequenced by Macrogen (Seoul, Korea). Sequences were analyzed using the CLC Genomics Workbench v.21 (QIAGEN Aarhus, Aarhus, Denmark).

3.8. Production of Selected Recombinant Anti-EGF Nanobodies

The genes coding the anti-EGF nanobodies were extracted from the pMAC phagemid with the restriction enzymes *NcoI*/*NotI* (New England Biolabs, Ipswich, MA, USA) and cloned in the expression vector pET22b with the same enzymes. Nanobody production was carried out as described above, for EGF.

3.9. Nanobody Purification

The anti-EGF nanobodies were also purified in two chromatographic stages. The first was with IEC, using the same serial connection of two columns described above. Both were equilibrated with half-diluted SMM9 medium. After sample loading in the same equilibrium buffer, each column was eluted separately. as explained previously. Buffer pH was also adjusted based on the theoretical isoelectric point of nanobodies, calculated as described above. The elution from the anion exchanger was diluted three times in water and further purified by IMAC, by adding the same amounts of imidazole as previously described. Fraction monitoring, diafiltering, sample analysis, nanobody purity, and concentration were performed as described above.

3.10. Nanobody Biotinylation

Nanobodies were diluted in 25-mM carbonate/bicarbonate buffer at a concentration around 1 mg/mL. Fifty microliters of biotin (H1759, Sigma-Aldrich, Burlington, MA, USA) at 10 mg/mL in DMSO was slowly added to nanobodies. The final molar ratio biotin:nanobody was 40:1. Reaction was stirred for six hours at RT, under protection from light. Free biotin was removed by dialyzing against PBS.

3.11. ELISA for Bilotinylated Anti-EGF Nanobodies

Polystyrene high-binding microtiter plates (Corning, Corning, NY, USA) were coated with 100 µL of rEGF at 5 µg/mL and incubated overnight at 4 °C. After washing three times with PBS, 0.1% Tween 20 (PBST), wells were blocked with 3% skimmed milk in PBS (300 µL/well) for 1 h at RT. Biotinylated nanobodies were serially diluted and incubated for one hour at RT. After washing, streptavidin conjugated to HRP (Biotechne R&D Systems, Minneapolis, MN, USA) diluted 1:200 was added for one hour at RT. The reaction was visualized, stopped, and measured, as described above. The KD estimation was carried out by following the method and fitting function described in [37]. A linear regression analysis using this function was performed using the MyCurveFit web server (https://mycurvefit.com/, last accessed on 4 May 2023).

Author Contributions: Conceptualization, A.G.-P. and E.M.; methodology, Y.S.-R., F.C.-C., O.S.-R., A.G.-P. and E.M.; investigation, Y.S.-R., J.S.-U., M.R.-C., F.C.-C., O.S.-R., A.G.-P. and E.M.; writing—original draft preparation, Y.S.-R., J.S.-U., M.R.-C., A.G.-P. and E.M.; writing—review and editing, Y.S.-R., F.C.-C., O.S.-R., A.G.-P. and E.M.; supervision, project administration and funding acquisition, E.M. All authors have read and agreed to the published version of the manuscript.

Funding: This research was funded by MINCIENCIAS, MINEDUCACIÓN, MINCIT and ICETEX through the Program NanoBioCancer (cod. FP44842-211-2018, project number 58676). A.G.-P. and E.M. thank the University of Medellin for its support.

Institutional Review Board Statement: Not applicable.

Informed Consent Statement: Not applicable.

Data Availability Statement: The data presented in this study are contained in the article tables.

Conflicts of Interest: The authors declare no conflict of interest.

Sample Availability: Not applicable. The phagemids and molecules used in this work were either purchased or produced in limited amounts to perform the reported experiments only.

References

1. Cohen, S.; Carpenter, G. Human Epidermal Growth Factor: Isolation and Chemical and Biological Properties. *Proc. Natl. Acad. Sci. USA* **1975**, *72*, 1317–1321. [CrossRef]
2. Singh, B.; Carpenter, G.; Coffey, R.J. EGF Receptor Ligands: Recent Advances. *F1000Research* **2016**, *5*, 2270. [CrossRef]
3. Mitsudomi, T. Molecular Epidemiology of Lung Cancer and Geographic Variations with Special Reference to EGFR Mutations. *Transl. Lung Cancer Res.* **2014**, *3*, 205–211. [PubMed]
4. Tahara, E.; Sumiyoshi, H.; Hata, J.; Yasui, W.; Taniyama, K.; Hayashi, T.; Nagae, S.; Sakamoto, S. Human Epidermal Growth Factor in Gastric Carcinoma as a Biologic Marker of High Malignancy. *Jpn. J. Cancer Res.* **1986**, *77*, 145–152. [PubMed]
5. Liu, T.-C.; Jin, X.; Wang, Y.; Wang, K. Role of Epidermal Growth Factor Receptor in Lung Cancer and Targeted Therapies. *Am. J. Cancer Res.* **2017**, *7*, 187–202. [PubMed]
6. Cheaito, K.; Bahmad, H.F.; Jalloul, H.; Hadadeh, O.; Msheik, H.; El-Hajj, A.; Mukherji, D.; Al-Sayegh, M.; Abou-Kheir, W. Epidermal Growth Factor Is Essential for the Maintenance of Novel Prostate Epithelial Cells Isolated from Patient-Derived Organoids. *Front. Cell Dev. Biol.* **2020**, *8*, 571677. [CrossRef]
7. Kalluri, R.; Weinberg, R.A. The Basics of Epithelial-Mesenchymal Transition. *J. Clin. Investig.* **2009**, *119*, 1420–1428. [CrossRef]
8. Heerboth, S.; Housman, G.; Leary, M.; Longacre, M.; Byler, S.; Lapinska, K.; Willbanks, A.; Sarkar, S. EMT and Tumor Metastasis. *Clin. Transl. Med.* **2015**, *4*, 6. [CrossRef]
9. Gonzalez, G.; Montero, E.; Leon, K.; Cohen, I.R.; Lage, A. Autoimmunization to Epidermal Growth Factor, a Component of the Immunological Homunculus. *Autoimmun. Rev.* **2002**, *1*, 89–95. [CrossRef]
10. Saavedra, D.; Crombet, T. CIMAvax-EGF: A New Therapeutic Vaccine for Advanced Non-Small Cell Lung Cancer Patients. *Front. Immunol.* **2017**, *8*, 269. [CrossRef]
11. García, B.; Neninger, E.; de la Torre, A.; Leonard, I.; Martínez, R.; Viada, C.; González, G.; Mazorra, Z.; Lage, A.; Crombet, T. Effective Inhibition of the Epidermal Growth Factor/Epidermal Growth Factor Receptor Binding by Anti–Epidermal Growth Factor Antibodies Is Related to Better Survival in Advanced Non–Small-Cell Lung Cancer Patients Treated with the Epidermal Growth Factor Cancer Vaccine. *Clin. Cancer Res.* **2008**, *14*, 840–846. [CrossRef] [PubMed]
12. Muyldermans, S. Nanobodies: Natural Single-Domain Antibodies. *Annu. Rev. Biochem.* **2013**, *82*, 775–797. [CrossRef] [PubMed]
13. Morrison, C. Nanobody Approval Gives Domain Antibodies a Boost. *Nat. Rev. Drug Discov.* **2019**, *18*, 485–487. [CrossRef]
14. Muyldermans, S. A Guide to: Generation and Design of Nanobodies. *FEBS J.* **2021**, *288*, 2084–2102. [CrossRef] [PubMed]
15. Valdés-Tresanco, M.S.; Molina-Zapata, A.; Pose, A.G.; Moreno, E. Structural Insights into the Design of Synthetic Nanobody Libraries. *Molecules* **2022**, *27*, 2198. [CrossRef] [PubMed]
16. Keam, S.J. Ozoralizumab: First Approval. *Drugs* **2023**, *83*, 87–92. [CrossRef] [PubMed]
17. Guardiola, S.; Varese, M.; Sánchez-Navarro, M.; Vincke, C.; Teixidó, M.; García, J.; Muyldermans, S.; Giralt, E. Blocking EGFR Activation with Anti-EGF Nanobodies via Two Distinct Molecular Recognition Mechanisms. *Angew. Chem. Int. Ed.* **2018**, *57*, 13843–13847. [CrossRef]
18. Guardiola, S.; Sánchez-Navarro, M.; Rosell, R.; Giralt, E.; Codony-Servat, J. Anti-EGF Nanobodies Enhance the Antitumoral Effect of Osimertinib and Overcome Resistance in Non-Small Cell Lung Cancer (NSCLC) Cellular Models. *Med. Oncol.* **2022**, *39*, 195. [CrossRef]
19. Contreras, M.A.; Serrano-Rivero, Y.; González-Pose, A.; Salazar-Uribe, J.; Rubio-Carrasquilla, M.; Soares-Alves, M.; Parra, N.C.; Camacho-Casanova, F.; Sánchez-Ramos, O.; Moreno, E. Design and Construction of a Synthetic Nanobody Library: Testing Its Potential with a Single Selection Round Strategy. *Molecules* **2023**, *28*, 3708. [CrossRef]
20. Haigler, H.; Ash, J.F.; Singer, S.J.; Cohen, S. Visualization by Fluorescence of the Binding and Internalization of Epidermal Growth Factor in Human Carcinoma Cells A-431. *Proc. Natl. Acad. Sci. USA* **1978**, *75*, 3317–3321. [CrossRef] [PubMed]
21. Kawamoto, T.; Sato, J.D.; Le, A.; Polikoff, J.; Sato, G.H.; Mendelsohn, J. Growth Stimulation of A431 Cells by Epidermal Growth Factor: Identification of High-Affinity Receptors for Epidermal Growth Factor by an Anti-Receptor Monoclonal Antibody. *Proc. Natl. Acad. Sci. USA* **1983**, *80*, 1337–1341. [CrossRef] [PubMed]
22. Anand, T.; Virmani, N.; Bera, B.C.; Vaid, R.K.; Vashisth, M.; Bardajatya, P.; Kumar, A.; Tripathi, B.N. Phage Display Technique as a Tool for Diagnosis and Antibody Selection for Coronaviruses. *Curr. Microbiol.* **2021**, *78*, 1124–1134. [CrossRef] [PubMed]
23. Rojas, G.; Pupo, A.; Gómez, S.; Krengel, U.; Moreno, E. Engineering the Binding Site of an Antibody against *N*-Glycolyl GM3: From Functional Mapping to Novel Anti-Ganglioside Specificities. *ACS Chem. Biol.* **2013**, *8*, 376–386. [CrossRef]
24. Hu, Y.; Lin, J.; Wang, Y.; Wu, S.; Wu, J.; Lv, H.; Ji, X.; Muyldermans, S.; Zhang, Y.; Wang, S. Identification of Serum Ferritin-Specific Nanobodies and Development towards a Diagnostic Immunoassay. *Biomolecules* **2022**, *12*, 1080. [CrossRef] [PubMed]
25. Hu, Y.; Zhang, C.; Lin, J.; Wang, Y.; Wu, S.; Sun, Y.; Zhang, B.; Lv, H.; Ji, X.; Lu, Y.; et al. Selection of Specific Nanobodies against Peanut Allergen through Unbiased Immunization Strategy and the Developed Immuno-Assay. *Food Sci. Hum. Wellness* **2023**, *12*, 745–754. [CrossRef]

26. Kaczmarek, J.Z.; Skottrup, P.D. Selection and Characterization of Camelid Nanobodies towards Urokinase-Type Plasminogen Activator. *Mol. Immunol.* **2015**, *65*, 384–390. [CrossRef]
27. Lakzaei, M.; Rasaee, M.J.; Fazaeli, A.A.; Aminian, M. A Comparison of Three Strategies for Biopanning of Phage-scFv Library against Diphtheria Toxin. *J. Cell Physiol.* **2019**, *234*, 9486–9494. [CrossRef]
28. Kulpakko, J.; Juusti, V.; Rannikko, A.; Hänninen, P.E. Detecting Disease Associated Biomarkers by Luminescence Modulating Phages. *Sci. Rep.* **2022**, *12*, 2433. [CrossRef]
29. Lunder, M.; Bratkovič, T.; Urleb, U.; Kreft, S.; Štrukelj, B. Ultrasound in Phage Display: A New Approach to Nonspecific Elution. *Biotechniques* **2008**, *44*, 893–900. [CrossRef]
30. Donatan, S.; Yazici, H.; Bermek, H.; Sarikaya, M.; Tamerler, C.; Urgen, M. Physical Elution in Phage Display Selection of Inorganic-Binding Peptides. *Mater. Sci. Eng. C* **2009**, *29*, 14–19. [CrossRef]
31. Conrath, K.E.; Lauwereys, M.; Galleni, M.; Matagne, A.; Frère, J.-M.; Kinne, J.; Wyns, L.; Muyldermans, S. β-Lactamase Inhibitors Derived from Single-Domain Antibody Fragments Elicited in the *Camelidae*. *Antimicrob. Agents Chemother.* **2001**, *45*, 2807–2812. [CrossRef] [PubMed]
32. de Marco, A. Recombinant Expression of Nanobodies and Nanobody-Derived Immunoreagents. *Protein Expr. Purif.* **2020**, *172*, 105645. [CrossRef] [PubMed]
33. Amcheslavsky, A.; Wallace, A.L.; Ejemel, M.; Li, Q.; McMahon, C.T.; Stoppato, M.; Giuntini, S.; Schiller, Z.A.; Pondish, J.R.; Toomey, J.R.; et al. Anti-CfaE Nanobodies Provide Broad Cross-Protection against Major Pathogenic Enterotoxigenic Escherichia Coli Strains, with Implications for Vaccine Design. *Sci. Rep.* **2021**, *11*, 2751. [CrossRef] [PubMed]
34. Nagy-Fazekas, D.; Stráner, P.; Ecsédi, P.; Taricska, N.; Borbély, A.; Nyitray, L.; Perczel, A. A Novel Fusion Protein System for the Production of Nanobodies and the SARS-CoV-2 Spike RBD in a Bacterial System. *Bioengineering* **2023**, *10*, 389. [CrossRef] [PubMed]
35. Salema, V.; Fernández, L.Á. High Yield Purification of Nanobodies from the Periplasm of *E. coli* as Fusions with the Maltose Binding Protein. *Protein Expr. Purif.* **2013**, *91*, 42–48. [CrossRef]
36. Kariuki, C.K.; Magez, S. Improving the Yield of Recalcitrant Nanobodies®by Simple Modifications to the Standard Protocol. *Protein Expr. Purif.* **2021**, *185*, 105906. [CrossRef]
37. Eble, J.A. Titration ELISA as a Method to Determine the Dissociation Constant of Receptor Ligand Interaction. *J. Vis. Exp.* **2018**, *2018*, 57334. [CrossRef]
38. Cohen, L.; Walt, D.R. Evaluation of Antibody Biotinylation Approaches for Enhanced Sensitivity of Single Molecule Array (Simoa) Immunoassays. *Bioconjug Chem.* **2018**, *29*, 3452–3458. [CrossRef]
39. Haque, M.; Forte, N.; Baker, J.R. Site-Selective Lysine Conjugation Methods and Applications towards Antibody–Drug Conjugates. *Chem. Commun.* **2021**, *57*, 10689–10702. [CrossRef]
40. Wade, J.D.; Domagala, T.; Rothacker, J.; Catimel, B.; Nice, E. Use of Thiazolidine-Mediated Ligation for Site Specific Biotinylation of Mouse EGF for Biosensor Immobilisation. *Lett. Pept. Sci.* **2001**, *8*, 211–220. [CrossRef]
41. Ferguson, K.M.; Berger, M.B.; Mendrola, J.M.; Cho, H.-S.; Leahy, D.J.; Lemmon, M.A. EGF Activates Its Receptor by Removing Interactions That Autoinhibit Ectodomain Dimerization. *Mol. Cell* **2003**, *11*, 507–517. [CrossRef] [PubMed]
42. Kuo, W.-T.; Lin, W.-C.; Chang, K.-C.; Huang, J.-Y.; Yen, K.-C.; Young, I.-C.; Sun, Y.-J.; Lin, F.-H. Quantitative Analysis of Ligand-EGFR Interactions: A Platform for Screening Targeting Molecules. *PLoS ONE* **2015**, *10*, e0116610. [CrossRef] [PubMed]
43. Moutel, S.; Bery, N.; Bernard, V.; Keller, L.; Lemesre, E.; De Marco, A.; Ligat, L.; Rain, J.C.; Favre, G.; Olichon, A.; et al. NaLi-H1: A Universal Synthetic Library of Humanized Nanobodies Providing Highly Functional Antibodies and Intrabodies. *eLife* **2016**, *5*, e16228. [CrossRef] [PubMed]
44. Predonzani, A.; Arnoldi, F.; López-Requena, A.; Burrone, O.R. In Vivosite-Specific Biotinylation of Proteins within the Secretory Pathway Using a Single Vector System. *BMC Biotechnol.* **2008**, *8*, 41. [CrossRef]
45. Cruz-Pacheco, A.F.; Monsalve, Y.; Serrano-Rivero, Y.; Salazar-Uribe, J.; Moreno, E.; Orozco, J. Engineered Synthetic Nanobody-Based Biosensors for Electrochemical Detection of Epidermal Growth Factor Receptor. *Chem. Eng. J.* **2023**, *465*, 142941. [CrossRef]

ANEXO 3.

Chemical Engineering Journal 465 (2023) 142941

Contents lists available at ScienceDirect

Chemical Engineering Journal

journal homepage: www.elsevier.com/locate/cej

Engineered synthetic nanobody-based biosensors for electrochemical detection of epidermal growth factor receptor

Andrés F. Cruz-Pacheco [a], Yeison Monsalve [a], Yunier Serrano-Rivero [b], Julieta Salazar-Uribe [b], Ernesto Moreno [b], Jahir Orozco [a,*]

[a] Max Planck Tandem Group in Nanobioengineering, Institute of Chemistry, Faculty of Natural and Exact Sciencies, University of Antioquia, Complejo Ruta N, Calle 67 No. 52-20, Medellín 050010, Colombia
[b] Faculty of Basic Sciences, University of Medellin, Medellin 050026, Colombia

ARTICLE INFO

Keywords:
Nanobody
Biosensor
Electrochemical detection
Screen-printed electrode bioconjugation chemistry
XPS analysis

ABSTRACT

Two engineered synthetic nanobody-based nanobiocomposite platforms were developed for label-free electrochemical detection of the epithelial growth factor receptor (EGFR) biomarker. Screen-printed carbon electrodes (SPCE) were decorated either with NiO nanoparticles (NPs) or poly(thiophene acetic acid) (PTAA) to link the anti-EGFR nanobody (Nb) and form nanobiocomposites for detecting the EGFR biomarker by electrochemical impedance spectroscopy (EIS). The nanoarchitectures were prepared by in situ electrosynthesis of NiO NPs or PTAA layers at SPCEs. A modified version of the 9G8 Nb (Nb9G8m), specific for the EGFR (anti-EGFR), was designed and produced as the nanobiosensor bioreceptor. This Nb was engineered to provide a hexahistidine tag (6xHis-tag) and a lysine (Lys) dual functionality to form a (6xHis-tag)/Ni^{2+} or Lys/PTAA interface. The biosensing interfaces were characterized by field-emission scanning electron microscopy, energy-dispersive X-ray spectroscopy, X-ray photoelectron spectroscopy, cyclic voltammetry, and EIS. The nanobody/nanobiocomposite-based biosensors detected EGFR proteins in a linear range from 0.25 to 50 μg mL^{-1} and 0.5 to 50 μg mL^{-1}, with limits of detection of 0.46 μg mL^{-1} and 1.14 μg mL^{-1}, for NiO- and PTAA-based platforms, respectively. The biosensing platforms offer high simplicity, specificity, and selectivity to detect EGFR, but Nbs can be readily engineered to detect other (glycol)proteins. Finally, as a proof of concept, the EGFR was detected in several tumor cell lines, differentiating biomarker expression among them.

1. Introduction

In the early 1990s, a distinct type of antibody composed only of a pair of heavy chains was found in members of the camelid family [1]. The single binding domain of these unique camelid antibodies was termed “nanobody” (Nb), in correspondence with its size on the nanometric scale, with around 2.5 nm in diameter and 4 nm in height [2]. Compared with typical antibodies, the single-domain nature of Nbs makes molecular manipulation easy and facilitates the production of a large variety of formats in which the fusion with other protein domains or the chemical conjugation with different molecules finds many different applications [3].

The design and construction of Nbs offer considerable advantages over their naturally occurring antibody counterparts, including high performance in affinity, thermo-, and long term-stability, shorter production time, and production against a myriad of antigens. Remarkably, on-demand engineered synthetic Nbs eliminate the need for animal immunization [4]. Furthermore, the intrinsic features of the Nb production and applications include the easy expression in bacteria and yeast because of the smaller size of a single immunoglobulin domain and the possibility of binding the target even at extreme pH conditions and high temperatures (80–92 °C) [5]. The high performance of novel Nb fragments can be exploited not only in the highly selective and sensitive biosensing development [6–8] but in prevention and diagnosis [9], enzymatic inhibition [10], as specific target molecules against Haptens [11], micro-organisms [12], T cell chimeric immunoreceptors [13], anti-idiotypic agents [14], antidote agents [15], and as signaling biomarkers and tumor treatment [16] using targeted NPs [17].

Modifying SPCEs with nanomaterials [18,19] and conducting polymers [20,21] to obtain tuned surface area for bioreceptor immobilization and improved electrochemical performance has received considerable attention in biosensing approaches. For example,

* Corresponding author.
E-mail address: grupotandem.nanobioe@udea.edu.co (J. Orozco).

https://doi.org/10.1016/j.cej.2023.142941
Received 22 December 2022; Received in revised form 20 March 2023; Accepted 10 April 2023
Available online 12 April 2023

rationally designed inorganic electrosynthesized metallic oxide NPs may contribute to massive bioreceptors immobilization but with proper orientation [22]. The metal chelate provided by coordination between the imidazole group in 6xHis-tag with the Ni^{2+} species existing in nickel oxide (NiO) nanostructures illustrates the highly oriented capture of bioreceptors, with shorter immobilization time compared to other methodologies. Besides, highly specific capture of the tagged bioreceptors occurs by the low abundance of naturally occurring histidine chains and the minimal interaction of other amino acid residues [23,24]. In contrast, amino-containing bioreceptors, including Nbs, can bind to chemical-activated carboxylic conducting polymer (FCPs) layers such as that from thiophenes through 1-ethyl(dimethylaminopropyl)carbodiimide (EDC)/N-hydroxysuccinimide (NHS) covalently coupling. The amide bond formation is straightforward but may lead to a random nanobody orientation [25]. Yet, several amino acid mutations or designed peptide tails can be added to favor a proper nanobody orientation, in which the binding site is exposed to the target.

EGFR is a transmembrane glycoprotein located at the cell surface, which plays an essential role as a target for antitumor strategies [26]. Abnormal levels can indicate the presence of some tumors of epithelial origin, such as CRC [27]. As the most prominent representative cell-surface receptor, the EGFR is crucial in external transducing signals through the membrane into the cell, controlling proliferation, differentiation, migration, and modulating apoptosis [28]. Different types of cancer have been associated with the hyperproliferation of cells by aberrant EGFR signaling due to overexpression or mutation [29]. Overexpression of EGFR has been associated with depth invasion of the tumor and, to a lesser extent, response to treatment [30]. Therefore, EGFR overexpression is one of the most critical cell events for identifying, initiating, and proliferating CRC [31].

This study used an anti-EGFR nanobody specially engineered for label-free electrochemical detection of the EGFR glycoprotein in two comparative assays based on the specific interaction of the Nbs at SPCE decorated with electrosynthesized NiO NPs or PTAA layers. The modification of SPCE surfaces through electrochemical potentiostatic methodologies made possible the easy and fast preparation of the interfaces to bind the anti-EGFR Nb. The anti-EGFR Nb was bio-conjugated with the Ni^{2+} ions in NiO via a metal chelate-based affinity bond in a highly oriented fashion, and the properties of the resultant nanocomposite-based platform were compared to that from the covalent linkage of the anti-EGFR Nb, engineered to favor proper orientation, to the exposed carboxyl groups of PTAA by the EDC/NHS chemistry. The nanostructured platforms and the anti-EGFR/EGFR binding event were studied in terms of morphology, chemical surface analysis, and electrochemical behavior. EGFR detection was followed by EIS upon different concentrations of EGFR-spiked buffers and several cell lines with variable levels of protein expressions.

2. Experimental procedures

The detailed procedure for obtaining and purifying the anti-EGFR Nb, structural and sequential characterization, and the procedures for the affinity tests with the antigen, are described in the supporting information (SI). In addition, the reagents and solutions used in all the tests, as well as the electrochemical, morphological, and chemical characterization by cyclic voltammetry (CV), EIS, field-emission scanning electron microscopy (FE-SEM), energy-dispersive X-ray spectroscopy (EDS) and X-ray photoelectron spectroscopy (XPS) of each stage of the platform nanoengineering are in the same section.

3. Results and discussion

3.1. Redesign of an anti-EGFR Nb for optimal nanosensor functionalization

An engineered version of the 9G8 (Nb9G8) nanobody [32], specific for the EGFR, was designed and produced as a nanobiosensor bioreceptor. First, the amino acid sequence of Nb9G8 was modified to achieve a dual option to link it to the nanosensing platform by complexing a histidine tag to metal chelates covering the SPCE or covalently coupling amino groups in the protein to carboxyl groups from the PTAA interface. In addition, several amino acid mutations were introduced, and a specially designed peptide tail was added to the C-terminus of the nanobody to favor a proper nanobody orientation, in which the binding site is exposed to the target in the solvent (Scheme. 1).

Three lysine residues, each carrying a positively charged amino group, were introduced in the peptide tail to optimize the functionalization through chemical conjugation. One of these lysines is part of an SV5 tag, which was included to facilitate protein detection using a commercial antibody specific to this tag. Furthermore, to avoid chemical conjugations leading to unfavorable nanobody orientations, we decided to mutate every lysine residue in the nanobody that is not relevant for EGFR binding or structural integrity. The crystal structure of Nb9G8 in complex with the EGFR [33] was used for these structural analyses.

The hypervariable loops (CDRs) of Nb9G8 contain one lysine in CDR3, a loop that plays an important role in antigen binding. Nonetheless, the Nb9G8-EGFR complex structure shows that this lysine neither interacts with the receptor nor has a role in anchoring the CDR3 conformation. Therefore, it can be replaced with a similar residue, like arginine. On the other hand, the framework region shows four lysine residues, all with their side chain pointing to the solvent. The five lysine residues were then mutated to arginine, which has a similar size and carries a guanidino group that retains the positive charge provided by lysine. As a result, the engineered nanobody contains only four amino groups –one at the N-terminal residue (lateral to the binding site) and three in the C-terminal peptide tail.

Finally, the peptide tail was completed with a 6xHis tag encoded in the pET22b(+) expression vector after the Not-I restriction site was used for cloning. The His-tag at the C-terminus served for protein purification by metal ion affinity chromatography (IMAC) and as a linking point at the NiO/SPCE interface.

3.2. Expression and purification of Nb9G8m

Nb9G8m was successfully produced using an expression system composed of the plasmid pET22b-Nb9G8m (Fig. S1A) and the *E. coli* strain BL21 (DE3) as host. SDS-PAGE and Western-blot showed a protein band of around 17 kDa corresponding to the designed nanobody (Fig. S1B). The pET22 system, used before to produce recombinant Nbs [34,35], inserts a pelB signaling peptide for protein secretion to the bacterial periplasm, where the Nb disulfide bond can be formed correctly. However, overproduction of the recombinant protein tends to form inclusion bodies that incorporate misfolded molecules. To avoid this undesired effect and improve Nb9G8m solubility, we modified several parameters in the culture conditions, such as culture medium, inductor concentration, temperature, time, and stirring. Also, a physical cell disruption method was implemented based on freeze/thaw cycles to release Nb9G8m to the supernatant. As a result, the recovery of soluble Nb9G8m using the original culture conditions was negligible (Fig. S1C) compared to the optimized procedure, which yielded a more significant Nb9G8m soluble fraction (Fig. S1D).

The soluble fraction of Nb9G8m was subjected to a purification process. Initially, only one chromatographic step –IMAC– was performed since this chromatography usually renders the protein of interest with high purity [36]. In this case, however, it was not enough (results not shown). Therefore, Nb9G8m purification was carried out, starting with an IEC chromatographic step, followed by IMAC. This way, the anion exchanger eliminated a significant quantity of contaminant proteins, while Nb9G8m bound to the cation exchanger with fewer contaminants (Fig. S1E), which were subsequently removed in the IMAC step. This chromatographic procedure yielded the Nb with high purity (>90%), with minor losses in the unbound protein and wash fractions

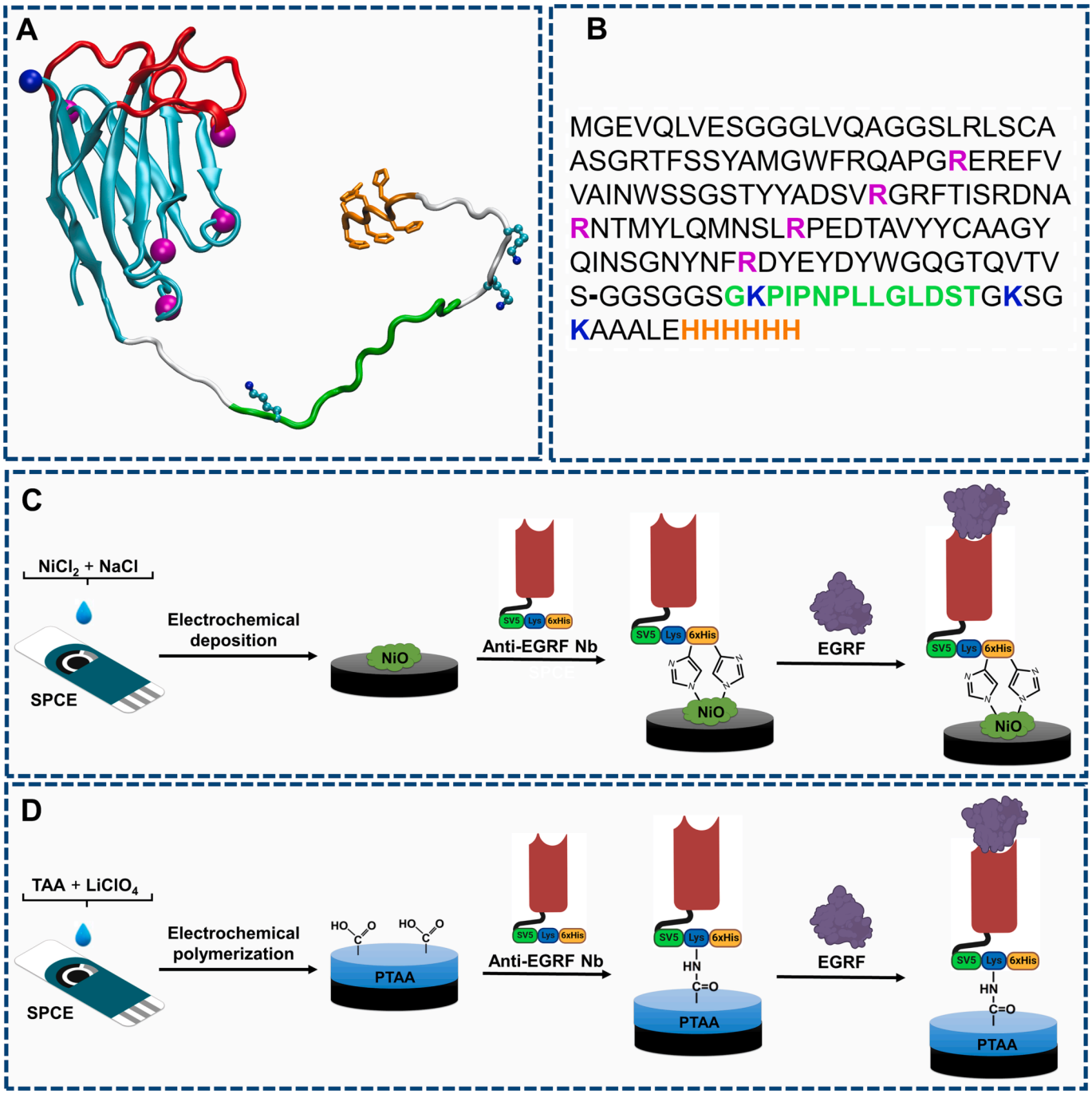

Scheme 1. Redesign of Nb 9G8 and coupling to the nanobiosensor surface. A) Structural model of the engineered nanobody. The protein backbone is shown in a cyan cartoon representation, with the three CDRs colored red. The N-terminus (carrying an amino group) is marked with a blue sphere, while the five positions mutated from Lys to Arg are marked with spheres in magenta. The C-terminal tail is colored in light gray, with the SV5 and 6xHis tags in green and orange, respectively, and the histidine side chains shown as sticks. The three lysines in the C-terminal tail are represented in balls and sticks. The C-terminal tail is very flexible, so the figure shows one possible conformation arbitrarily chosen among an ensemble of conformations produced by the MODPED server. B) Amino acid sequence of the engineered nanobody. The mutated positions are highlighted in magenta, while the three lysines in the C-terminal tail are marked in bold blue. The SV5 and 6xHis tags are highlighted in green and orange, respectively. C,D) Schematic illustration of the modification of SPCE with C) BSA/anti-EGFR/NiO nanobiocomposite and D) BSA/anti-EGFR/PTAA to detect EGFR protein. $NiCl_2$, nickel chloride; NaCl, sodium chloride; NiO, nickel oxide; anti-EGFR Nb, epidermal growth factor receptor Nb; SV5Tag, SV5 peptide; Lys, lysine; 6xHis, 6 histidines tag; EGFR, epidermal growth factor receptor; TAA, thiophene acetic acid; $LiClO_4$, lithium perchlorate; PTAA, poly(thiophene acetic acid).

(Fig. S1F).

3.3. Characterization of nanostructured platforms

The methodologies used to immobilize the anti-EGFR Nb at SPCE were designed based on the functionalities generated by protein engineering. The electrochemical nanobiosensors developed with the nanostructured SPCEs for detecting the EGFR protein by EIS are shown in Scheme 1. First, Ni NPs were electrosynthesized in situ in the presence of NaCl as a supporting electrolyte in the electrochemical reduction of

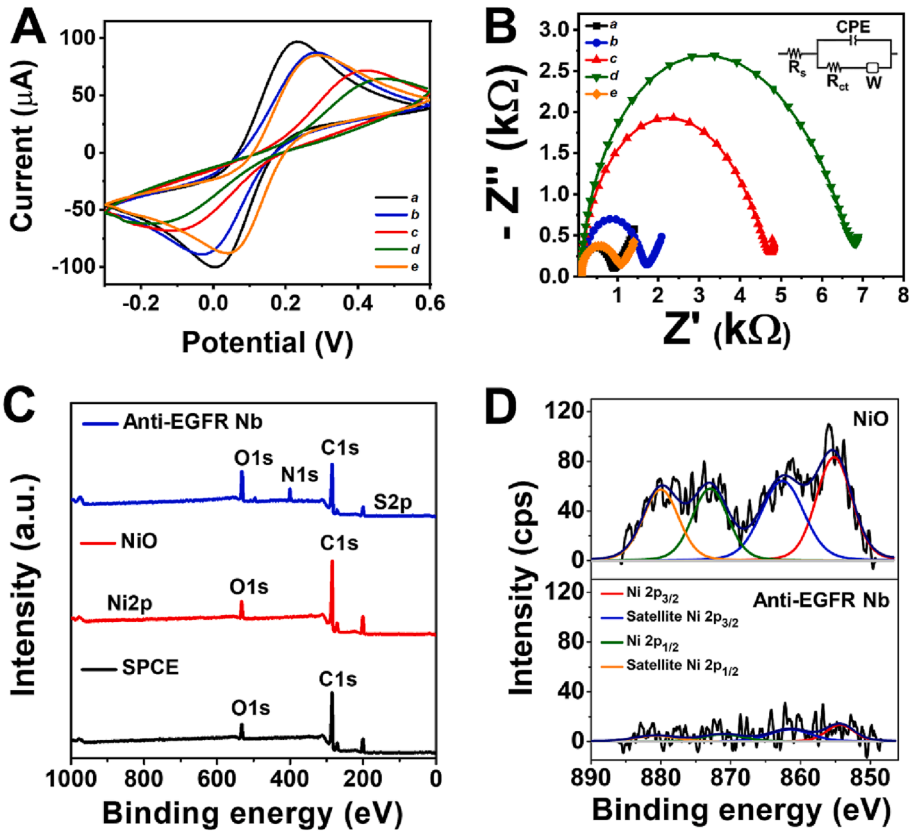

Fig. 1. A) CV and B) EIS response at each step of SPCE modification for NiO-based platform recorded in a 1X PBS pH 7.4 solution containing 5 mM $[Fe(CN)_6]^{3-/4-}$: a) bare SPCE, b) NiO, c) anti-EGFR Nb, d) BSA and e) EGFR (50 μg mL^{-1}). C) Survey spectra for each step of the NiO-platform assembly. D) Corresponding Ni2p core level spectra for NiO bio-conjugation.

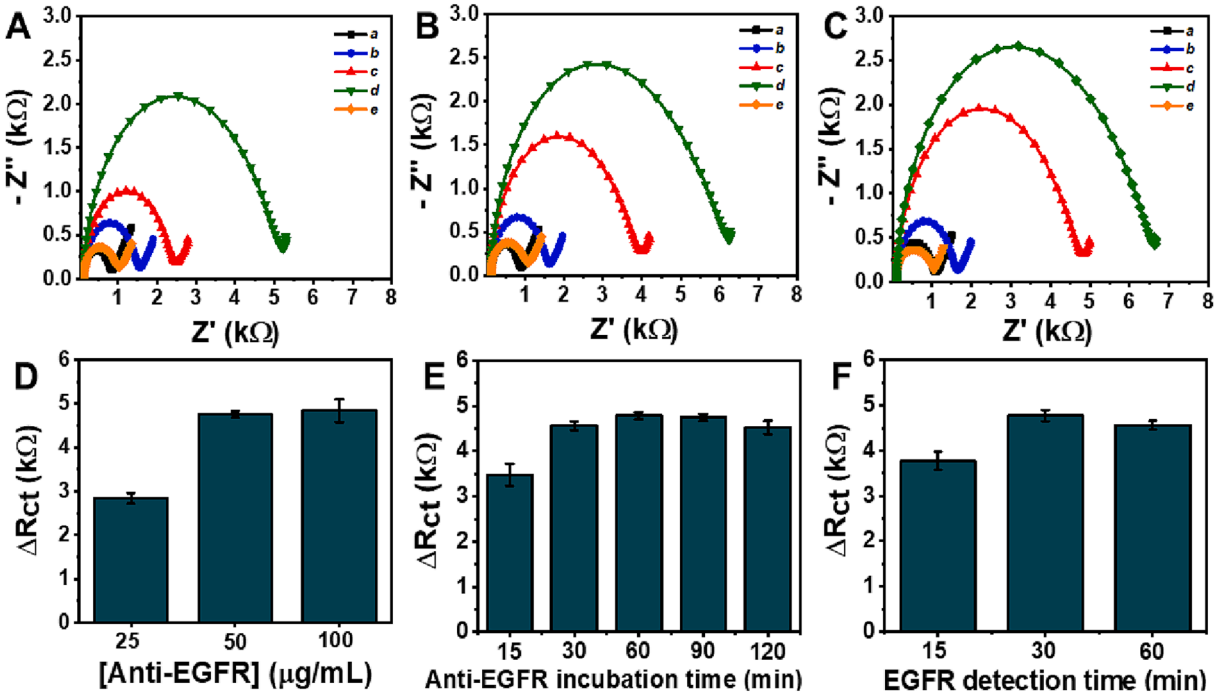

Fig. 2. Optimization of the anti-EGFR nanobody concentration on the NiO-based biosensor: a) bare SPCE, b) NiO NPs, c) anti-EGFR Nb, d) BSA, and e) EGFR for A) 25, B) 50, and C) 100 μg mL^{-1}. The histograms show D) the summary and quantification of the ΔR_{ct} for the anti-EGFR concentration experiment, E) the anti-EGFR incubation time, and F) the EGFR incubation time. Error bars indicate the standard deviation of duplicate measurements.

the Ni salt (Fig. S2A) by the "H_2 coevolution method", i.e., the reduced Ni on the graphitic surface of the SPCE serves to catalyze the evolution of H_2 at the applied reduction potential, producing visible bubbles that act like a blockage in the growth stages of Ni NPs [37]. NiO NPs were obtained by electrochemical oxidation of Ni in phosphate buffer (10X PB, pH 7.4) by CV, as shown in Fig. S2B. We can notice two pronounced oxidation and reduction peaks characteristic of Ni oxidation at pH 7.4, which decreased with the number of cycles [38]. The electrochemical oxidation was stopped after 40 CV cycles since almost stable response curves were obtained. The concentration of $NiCl_2$ was tested from 5 to 15 mM. However, 10 mM $NiCl_2$ was selected as the optimal concentration in agreement with previous works [37] since the electrochemical response by CV and EIS (Fig. S2C and D) was very similar in all concentrations. Therefore, this effect corroborated the controlled electrodeposition of Ni by using H_2 bubbles as blocking agents [37]. The morphology and elemental composition of the nanostructured NiO and PTAA platforms were characterized by FE-SEM and EDS. Fig. S3A and S3B show the FE-SEM images of electrodeposited NiO NPs on SPCE. Image analysis with the ImageJ software revealed that the NPs had a size of 56 ± 7 nm (n = 60), and the surface coverage was 0.57 %. The EDS analysis was performed at various points on the surface of the working electrode and confirmed the presence of nickel (26 %) and oxygen (74 %), associated with the NiO NPs formation.

The architecture of the PTAA-based nanobiosensor is shown in Scheme 1B. The PTAA film was electrosynthesized on SPCE in the presence of the perchlorate (ClO_4^-) counterion to compensate for the monomer-positive charges. Electropolymerization of TAA monomer was carried out at a fixed potential of + 1.1 V to generate the radical, cationic species $TAA^{\bullet+}$ involved in the nucleation and growth processes of the PTAA polymer chain [39]. Different values of electric charge involved in the potentiostatic polymerization of the PTAA layer were evaluated to achieve an interface with a high density of carboxylic acid groups, as shown in Figs. S4 and S5. The synthesis of PTAA up to an electrical charge of 600 μC was selected to form a stable film with a high density of carboxyl groups, ideal for bioconjugation processes and without causing damage by overoxidation as occurred with polymerization carried out up to 1200 μC.

3.4. Assembly and characterization of the biosensing interface

The investigation of electrochemical interfacial properties of NiO- or PTAA-based platforms and assembly of the detection assay using anti-EGFR Nb coupled to the nanostructures was performed by CV and EIS, as shown in Fig. 1A-B and S6A-B. Each SPCE modification step was followed by the electroactive area (A_e) calculated with the Randles-Sevcik equation shown in SI-Eq 1 and summarized in Table S1 and S2. The cyclic voltammograms in Fig. 1A show quasi-reversible peaks with constant anodic and cathodic peak separations at all stages of biosensor assembly.

First, the successful electrodeposition of NiO NPs was corroborated by the decreased A_e of the NiO interface (10.3 mm^2) compared to the bare SPCE (13.2 mm^2) due to the semiconducting properties of the NiO NPs [40]. After immobilizing the anti-EGFR Nb on the NiO NPs, the A_e decreased to 5.1 mm^2, demonstrating the effective coupling between the 6xHis tag of the Nb and the NiO NPs. The Nb-metal ions affinity interaction was generated through the coordination of the Ni^{2+} cations of NiO with the free nitrogen electrons of the imidazole ring in His to orient the Nb. Remarkably, at pH values < 6.0, the imidazole groups of histidine involved in the coordination bond can be protonated and prevent the union of Nb with NiO NPs [41]. Therefore, electrochemical measurements were performed in 1X PBS pH 7.4 solution containing 5 mM $[Fe(CN)_6]^{3-/4-}$. The A_e decreased to 4.0 mm^2 due to the insulating nature of bovine serum albumin (BSA) used as a blocking agent to prevent non-specific adsorption in the detection steps. The CV results demonstrated the customized assembly of an engineered Nb-based bio-interface using a simple and fast methodology without additional bioconjugation steps compared to the PTAA-based platform, which requires activation of carboxylic acid groups with EDC/NHS chemistry, as discussed in the SI. Finally, the effective immunoreaction between EGFR and the BSA/anti-EGFR/NiO/SPCE-based nanobiosensor showed an increase in A_e up to 11.3 mm^2 due to the high amount of N-glycosylation in the EGFR structure. N-glycosylation contributes up to 50 kDa to the total

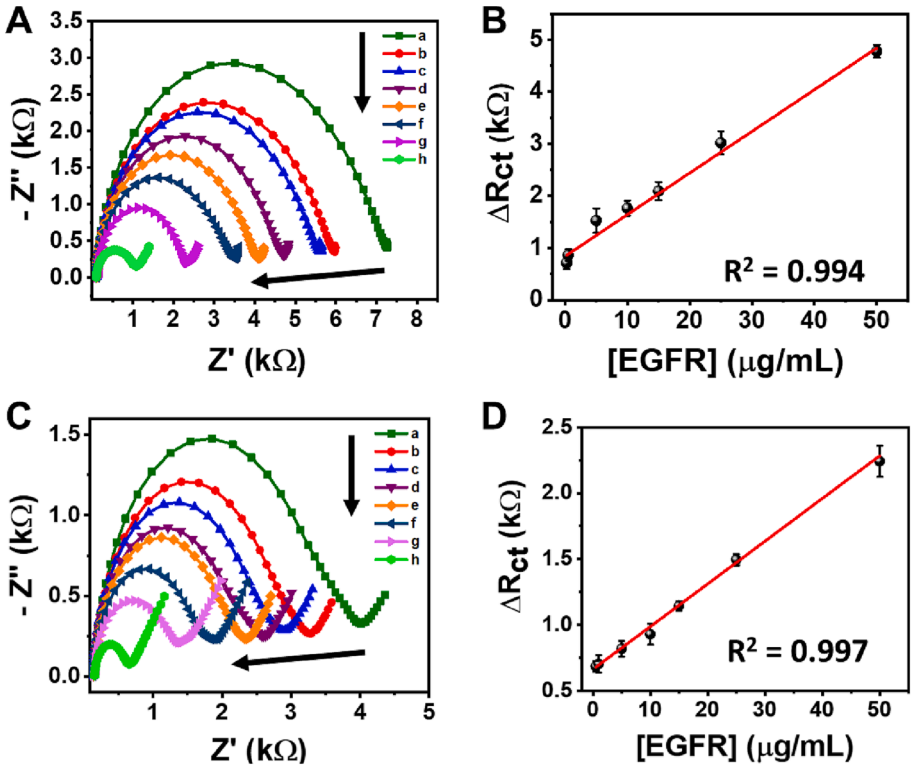

Fig. 3. A) EIS signals acquired from the label-free electrochemical NiO-based biosensor upon different EGFR concentrations, i.e., (a-h) 0, 0.25, 0.5, 5, 10, 15, 25, and 50 μg mL^{-1} EGFR. B) Resultant linear regression curve of ΔR_{ct} upon different concentrations of EGFR. C) EIS signals acquired from the label-free electrochemical PTAA-based biosensor upon different EGFR concentrations, i.e., (a-h) 0, 0.5, 1, 5, 10, 15, 25, and 50 μg mL^{-1} EGFR. D) Resultant linear regression curve of ΔR_{ct} upon different concentrations of EGFR.

molecular weight of the extracellular domain of the EGFR (~110 kDa) [42]. Furthermore, in the molecular probe used here, the extracellular domain of the EGFR is fused to an antibody Fc fragment, which contributes two additional N-glycosylation sites. Therefore, the partially neutral charge of the target enhanced the diffusion of the redox probe towards the electrode surface, and the detection was correlated with the A_e increase by CV.

The biosensors' effective architecture and target detection were confirmed by EIS, monitoring the resistance to electron transfer in the NiO- and PTAA-based platforms. Fig. 1B and S6C-D show the Nyquist diagrams derived from EIS, where the impedance data was presented in a complex plane with the real part (Z') plotted on the x-axis and the imaginary part (-Z'') plotted on the y-axis [43]. The EIS spectra were fitted using Randles equivalent circuit for electron transfer reactions with mass transfer control at low frequencies (ω), inserted in Fig. 1B. The equivalent circuit consists of a solution resistance (R_s), a charge transfer resistance (R_{ct}), and a constant phase element (CPE). $CPE = -1/(i\omega C)^n$ for a non-ideal capacitor, where n is the exponent of the CPE (1 for a pure capacitor and 0.5 for non-uniform and rough surfaces). Z_w represents the Warburg impedance for diffusion-controlled processes of the species in solution and corresponds to a straight line in the complex plane plots [43].

Table S2 summarizes the calculated data from the EIS analysis. The R_{ct} of NiO NP-modified SPCE increased to 1526.8 ± 113.4 Ω compared to bare SPCE (R_{ct} = 743.8 ± 76.2 Ω), supporting the CV results for efficient NiO electrosynthesis. Immobilization of anti-EGFR Nb on the NiO NPs was verified from an increased semicircle in the Nyquist plot with an R_{ct} of 4374.9 ± 57.9 Ω. Such an increase is due to hindered electron transfer from the redox probe at the Nb-coated platform. The free sites not covered with Nb were blocked with BSA, and the insulating nature of this biomolecule produced an increase in R_{ct} equal to 6262.4 ± 74.2 Ω. These results confirmed the simple and fast assembly process of the synthetic Nb-based nanobiosensor on NiO NPs like the CV analysis. The significant decrease in R_{ct} confirmed the immunocomplex formation to 773.4 ± 15.4 Ω. This result corroborated the successful molecular biorecognition event since the glycosylated EGFR decreased the difficulty of the redox probe to diffuse toward the electrode surface. The PTAA-based biosensor assembly described in the SI showed similar electrochemical responses to the NiO-based platform and the EGFR target biosensing with decreased R_{ct}. In this way, the activity of the anti-EGFR Nb synthesized *in vitro* for binding with EGFR was demonstrated electrochemically, considering the chemical properties of each biomolecule.

In addition, XPS analysis was used to study the mechanism of surface nanostructuring and anti-EGFR Nb binding in the assembly of NiO-NPs and PTAA-based biosensors. XPS analysis of the PTAA-based biosensor assembly was detailed in Figs. S7A-H. The survey spectra in Fig. 1C show the evolution of signals for C1s, O1s, and Ni2p in the NiO NP-modified SPCE. Besides, the emergence of signals for N1s and S2p after Nb immobilization. Fig. 1D shows the high-resolution spectra of the Ni2p core level corresponding to the electrochemically synthesized NiO NPs on SPCE. The Ni2p spectral line showed a multiplet division with two key components at 855.2 eV and 872.9 eV with satellite peaks at 862.6 eV and 880.0 eV corresponding to $Ni2p_{3/2}$ and $Ni2p_{1/2}$, respectively. The splitting peak separation (ΔE) was 17.7 eV. Since the peak position of Ni2p line cannot be assigned to a single chemical state, the range of energies of each component is associated with Ni^{2+} in NiO or $Ni(OH)_2$ [44]. This result was supported by the analysis of the core level spectrum of O1s shown in Fig. S8A, which presents a component at 531.6 eV assigned to lattice oxygen in NiO. Likewise, the components at high binding energies are attributed to OH groups, possibly due to the spontaneous hydroxylation of the Ni surface and carboxylates present in SPCE [44]. The components in the O1s spectrum at 532.4 and 533.5 eV and in the C1s spectrum (Fig. S8B) at 284.5, 286.2, and 289.0 eV for C-(C,H), C-O and (C = O)–OH bonds, respectively, were associated with the graphitic carbon of the NiO NPs uncoated working electrode, as evidenced in the FE-SEM images in Fig. S2. The effective immobilization of anti-EGFR Nb on NiO NPs was clearly evidenced by the decrease in intensity of the Ni2p spectral line shown in Fig. 1D. The emerging peaks in the high-resolution spectra of O1s, C1s, N1s, and S2p (Figs. S8C-F) show the typical signals of the peptide bond and the amino acid residues present in the primary structure of the Nb attached to the NiO NPs. Thus, the components at 532.7 eV in O1s, 588.3 eV in C1s, and 400.2 eV in N1s were attributed to the amide bond ((C = O) − NH) [45]. C − S bond in the cysteine and methionine residues of Nb was observed at 286.5 eV in the C1s spectrum, and the new doublet peaks of the S2p spectrum at 163.9 and 165.4 eV. A small component of 534.8 eV in O1s was related to OH groups in the protein chain.

The biofunctionalization of NiO or PTAA nanostructures with anti-EGFR Nb were differentiated in the N1s spectra of both platforms. For example, the N1s spectrum (Fig. S8E) of Nb coupled to the NiO platform shows a small component at 402.2 eV corresponding to terminal amines ($C - NH_3^+$) of free lysines, which were protonated under the vacuum conditions of the XPS analysis [44]. In contrast, Fig. S7E shows the N1s core level spectrum of the Nb-PTAA-based platform with a component at 398.4 eV related to the C=N bond of free imidazole ring and a signal at 402.4 eV, probably from the free protonated imidazole ring ($C{=}NH^+{-}$) in the 6xHis tag. Therefore, XPS analysis corroborated the effective bioengineering of the synthetic Nb for proper bioconjugated chemistry in biosensor development.

3.5. Optimization of experimental parameters involved in EGFR detection

To compare how the moieties generated at the nanobody and the two approaches to immobilize them at the SPCE through the 6x-his-tag or Lys residues at the C-terminal tail impact the analytical performance of the nanocomposite biosensing interfaces, we first optimized the binding conditions. For example, we studied the optimal concentration of anti-EGFR Nb and incubation time on the NiO and PTAA nanostructures and the optimal incubation time for the EGFR glycoprotein. A higher ΔR_{ct} value between R_{ct}(BSA) and R_{ct}(EGFR) containing 50 μg mL^{-1} of EGFR was taken as a criterion to select the optimal values in both the NiO-based and PTAA-based platforms described in the S.I. First, 25, 50, and 100 μg mL^{-1} of anti-EGFR Nb were incubated on the surface of NiO-NPs-modified SPCE for 90 min to obtain the optimal concentration for EGFR detection (Fig. 2A-D). Immobilization of 50 and 100 μg mL^{-1} of anti-EGFR Nb resulted in an ΔR_{ct} of 4745.7 ± 75.9 Ω and 4830.1 ± 255.9 Ω, respectively, compared to the lowest ΔR_{ct} value for 25 μg mL^{-1} (2835.8 ± 125.4 Ω). Therefore, a concentration of 50 μg mL^{-1} provided a sufficiently dense surface of Nbs to maximize interaction with EGFR.

Anti-EGFR Nb immobilization for 15, 30, 60, 90, and 120 min were evaluated (Fig. S9). Immobilization of anti-EGFR Nb for 15 min (3475.8 ± 246.9 Ω) was insufficient. However, 30 (4566.1 ± 99.6 Ω), 60 (4783.6 ± 84.4 Ω), 90 (4745.7 ± 75.9 Ω), and 120 min (4523.1 ± 147.9 Ω) were not statistically significantly different (Fig. 2E). Therefore, 30 min was optimal for the 6xHis-tag/Ni^{2+} coordinated bond formation. Finally, optimization of the interaction times of EGFR with the assembled biosensors is shown in Fig. 2F and S10. Immune complex formation on the electrode surface was insufficient in only 15 min of reaction (3775.9 ± 201.3 Ω) compared to 30 and 60 min, with ΔR_{ct} values of 4778.1 ± 122.6 Ω and 4566.1 ± 99.6 Ω, respectively. Whereby 30 min was chosen as the optimal EGFR detection time to evaluate the analytical performance of the biosensor. In the same sense, the optimal conditions to detect EGFR on the PTAA-based biosensor required immobilizing 50 μg mL^{-1} for 60 min of anti-EGFR Nb on the activated carboxylic acids of the PTAA interface, as shown sequentially in the Figs. S11-13. Likewise, the EGFR biosensing time took 60 min, possibly because a fraction of the anti-EGFR Nb may have bound to PTAA through the amino group in the N-terminal residue, causing the antigen-Nb affinity interaction to be slightly delayed in comparison with the highly oriented NiO NPs-based biosensor.

3.6. Analytical performance

We evaluated the analytical performance of both biosensor platforms under optimized conditions by EIS in 1X PBS containing 5 mM $[Fe(CN)_6]^{3-/4-}$. The detection with increasing concentrations of EGFR generated decreased R_{ct} due to the partially neutral charge of the immunocomplex, which promotes the diffusion of the redox probe toward the electrode interface, as explained above. Fig. 3 shows the calibration curves of NiO NPs and PTAA-based biosensor platforms by estimating the ΔR_{ct} for the different solutions with known EGFR concentrations. The linear correlation between ΔR_{ct} and the EGFR glycoprotein concentration of the NiO NP-based platform in a range of 0.25 to 50 μg mL^{-1} exhibited a linear regression equation expressed as $\Delta R_{ct} = 79.89[EGFR] + 842.47$ with a correlation coefficient $R^2 = 0.994$ (Fig. 3B). Meanwhile, Fig. 3D shows the detection of EGFR on the PTAA-based platform in a linear range between 0.5 and 50 μg mL^{-1} with an equation described as $\Delta R_{ct} = 32.39[EGFR] + 663.72$ and an $R^2 = 0.997$. The limit of detection (LOD = 3SD/slope), the limit of quantification (LOQ = 10SD/slope), and sensitivity (S = slope/A_e) were calculated taking into account the standard deviation (SD) for R_{ct}(BSA), the slope of the calibration curves and the A_e for each assembled platform. The LOD, LOQ, and sensitivity of the NiO NPs-based platform were 0.46 μg mL^{-1}, 1.55 μg mL^{-1}, and 19.97 Ω μg^{-1} mL mm^{-2}, respectively, using an SD of 12.41 Ω (n = 10) for measurements in the absence of EGFR protein. Similarly, the PTAA-based platform presented analytical performance with a LOD, LOQ, and sensitivity of 1.14 μg mL^{-1}, 3.87 μg mL^{-1}, and 5.68 Ω μg^{-1} mL mm^{-2}, respectively, with an SD of the blank signal of 12.32 Ω (n = 10). LOD and LOQ of the NiO-NPs platform were lower than those from PTAA. This could be explained by the conformational freedom of the immobilized Nb through the 6xHis-tag that adopts a more upright, end-on orientation with better flexibility and provides closer packing, resulting in a higher surface area accessible to the target [46], compared to covalent immobilization of Nbs via the Lys-tag, which may reduce bioreceptor flexibility on the surface that hampers interaction with EGFR. The methods were reproducible with a relative standard deviation (RSD) below 5% for EGFR detection using three replicate assays for all concentrations tested. Additionally, Fig. S14 shows the Nyquist spectra with high inter-device reproducibility assembled on the SPCEs at optimal conditions with RSD of 1.6 and 2.3 % for the NiO NPs and PTAA-based platforms, respectively.

In the same fashion, we constructed an enzyme-linked immunosorbent assay (ELISA) adsorbing different known concentrations of EGFR onto a 96-well plate and using an anti-SV5 antibody (anti-SV5 Ab) coupled with horseradish peroxidase (HRP) to support the impedimetric results and test the SV5 tag (SV5tag) in the C-terminal region of the Nb. Fig. S15 shows the ELISA with a linear regression equation expressed as Absorbance = 0.78[EGFR] + 0.10 and an $R^2 = 0.984$, with a blank SD equal to 0.003 (n = 10). The LOD and LOQ of the ELISA were 10 ng mL^{-1} and 40 ng mL^{-1}, respectively. Including an SV5 or equivalent tag as part of a C-terminal tail is a useful feature that may be implemented in engineered nanobody-based biosensors. In this context, bioengineering of the 6xHis-, Lys-, and SV5- tags added to the C-terminal part of the engineered Nb was confirmed.

Table S3 compares the analytical performance of nanostructured platforms based on the engineered Nb with the ELISA assay and other biosensors described for EGFR detection. Although the LODs achieved in the nanostructured platforms are not as low as those reported by other authors or the ELISA, the platforms based on NiO-NPs and PTAA offered adequate sensitivity for detecting tumor cells with surface-expressed EGFR, without any further purification, as demonstrated below. Other inherent advantages of the NiO NP-based platform developed with the engineered Nb were the time required to prepare the biosensor (1 h) and the assay time of 30 min required for effective target interaction. Overall, the on-demand engineered Nb demonstrated a versatile approach to orient these bioreceptors at the surface of nanoarchitectures with a similar working linear range. The NiO-based nanobiocomposite had a 2.5-fold lower LOD concerning the PTAA-based interface due to a possible better orientation when coupling through NiO NPs. In addition, it highlights the benefits of the unique assembly from on-demand designed Nbs. On the other hand, natural Nb-based approaches using signaling systems such as Föster resonance energy transfer (FRET) or fluorescent signaling systems take > 1 h to detect the target [47,48]. In this way, the simple, fast, and portable detection on the SPCE decorated with the nanobiocomposite proved suitable for developing miniaturized systems compatible with the point-of-care concept.

3.7. Specificity and selectivity

The specificity and selectivity of the nano-biosensors were tested with different biomolecules that could interfere with the EGFR protein determination. Therefore, we evaluated the potential cross-reactivity of the EGFR protein to carcinoembryonic antigen (CEA), p53 antigen, and IgG antibody (IgG). Notably, the IgG antibody contains the same type of Fc moiety in the fusion EGFR-Fc protein used here as the probe.

The interfering species were measured ten times more concentrated than the target to corroborate the reliability of the assay. Fig. 4 shows the impedimetric response assays for the two platforms in the presence of the three possible interferents at 5 μg mL^{-1}, the mix of them, and the mix with 0.5 μg mL^{-1} target. Fig. 4A and 4C show the Nyquist plot from EIS measurements and the corresponding ΔR_{ct}. The results in Fig. 4B and 4D show that the ΔR_{ct} expressed in Ω was higher for the EGFR protein (861.85 ± 110.45 and 685.89 ± 40.76 Ω) and EGFR protein and the mix (853.17 ± 111.56 and 771.33 ± 39.83 Ω) compared to CEA (56.81 ± 53.03 and 115.17 ± 18.98 Ω), p53 (105.17 ± 35.63 and 132.58 ± 18.57 Ω), IgG (57.85 ± 76.44 and 112.85 ± 17.89 Ω) and the mix (85.52 ± 49.26 and 163.23 ± 52.57 Ω), for the NiO- and PTAA-based platforms, respectively. In addition, the ΔR_{ct} signal for the EGFR protein showed significant statistical differences when compared with the blank and the other proteins tested individually or mixed, with a level of statical significance of 95% ($p < 0.05$). These results indicate that the biosensor was highly selective and specific for EGFR protein detection.

3.8. EGFR detection in the whole cancer cell membrane

As proof of concept, both platforms were tested with cell lines expressing different levels of EGFR in the membrane. Fig. 5A and 5C show the Nyquist diagrams of the biosensors incubated with each cell line ($1x10^6$ cell mL^{-1}). The impedimetric signals show a clear differentiation and hierarchy among cell lines in both platforms, with a decrease in the R_{ct} signal caused by the glycosylations on the cell surface. Fig. 5B and 5D show the adjustment value for the ΔR_{ct} of the different cell lines. A higher level of EGFR expression was evidenced in A431 cells, followed by the SW480, SW620, and the HEK293 cell line used as control. This result agrees with previous reports since the A431 cell line, isolated from an epidermoid carcinoma, expresses abnormally high levels of EGFR and is a standard positive control for EGFR expression [49]. Likewise, the SW480 and SW620 cell lines derived from a colon adenocarcinoma and a lymph node metastasis showed a higher ΔR_{ct} than the normal HEK293 cells used as non-neoplastic control [50–52]. This effect is consistent with previous reports [53], in which EGFR overexpression is found in CRC cell lines, particularly in SW480 (stage II) cell lines where membrane receptors are crucial for abnormal cell proliferation.

4. Conclusions

We successfully developed two nanostructured platforms based on NiO NPs and PTAA for the specific binding of an engineered anti-EGFR nanobody as a molecular recognition element in label-free impedimetric detection of the EGFR glycoprotein. The amino acid sequence of the Nb was engineered to provide a 6xHis-tag and a Lys dual functionality to link it to the nanosensing platform by complexing to metal chelates or

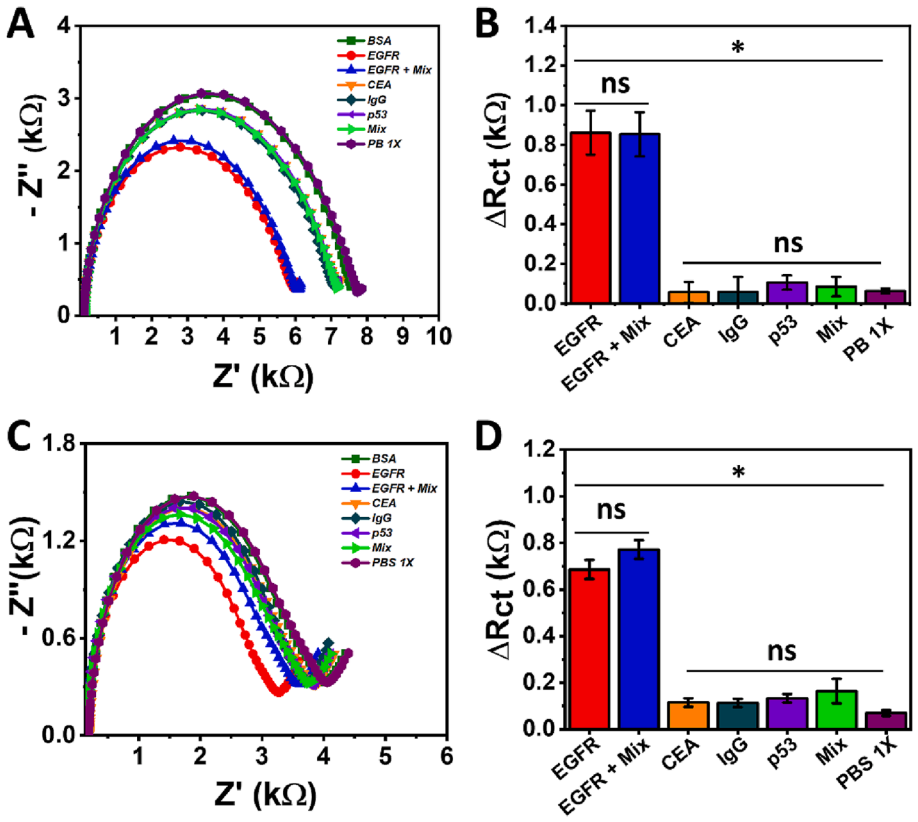

Fig. 4. Nyquist plot for 0.5 μg mL^{-1} EGFR and 10-fold (5 μg mL^{-1}) interfering species and the mixture of all proteins and antibodies, respectively, in a 1X PBS pH 7.4 solution for A) NiO- and C) PTAA-based biosensor. The difference in the ΔR_{ct} for each sample in B) NiO- and D) PTAA-based biosensor. * Indicates significant differences with $p < 0.05$ and ns denotes no significant differences ($p < 0.05$).

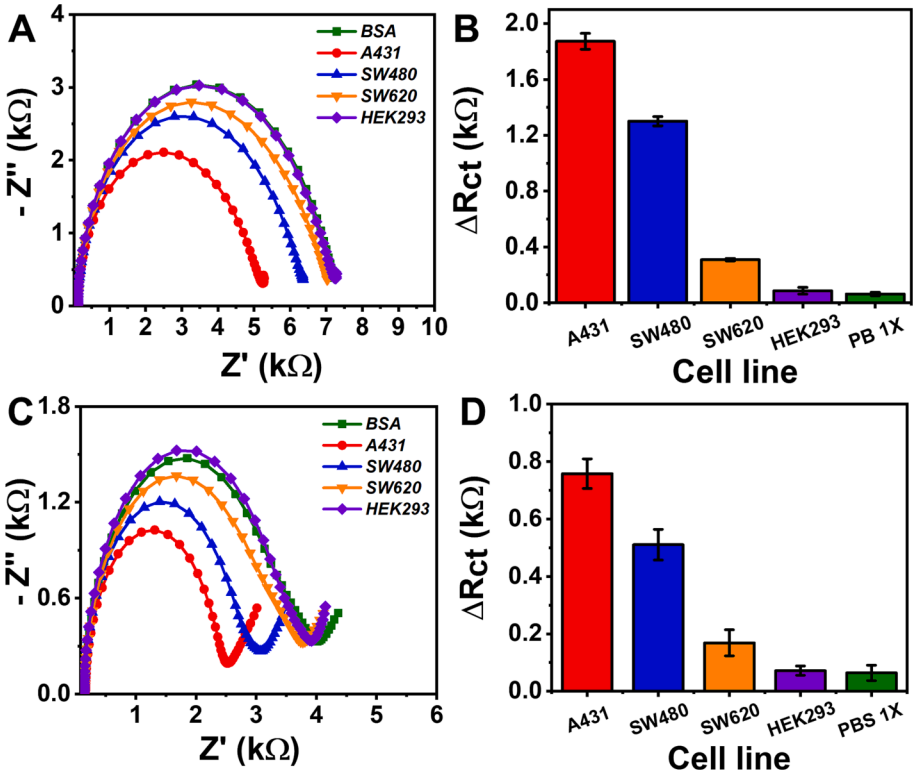

Fig. 5. Change in EIS response of the biosensor of different cell lines for A) NiO- and C) PTAA-based biosensor. The difference in the ΔR_{ct} for each sample in B) NiO- and D) PTAA-based biosensor. Error bars indicate the standard deviation of duplicate measurements.

covalently coupling to the interface, respectively. Electropolymerization and potentiostatic electrodeposition were robust techniques for obtaining highly reproducible NiO NPs and PTAA thin films. Electrochemical techniques, XPS, and other physicochemical analyses characterized the successful assembly of the biosensor platforms. The obtained nanobiosensors monitored the EGFR glycoprotein using EIS and discriminated cancer cells with different levels of EGFR expression with high specificity and reproducibility. In addition, the functionality of engineered anti-EGFR Nb was compared on both platforms assembled in parallel, demonstrating the reliability of coordination interaction between Ni^{2+} of NiO NPs with the 6xHis-tag and the covalent bond between the carboxyl groups of PTAA and the Lys-tag of Nbs. Although both proposed platforms had adequate performance, bioengineering Nbs with end-Lys tags may improve the more upright orientation of the bioreceptor with high coverage on functional polymer-based substrates to detect targets in a few minutes, like the His-tag strategy proposed. Overall, engineered Nb-based platforms hold promise for developing robust, low-cost, and easily miniaturized detection devices for cancer-related biomarker detection.

CRediT authorship contribution statement

Andrés F. Cruz-Pacheco: Conceptualization, Methodology, Formal analysis, Investigation, Data curation, Writing – original draft. **Yeison Monsalve:** Conceptualization, Methodology, Formal analysis, Investigation, Data curation, Writing – original draft. **Yunier Serrano-Rivero:** Methodology, Formal analysis, Investigation, Writing – original draft. **Julieta Salazar-Uribe:** Methodology, Formal analysis, Investigation. **Ernesto Moreno:** Methodology, Formal analysis, Investigation. **Jahir Orozco:** Conceptualization, Formal analysis, Writing – review & editing, Supervision, Project administration, Funding acquisition.

Declaration of Competing Interest

The authors declare that they have no known competing financial interests or personal relationships that could have appeared to influence the work reported in this paper.

Data availability

The authors are unable or have chosen not to specify which data has been used.

Acknowledgments

The work has been funded by MINCIENCIAS, MINEDUCACIÓN, MINCIT, and ICETEX through the Program Ecosistema Científico Cod. FP44842-211-2018, project numbers 58536 and 58676. J.O. thanks support from The University of Antioquia and the Max Planck Society through the cooperation agreement 566-1, 2014. E.M., thanks for the support from the University of Medellin. We thank EPM and The Ruta N complex for hosting the Max Planck Tandem Groups.

Appendix A. Supplementary data

Supplementary data to this article can be found online at https://doi.org/10.1016/j.cej.2023.142941.

References

[1] C. Hamers-Casterman, T. Atarhouch, S. Muyldermans, G. Robinson, C. Hammers, E. B. Songa, N. Bendahman, R. Hammers, Naturally occurring antibodies devoid of light chains, Nature. 363 (1993) 446–448, https://doi.org/10.1038/363446a0.
[2] B. Li, X. Qin, L.-Z. Mi, Nanobodies: from structure to applications in non-injectable and bispecific biotherapeutic development, Nanoscale. 14 (2022) 7110–7122.
[3] S. Muyldermans, Nanobodies: Natural single-domain antibodies, Annu. Rev. Biochem. 82 (2013) 775–797, https://doi.org/10.1146/annurev-biochem-063011-092449.
[4] M.S. Valdés-Tresanco, A. Molina-Zapata, A.G. Pose, E. Moreno, Structural Insights into the Design of Synthetic Nanobody Libraries, Molecules. 27 (2022) 1–18, https://doi.org/10.3390/molecules27072198.
[5] T. De Meyer, S. Muyldermans, A. Depicker, Nanobody-based products as research and diagnostic tools, Trends Biotechnol. 32 (2014) 263–270, https://doi.org/10.1016/j.tibtech.2014.03.001.
[6] Q. Zhou, G. Li, K. Chen, H. Yang, M. Yang, Y. Zhang, Y. Wan, Y. Shen, Y. Zhang, Simultaneous unlocking optoelectronic and interfacial properties of c60 for ultrasensitive immunosensing by coupling to metal-organic framework, Anal. Chem. 92 (2020) 983–990, https://doi.org/10.1021/acs.analchem.9b03915.
[7] D. Pan, G. Li, H. Hu, H. Xue, M. Zhang, M. Zhu, X. Gong, Y. Zhang, Y. Wan, Y. Shen, Direct Immunoassay for Facile and Sensitive Detection of Small Molecule Aflatoxin B1 based on Nanobody, Chem. - A Eur. J. 24 (2018) 9869–9876, https://doi.org/10.1002/chem.201801202.
[8] Q. Zhou, G. Li, Y. Zhang, M. Zhu, Y. Wan, Y. Shen, Highly Selective and Sensitive Electrochemical Immunoassay of Cry1C Using Nanobody and π-π Stacked Graphene Oxide/Thionine Assembly, Anal. Chem. 88 (2016) 9830–9836, https://doi.org/10.1021/acs.analchem.6b02945.
[9] B. Kovalchuk, A.S. Berghoff, M.A. Karreman, K. Frey, M. Piechutta, M. Fischer, J. Grosch, S. Heiland, M.O. Breckwoldt, F. Hilberg, W. Wick, F. Winkler, Nintedanib and a bi-specific anti-VEGF/Ang2 nanobody selectively prevent brain metastases of lung adenocarcinoma cells, Clin. Exp. Metastasis. 37 (2020) 637–648, https://doi.org/10.1007/s10585-020-10055-x.
[10] J. Liu, Y. Jiang, X. Chen, L. Chen, X. Zhang, D. Cui, Y. Li, Z. Liu, Q. Zhao, A. Diao, Development of active affibody aggregates induced by a self-assembling peptide for high sensitive detection of alpha-fetoprotein, Chem. Eng. J. 436 (2022), 135208, https://doi.org/10.1016/j.cej.2022.135208.
[11] S. Spinelli, L.G.J. Frenken, P. Hermans, T. Verrips, K. Brown, M. Tegoni, C. Cambillau, M. Biologiques, C.J. Aiguier, Camelid Heavy-Chain Variable Domains Provide Efficient Combining Sites to, Biochemistry. 1217–1222 (2000).
[12] A. Ganji, M. Islami, M. Ejtehadifar, E. Zarei-Mehrvarz, M. Darvish, Nanobody and aptamer as targeting moiety against bacterial toxins: Therapeutic and diagnostic applications, Rev. Res. Med. Microbiol. 30 (2019) 183–190, https://doi.org/10.1097/MRM.0000000000000175.
[13] N. An, Y.N. Hou, Q.X. Zhang, T. Li, Q.L. Zhang, C. Fang, H. Chen, H.C. Lee, Y. J. Zhao, X. Du, Anti-Multiple Myeloma Activity of Nanobody-Based Anti-CD38 Chimeric Antigen Receptor T Cells, Mol. Pharm. 15 (2018) 4577–4588, https://doi.org/10.1021/acs.molpharmaceut.8b00584.
[14] M. Shu, Y. Xu, D. Wang, X. Liu, Y. Li, Q. He, Z. Tu, Y. Qiu, Y. Ji, X. Wang, Anti-idiotypic nanobody: A strategy for development of sensitive and green immunoassay for Fumonisin B1, Talanta. 143 (2015) 388–393, https://doi.org/10.1016/j.talanta.2015.05.010.
[15] D. Schumacher, J. Helma, A.F.L. Schneider, H. Leonhardt, C.P.R. Hackenberger, Nanobodies: Chemical Functionalization Strategies and Intracellular Applications, Angew. Chemie - Int. Ed. 57 (2018) 2314–2333, https://doi.org/10.1002/anie.201708459.
[16] L. Wang, Y. Ding, N. Li, Y. Chai, Q. Li, Y. Du, Z. Hong, L. Ou, Nanobody-based polyvinyl alcohol beads as antifouling adsorbents for selective removal of tumor necrosis factor-α, Chinese Chem. Lett. 33 (2022) 2512–2516, https://doi.org/10.1016/j.cclet.2021.12.087.
[17] W. Wu, L. Shi, Y. Duan, S. Xu, L. Shen, T. Zhu, L. Hou, X. Meng, B. Liu, Nanobody modified high-performance AIE photosensitizer nanoparticles for precise photodynamic oral cancer therapy of patient-derived tumor xenograft, Biomaterials. 274 (2021), 120870, https://doi.org/10.1016/j.biomaterials.2021.120870.
[18] D. Echeverri, A.F. Cruz-Pacheco, J. Orozco, Capacitive nanobiosensing of β-1,4-galactosyltransferase-V colorectal cancer biomarker, Sensors Actuators: B. Chemical. 374 (2023) 132784.
[19] S. Cajigas, D. Alzate, J. Orozco, Gold/DNA-based nanobioconjugate for electrochemical detection of zika virus, Microchimica Acta 187 (594) (2020).
[20] A.F. Cruz-Pacheco, J. Quinchia, J. Orozco, Nanostructured poly(thiophene acetic acid)/Au/poly(methylene blue) interface for electrochemical immunosensing of p53 protein, Sensors Actuators: B. Chemical. 190 (2023) 136.
[21] A.F. Cruz-Pacheco, J. Quinchia, J. Orozco, Cerium oxide-doped PEDOT nanocomposite for label-free electrochemical immunosensing of anti-p53 autoantibodies, Microchimica Acta 189 (2022) 228.
[22] J. Quinchia, D. Echeverri, A.F. Cruz-Pacheco, M.E. Maldonado, J.A. Orozco, Electrochemical biosensors for determination of colorectal tumor biomarkers, Micromachines. 11 (2020) 1–46, https://doi.org/10.3390/MI11040411.
[23] A. Mashkoori, A. Mostafavi, T. Shamspur, M. Torkzadeh-Mahani, Electrochemical enzyme-based blood uric acid biosensor: new insight into the enzyme immobilization on the surface of electrode via poly-histidine tag, Microchim. Acta. 189 (2022), https://doi.org/10.1007/s00604-022-05408-0.
[24] C.L. Meyerkord, H. Fu, Protein-protein interactions: Methods and applications: Second edition, Protein-Protein Interact. Methods Appl. Second Ed. 1278 (2015) 1–613. doi: 10.1007/978-1-4939-2425-7.
[25] N. Aydemir, J. Malmström, J. Travas-Sejdic, Conducting polymer based electrochemical biosensors, Phys. Chem. Chem. Phys. 18 (2016) 8264–8277, https://doi.org/10.1039/c5cp06830d.
[26] P. Wee, Z. Wang, Epidermal Growth Factor Receptor Cell Proliferation Signaling Pathways, Cancers (Basel) (2017) 1–45, https://doi.org/10.3390/cancers9050052.

[27] M.W. Saif, Colorectal cancer in review: The role of the EGFR pathway, Expert Opin. Investig. Drugs. 19 (2010) 357–369, https://doi.org/10.1517/13543781003593962.
[28] S.L. Grant, A. Hammacher, A.M. Douglas, G.A. Goss, R.K. Mansfield, J.K. Heath, C. G. Begley, An unexpected biochemical and functional interaction between gp130 and the EGF receptor family in breast cancer cells, Oncogene. 21 (2002) 460–474, https://doi.org/10.1038/sj.onc.1205100.
[29] O.M. Fischer, S. Hart, A. Gschwind, A. Ullrich, EGFR signal transactivation in cancer cells, Biochem. Soc. Trans. 31 (2003) 1203–1208, https://doi.org/10.1042/bst0311203.
[30] G. Lin, X.J. Sun, Q.B. Han, Z. Wang, Y.P. Xu, J.L. Gu, W. Wu, G. Zhang, J.L. Hu, W. Y. Sun, W.M. Mao, Epidermal growth factor receptor protein overexpression and gene amplification are associated with aggressive biological behaviors of esophageal squamous cell carcinoma, Oncol. Lett. 10 (2015) 901–906, https://doi.org/10.3892/ol.2015.3277.
[31] J.A. McKay, L.J. Murray, S. Curran, V.G. Ross, C. Clark, G.I. Murray, J. Cassidy, H. L. McLeod, Evaluation of the epidermal growth factor receptor (EGFR) in colorectal tumours and lymph node metastases, Eur. J. Cancer. 38 (2002) 2258–2264, https://doi.org/10.1016/S0959-8049(02)00234-4.
[32] R.C. Roovers, M.J.W.D. Vosjan, T. Laeremans, R. El Khoulati, R.C.G. De Bruin, K. M. Ferguson, A.J. Verkleij, G.A.M.S. Van Dongen, P.m.p., Van Bergen En Henegouwen, A biparatopic anti-EGFR nanobody efficiently inhibits solid tumour growth, Int. J. Cancer. 129 (2011) 2013–2024, https://doi.org/10.1002/ijc.26145.
[33] K.R. Schmitz, A. Bagchi, R.C. Roovers, P.M.P. Van Bergen En, K.M.F. Henegouwen, Structural evaluation of EGFR inhibition mechanisms for nanobodies/VHH domains, Structure. 21 (2013) 1214–1224, https://doi.org/10.1016/j.str.2013.05.008.
[34] A. Noor, G. Walser, M. Wesseling, P. Giron, A.-M. Laffra, F. Haddouchi, J. De Grève, P. Kronenberger, Production of a mono-biotinylated EGFR nanobody in the E. coli periplasm using the pET22b vector, BMC Res Notes 11 (1) (2018).
[35] J.Z. Kaczmarek, P.D. Skottrup, Selection and characterization of camelid nanobodies towards urokinase-type plasminogen activator, Mol. Immunol. 65 (2015) 384–390, https://doi.org/10.1016/j.molimm.2015.02.011.
[36] A. González Pose, R. Montesino Seguí, R. Maura Pérez, F. Hugues Salazar, I. Cabezas Ávila, C. Altamirano Gómez, O. Sánchez Ramos, J. Roberto Toledo, Characterisation of a new molecule based on two E2 sequences from bovine viral diarrhoea-mucosal disease virus fused to the human immunoglobulin Fc fragment, J Vet. Res. 65 (2021) 27–37, https://doi.org/10.2478/jvetres-2021-0006.
[37] M.P. Zach, R.M. Penner, Nanocrystalline nickel nanoparticles, Adv. Mater. 12 (2000) 878–883, https://doi.org/10.1002/1521-4095(200006)12:12<878::AID-ADMA878>3.0.CO;2-X.
[38] L.-F. Huang, M.J. Hutchison, R.J. Santucci, J.R. Scully, J.M. Rondinelli, Improved Electrochemical Phase Diagrams from Theory and Experiment: The Ni-Water System and Its Complex Compounds, J. Phys. Chem. C. 121 (18) (2017) 9782–9789.
[39] P.N. Bartlett, D.H. Dawson, Electrochemistry of poly(3-thiopheneacetic acid) in aqueous solution: Evidence for an intramolecular chemical reaction, J. Mater. Chem. 4 (1994) 1805–1810, https://doi.org/10.1039/JM9940401805.
[40] A. Noorbakhsh, A. Salimi, Development of DNA electrochemical biosensor based on immobilization of ssDNA on the surface of nickel oxide nanoparticles modified glassy carbon electrode, Biosens. Bioelectron. 30 (2011) 188–196, https://doi.org/10.1016/j.bios.2011.09.010.
[41] M. Ganesana, G. Istarnboulie, J.L. Marty, T. Noguer, S. Andreescu, Site-specific immobilization of a (His)6-tagged acetylcholinesterase on nickel nanoparticles for highly sensitive toxicity biosensors, Biosens. Bioelectron. 30 (2011) 43–48, https://doi.org/10.1016/j.bios.2011.08.024.
[42] K. Kaszuba, M. Grzybek, A. Orłowski, R. Danne, T. Róg, K. Simons, Ü. Coskun, I. Vattulainen, N-Glycosylation as determinant of epidermal growth factor receptor conformation in membranes, Proc. Natl. Acad. Sci. U. S. A. 112 (2015) 4334–4339, https://doi.org/10.1073/pnas.1503262112.
[43] C.M.A. Brett, Electrochemical Impedance Spectroscopy in the Electrochemical Sensors and Biosensors, Molecules. 27 (2022) 1497.
[44] N. Weidler, J. Schuch, F. Knaus, P. Stenner, S. Hoch, A. Maljusch, R. Schäfer, B. Kaiser, W. Jaegermann, X-ray Photoelectron Spectroscopic Investigation of Plasma-Enhanced Chemical Vapor Deposited NiOx, NiOx(OH)y, and CoNiOx(OH)y: Influence of the Chemical Composition on the Catalytic Activity for the Oxygen Evolution Reaction, J. Phys. Chem. C. 121 (2017) 6455–6463, https://doi.org/10.1021/acs.jpcc.6b12652.
[45] D.M. Eby, K. Artyushkova, A.K. Paravastu, G.R. Johnson, Probing the molecular structure of antimicrobial peptide-mediated silica condensation using X-ray photoelectron spectroscopy, J. Mater. Chem. 22 (2012) 9875–9883, https://doi.org/10.1039/c2jm30837a.
[46] D. Wasserberg, J. Cabanas-Danés, J. Prangsma, S. O'Mahony, P.A. Cazade, E. Tromp, C. Blum, D. Thompson, J. Huskens, V. Subramaniam, P. Jonkheijm, Controlling Protein Surface Orientation by Strategic Placement of Oligo-Histidine Tags, ACS Nano. 11 (2017) 9068–9083, https://doi.org/10.1021/acsnano.7b03717.
[47] X. Qiu, K.D. Wegner, Y.T. Wu, P.M.P. Van Bergen En, T.L. Henegouwen, N. H. Jennings, Nanobodies and antibodies for duplexed EGFR/HER2 immunoassays using terbium-to-quantum dot FRET, Chem. Mater. 28 (2016) 8256–8267, https://doi.org/10.1021/acs.chemmater.6b03198.
[48] K.D. Wegner, S. Lindén, Z. Jin, T.L. Jennings, R. El Khoulati, P.M.P. Van Bergen En, N.H. Henegouwen, Nanobodies and nanocrystals: Highly sensitive quantum dot-based homogeneous FRET immunoassay for serum-based EGFR detection, Small. 10 (2014) 734–740, https://doi.org/10.1002/smll.201302383.
[49] R.K. Schmidt-Ullrich, R.B. Mikkelsen, P. Dent, D.G. Todd, K. Valerie, B. D. Kavanagh, J.N. Contessa, W.K. Rorrer, P.B. Chen, Radiation-induced proliferation of the human A431 squamous carcinoma cells is dependent on EGFR tyrosine phosphorylation, Oncogene. 15 (1997) 1191–1197, https://doi.org/10.1038/sj.onc.1201275.
[50] Z. Wang, X. Zhang, Z. Yang, H. Du, Z. Wu, J. Gong, J. Yan, Q. Zheng, MiR-145 regulates PAK4 via the MAPK pathway and exhibits an antitumor effect in human colon cells, Biochem. Biophys. Res. Commun. 427 (2012) 444–449, https://doi.org/10.1016/j.bbrc.2012.06.123.
[51] Y. Xu, P. Soo, F. Walker, H.H. Zhang, N. Redpath, C.W. Tan, N.A. Nicola, T. E. Adams, T.P. Garrett, J.G. Zhang, A.W. Burgess, LRIG1 extracellular domain: Structure and function analysis, J. Mol. Biol. 427 (2015) 1934–1948, https://doi.org/10.1016/j.jmb.2015.03.001.
[52] Y. Li, Z. Sun, B. Liu, Y. Shan, L. Zhao, L.i. Jia, Tumor-suppressive miR-26A and miR-26B inhibit cell aggressiveness by regulating fut4 in colorectal cancer, Cell Death Dis. 8 (6) (2017) e2892–e.
[53] T. Holbro, R.R. Beerli, F. Maurer, M. Koziczak, C.F. Barbas, N.E. Hynes, The ErbB2/ErbB3 heterodimer functions as an oncogenic unit: ErbB2 requires ErbB3 to drive breast tumor cell proliferation, Proc. Natl. Acad. Sci. U.S.A. 100 (15) (2003) 8933–8938.